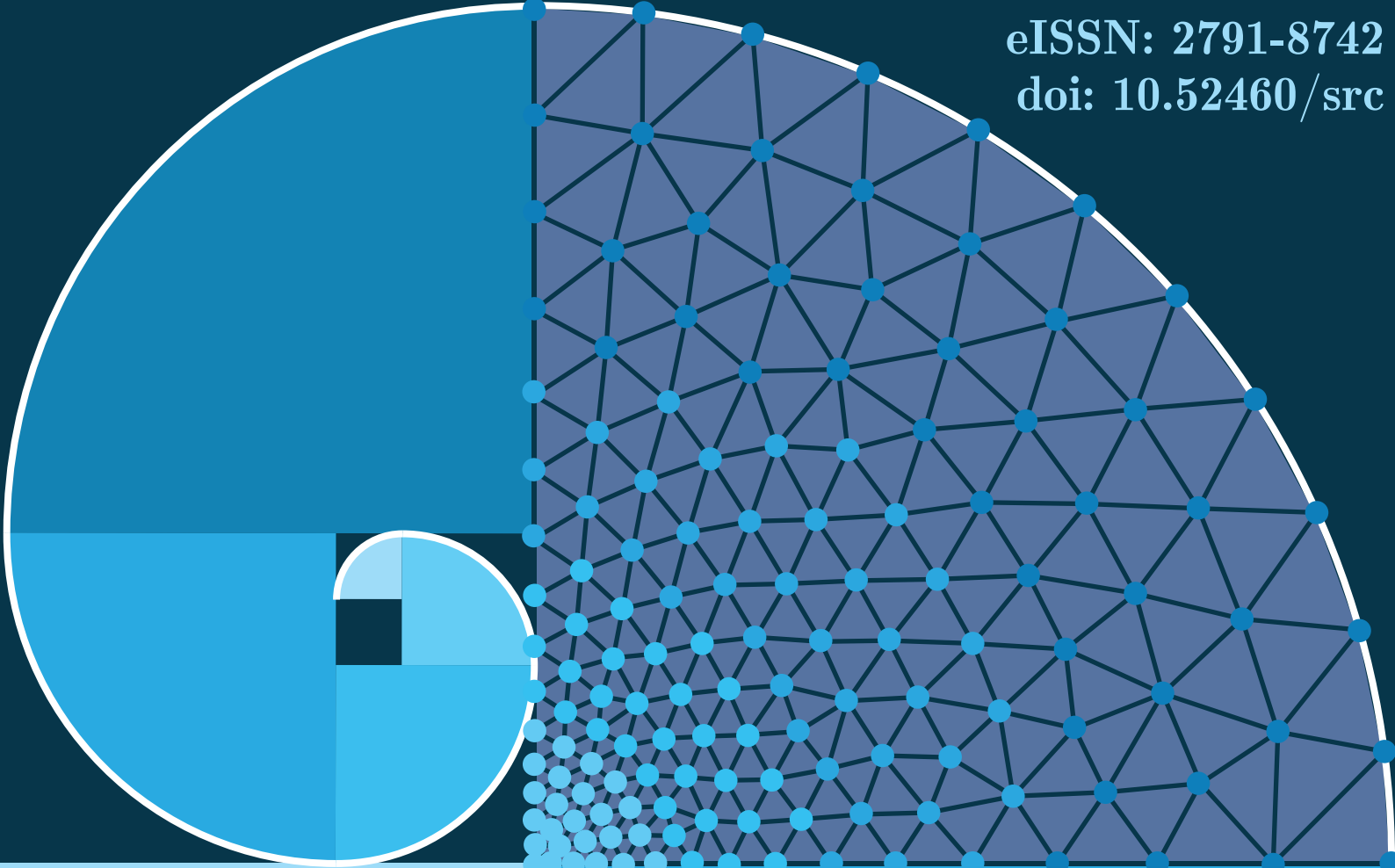
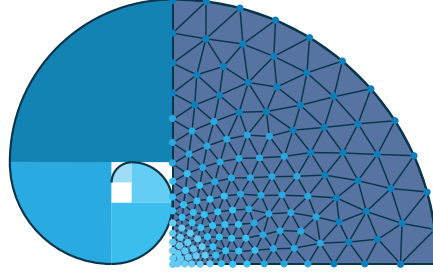


eISSN: 2791-8742  
doi: 10.52460/src



**Scientific  
Research  
Communications**

**Volume 1  
Issue 1  
July 2021**



# Scientific Research Communications

Volume 1, Issue 1, 2021

---

## Editorial

### Editor-in-Chief

Mehmet EVİK

### Associate Editors

Ahmet AYKAÇ

Ayşe KALAYCI ÖNAÇ

Faruk ÖZGER

Gökçen BOMBAR

Sedat YALÇINKAYA

Sercan ACARER

Umut CEYHAN

### Office

Ahenk KARCI

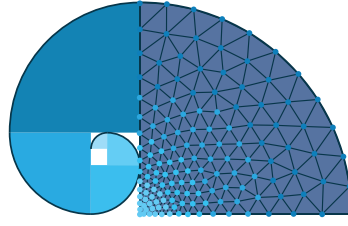
Hande GÜNDEL

Furkan EMREM

### Publisher

Prof. Dr. Mehmet EVİK

İzmir International Guest Students Association



# Scientific Research Communications

Volume 1, Issue 1, 2021

---

## Contents

### Research Articles

#### **Some Compact Operators on the Hahn Space**

E. Malkowsky

#### **Watt Six-Bar Compliant Mechanism Analysis based on Kinematic and Dynamic Responses**

Ç. Uyulan and B. İpek

#### **Re-examine Conventional Concepts in Urban Design: The Conflict between Urban Space Utilization and the Elements of Power and Control - Case of Hawkers within Amman, Jordan**

D. Abdel-Aziz

#### **Ensemble of Classifiers and Term Weighting Schemes for Sentiment Analysis in Turkish**

A. Onan

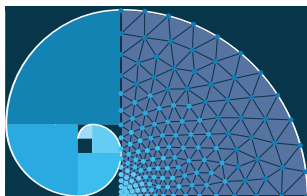
#### **The Impact of COVID-19 on Users' Visit to the Shopping Centers in Libya**

H. M. S. Almansouri and M. Çetin

### Review Articles

#### **On Local Scouring at Single Piers**

A. H. Cardoso and C. M. S. Fael and R. M. M. Lança



# Some Compact Operators on the Hahn Space

Eberhard Malkowsky<sup>1,\*</sup> 

<sup>1</sup>University Union Nikola Tesla, Faculty of Management, Belgrade, Serbia

\*Corresponding author: Eberhard.Malkowsky@math.uni-giessen.de; ema@pmf.ni.ac.rs

Received: 17.02.2021

Accepted: 30.05.2021

## Abstract

We establish the characterisations of the classes of bounded linear operators from the generalised Hahn sequence space  $h_d$ , where  $d$  is an unbounded monotone increasing sequence of positive real numbers, into the spaces  $[c_0]$ ,  $[c]$  and  $[c_\infty]$  of sequences that are strongly convergent to zero, strongly convergent and strongly bounded. Furthermore, we prove estimates for the Hausdorff measure of noncompactness of bounded linear operators from  $h_d$  into  $[c]$ , and identities for the Hausdorff measure of noncompactness of bounded linear operators from  $h_d$  to  $[c_0]$ , and use these results to characterise the classes of compact operators from  $h_d$  to  $[c]$  and  $[c_0]$ .

**2020 Mathematics Subject Classification:** 46A45, 40C05, 46B45, 47H08

**Keywords:** The Hahn sequence space; bounded linear operators; Hausdorff measure of noncompactness; compact operators

## 1. Introduction and Notations

We use the standard notations  $\omega$  for the set of all complex sequences  $x = (x_k)_{k=1}^\infty$ , and  $\ell_\infty$ ,  $c$ ,  $c_0$  and  $\phi$  for the sets of all bounded, convergent, null and finite sequences, that is, sequences terminating in zeros. We also write  $e = (e_k)_{k=1}^\infty$  and  $e^{(n)} = (e_k^{(n)})_{k=1}^\infty$  ( $n \in \mathbb{N}$ ) for the sequences with  $e_k = 1$  for all  $k$ , and  $e_n^{(n)} = 1$  and  $e_k^{(n)} = 0$  for  $k \neq n$ .

We recall that a *BK* space  $X$  is a Banach sequence space with continuous coordinates  $P_n : X \rightarrow \mathbb{C}$  ( $n \in \mathbb{N}$ ), where  $P_n(x) = x_n$  for all  $x = (x_k)_{k=1}^\infty \in X$ . A *BK* space  $X \supset \phi$  is said to have *AK* if  $x = \lim_{m \rightarrow \infty} x^{[m]}$  for all  $x = (x_k)_{k=1}^\infty \in X$ , where  $x^{[m]} = \sum_{k=1}^m x_k e^{(k)}$  denotes the  $m$ -section of the sequence  $x$ . It is well known that the sets  $\ell_\infty$ ,  $c$ , and  $c_0$  are *BK* spaces with their natural norms  $\|x\|_\infty = \sup_k |x_k|$ ,  $c_0$  has *AK*, every sequence  $x = (x_k)_{k=1}^\infty \in c$  has a unique representation  $x = \xi e + \sum_{k=1}^\infty (x_k - \xi) e^{(k)}$ , where  $\xi = \lim_{k \rightarrow \infty} x_k$ , and finally,  $\ell_\infty$  is not separable and consequently has no Schauder basis. Let  $X \subset \omega$ . Then the set  $X^\beta = \{a \in \omega : \sum_{k=1}^\infty a_k x_k \text{ converges for all } x \in X\}$  is the  $\beta$ -dual of  $X$ . Let  $A = (a_{nk})_{n,k=1}^\infty$  be an infinite matrix of complex numbers,  $A_n = (a_{nk})_{k=1}^\infty$  and  $A^k = (a_{nk})_{n=1}^\infty$  be the sequences in the  $n^{\text{th}}$  row and the  $k^{\text{th}}$  column of  $A$ , and  $X$  and  $Y$  be subsets of  $\omega$ . Then we write  $A_n x = \sum_{k=1}^\infty a_{nk} x_k$  and  $Ax = (A_n x)_{n=1}^\infty$  for  $x = (x_k)_{k=1}^\infty$  provided all the series converge. The set  $X_A = \{x \in \omega : Ax \in X\}$  is called the *matrix domain of A in X*, and  $(X, Y)$  denotes the class of all matrix transformations from  $X$  into  $Y$ , that is,  $A \in (X, Y)$  if and only if  $X \subset Y_A$ .

The reader interested in the theory of sequence spaces and matrix transformations is referred to

the monographs Boos (2000); de Malafosse et al. (2021); Kamthan and Gupta (1981); Malkowsky and Rakočević (2019); Ruckle (1981); Wilansky (1984); Zeller and Beekmann (1968).

If  $X$  and  $Y$  are Banach spaces, we use the standard notation  $\mathcal{B}(X, Y)$  for the Banach space of all bounded linear operators  $L : X \rightarrow Y$  with the operator norm  $\|L\| = \sup\{|L(x)| : \|x\| = 1\}$ ; the space  $X^* = \mathcal{B}(X, \mathbb{C})$  is called the continuous dual of  $X$ ; its norm is  $\|f\| = \sup\{|f(x)| : \|x\| = 1\}$  for all  $f \in X^*$ . Also  $\mathcal{K}(X, Y)$  denotes the class of all compact operators in  $\mathcal{B}(X, Y)$ .

The following well-known result gives the relation between  $(X, Y)$  and  $\mathcal{B}(X, Y)$ .

**Proposition 1.1** *Let  $X$  and  $Y$  be BK spaces.*

(a) *If  $A \in (X, Y)$ , then  $L_A \in \mathcal{B}(X, Y)$ , where  $L_A(x) = Ax$  for all  $x \in X$ , that is, matrix maps between BK spaces are continuous (Wilansky, 1984, Theorem 4.2.8).*

(b) *If  $X$  has AK, then every operator  $L \in \mathcal{B}(X, Y)$  can be represented by a matrix  $A \in (X, Y)$  such that*

$$Ax = L(x) \text{ for all } x \in X \text{ (Jarrah and Malkowsky, 2003, Theorem 1.9).} \quad (1.1)$$

The operator  $\Delta : \omega \rightarrow \omega$  of the so-called forward differences is defined by  $\Delta x_k = x_k - x_{k+1}$  ( $k = 1, 2, \dots$ ). The set  $h = \{x \in \omega : \sum_{k=1}^{\infty} k|\Delta x_k| < \infty\} \cap c_0$  was defined by Hahn in 1922 (see Hahn (1922)) in connection with the theory of singular integrals; Hahn showed that  $h$  is a BK space with  $\|x\|' = \sum_{k=1}^{\infty} k|\Delta x_k| + \sup_k |x_k|$  for all  $x = (x_k)_{k=1}^{\infty} \in h$ . Rao (1990) showed that the Hahn space is a BK space with AK with the norm  $\|x\| = \sum_{k=1}^{\infty} k|\Delta x_k|$  for all  $x = (x_k)_{k=1}^{\infty} \in h$ .

Goes (1972) introduced and studied the generalised Hahn space  $h_d$  for arbitrary complex sequences  $d = (d_k)_{k=1}^{\infty}$  with  $d_k \neq 0$  for all  $k$  by  $h_d = \{x \in \omega : \sum_{k=1}^{\infty} |d_k| \cdot |\Delta x_k| < \infty\} \cap c_0$  with the norm

$$\|x\|_d = \sum_{k=1}^{\infty} |d_k| \cdot |\Delta x_k| \text{ for all } x = (x_k)_{k=1}^{\infty} \in h_d. \quad (1.2)$$

The following result is known.

**Proposition 1.2** *Let  $d$  be a increasing unbounded sequence of positive reals.*

(a) *Then  $h_d$  with the norm in (1.2) is a BK space with AK (Malkowsky et al., 2021, Proposition 2.1).*

(b) *We write*

$$bs_d = \left\{ a \in \omega : \sup_n \frac{1}{d_n} \left| \sum_{k=1}^n a_k \right| \right\} \text{ and } \|a\|_{bs_d} = \sup_n \frac{1}{d_n} \left| \sum_{k=1}^n a_k \right| \text{ for all } a \in bs_d.$$

*Then  $h_d^\beta = bs_d$  and  $h_d^\beta$  and  $h_d^*$  are norm isomorphic (Malkowsky et al., 2021, Proposition 2.3).*

Recent research on the Hahn space and its generalisations can be found, for instance, in Das (2017); Kirişci (2013a); Raj and Kilişman (2014); Rao and Srinivasalu (1996); Rao and Subramanian (2002) and the survey paper Kirişci (2013b).

Throughout, we use the convention that every term with a subscript  $\leq 0$  is equal to zero. The

sets

$$\begin{aligned}
 [c_0] &= \left\{ x \in \omega : \lim_{n \rightarrow \infty} \frac{1}{n} \sum_{k=1}^n |kx_k - (k-1)x_{k-1}| = 0 \right\}, \\
 [c] &= [c_0] \oplus e = \{x \in \omega : x - \xi e \in [c_0] \text{ for some } \xi \in \mathbb{C}\} \text{ and} \\
 [c_\infty] &= \left\{ x \in \omega : \sup_n \frac{1}{n} \sum_{k=1}^n |kx_k - (k-1)x_{k-1}| < \infty \right\}
 \end{aligned}$$

of sequences that are strongly convergent to zero, strongly convergent and strongly bounded were first introduced and studied in the papers Borwein (1960), and Kuttner and Thorpe (1979). Generalizations of these spaces were considered by Mòricz (1989), the research papers Djolović and Malkowsky (2012, 2013); Jarrah and Malkowsky (2002); Malkowsky (1995, 2000, 2013); Malkowsky and Nergiz (2015); Malkowsky and Rakočević (1998, 2000), and the survey paper Malkowsky (2017).

The following result is well-known.

**Proposition 1.3** (Malkowsky, 1995, Theorem 2) *The sets  $[c_0]$ ,  $[c]$  and  $[c_\infty]$  are BK spaces with*

$$\|x\|_{[c_\infty]} = \sup_n \frac{1}{n} \sum_{k=1}^n |kx_k - (k-1)x_{k-1}|;$$

$[c_0]$  is a closed subspace of  $[c]$ , and  $[c]$  is a closed subspace of  $[c_\infty]$ ;  $[c_0]$  has AK and every sequence  $x = (x_k)_{k=1}^\infty \in [c]$  has a representation

$$x = \xi e + \sum_{k=1}^{\infty} (x_k - \xi) e^{(k)}, \quad (1.3)$$

where  $\xi$  is the unique complex number such that  $x - \xi e \in [c_0]$ , the so-called  $[c]$ -limit of  $x$ .

In this paper, we characterise the classes  $\mathcal{B}(h_d, [c_0])$ ,  $\mathcal{B}(h_d, [c])$  and  $\mathcal{B}(h_d, [c_\infty])$ , when  $d$  is a monotone increasing unbounded sequence of positive real numbers. Furthermore, we establish estimates for the Hausdorff measure of noncompactness of operators in the class  $\mathcal{B}(h_d, [c])$ , and identities for the Hausdorff measure of noncompactness of operators in the class  $\mathcal{B}(h_d, [c_0])$ . Finally, we characterise the classes  $\mathcal{K}(h_d, [c])$  and  $\mathcal{K}(h_d, [c_0])$ .

## 2. The Classes $\mathcal{B}(h_d, Y)$ for $Y \in \{[c_\infty], [c], [c_0]\}$

Throughout let  $d$  be an unbounded increasing sequence of positive real numbers.

We are going to characterise the classes  $\mathcal{B}(h_d, Y)$  and compute the operator norm of  $L \in \mathcal{B}(h_d, Y)$  for  $Y \in \{[c_\infty], [c], [c_0]\}$ . Since  $h_d$  is a BK space with AK by Proposition 1.2 (a), and each space  $Y$  is a BK space by Proposition 1.3, each operator  $L \in \mathcal{B}(h_d, Y)$  can be represented by a matrix  $A \in (h_d, Y)$  as in (1.1) by Proposition 1.1 (b). We will use this fact and notation throughout the paper.

We need the following definition and results which we state here for the reader's convenience.

**Definition 2.1** (Wilansky, 1984, Definition 7.4.2) Let  $X$  be a BK space. A subset  $E$  of the set  $\phi$  called a *determining set* for  $X$  if  $D(X) = \bar{B}_X \cap \phi$  is the absolutely convex hull of  $E$ .

**Proposition 2.2** (Wilansky, 1984, Theorem 8.3.4) *Let  $X$  be a BK space with AK,  $E$  be a determining set for  $X$ , and  $Y$  be an FK space. Then  $A \in (X, Y)$  if and only if:*

(i) *The columns of  $A$  belong to  $Y$ , that is,  $A^k = (a_{nk})_{n=1}^\infty \in Y$  for all  $k$ ,*

and

(ii)  *$L(E)$  is a bounded subset of  $Y$ , where  $L(x) = Ax$  for all  $x \in X$ .*

**Proposition 2.3** (Malkowsky et al., 2021, Proposition 3.2) *The set*

$$E = \left\{ \frac{1}{d_m} \cdot e^{[m]} : m \in \mathbb{N} \right\} \quad (2.1)$$

is a determining set for  $h_d$ .

**Theorem 2.4** *We have*

(a)  *$L \in \mathcal{B}(h_d, [c_\infty])$  if and only if*

$$\|A\|_{(h_d, [c_\infty])} = \sup_{l, m} \frac{1}{ld_m} \sum_{n=1}^l \left| n \sum_{k=1}^m a_{nk} - (n-1) \sum_{k=1}^m a_{n-1, k} \right| < \infty; \quad (2.2)$$

(b)  *$L \in \mathcal{B}(h_d, [c])$  if and only if (2.2) holds and*

$$\left\{ \begin{array}{l} \text{for each } k \in \mathbb{N}, \text{ there exists } \alpha_k \in \mathbb{C} \text{ such that} \\ \lim_{l \rightarrow \infty} \frac{1}{l} \sum_{n=1}^l |na_{nk} - (n-1)a_{n-1, k} - \alpha_k| = 0; \end{array} \right\} \quad (2.3)$$

(c)  *$L \in \mathcal{B}(h_d, [c_0])$  if and only if (2.2) holds and*

$$\lim_{l \rightarrow \infty} \frac{1}{l} \sum_{n=1}^l |na_{nk} - (n-1)a_{n-1, k}| = 0 \text{ for each } k. \quad (2.4)$$

(d) *If  $L \in \mathcal{B}(h_d, Y)$  for  $Y \in \{[c_0], [c], [c_\infty]\}$ , then*

$$\|L\| = \|A\|_{(h_d, [c_\infty])}. \quad (2.5)$$

**Proof.** (a) Let  $L \in \mathcal{B}(h_d, [c_\infty])$ .

Since the set  $E$  in (2.1) is a determining set for  $h_d$  by Proposition 2.3, we apply Proposition 2.2, and show that the matrix  $A$  that represents  $L$  satisfies the conditions in (i) and (ii) of Proposition 2.2.

We write  $C = (c_{nm})_{n, m=1}^\infty$  for the matrix with

$$c_{nm} = n \sum_{k=1}^m a_{nk} \text{ for } n, m = 1, 2, \dots$$

and

$$\Delta_n^- c_{nm} = c_{nm} - c_{n-1, m} \text{ for } n, m = 1, 2, \dots$$

Let  $m \in \mathbb{N}$  be given and  $y^{(m)} = (1/d_m)e^{[m]} \in E$ . Then we have

$$A_n y^{(m)} = \sum_{k=1}^\infty a_{nk} y_k^{(m)} = \frac{1}{d_m} \sum_{k=1}^m a_{nk} = \frac{1}{nd_m} c_{nm} \text{ for all } n,$$

hence

$$\begin{aligned} \|Ay^{(m)}\|_{[c_\infty]} &= \sup_l \frac{1}{l} \sum_{n=1}^l |nA_n y^{(m)} - (n-1)A_{n-1} y^{(m)}| \\ &= \sup_l \frac{1}{ld_m} \sum_{n=1}^l |\Delta_n^- c_{nm}| \leq \|A\|_{(h_d, [c_\infty])} < \infty. \end{aligned}$$

So (2.2) yields the condition in (ii) of Proposition 2.2.

It remains to show that the condition in (i) of Proposition 2.2 is redundant.

We have

$$a_{nm} = d_m A_n y^{(m)} - d_{m-1} A_n y^{(m-1)} = \frac{1}{n} (c_{nm} - c_{n,m-1}) \text{ for all } n \text{ and } m,$$

hence

$$|na_{nm} - (n-1)a_{n,m-1}| = |c_{nm} - c_{n,m-1} - (c_{n-1,m} - c_{n-1,m-1})| = |\Delta_n^- c_{nm}| + |\Delta_n^- c_{n,m-1}|$$

and

$$\begin{aligned} \|A^m\|_{[c_\infty]} &= \sup_l \frac{1}{l} \sum_{n=1}^l |na_{nm} - (n-1)a_{n,m-1}| \\ &\leq d_m \sup_l \frac{1}{ld_m} \sum_{n=1}^l |\Delta_n^- c_{nm}| + d_{m-1} \sup_l \frac{1}{ld_{m-1}} \sum_{n=1}^l |\Delta_n^- c_{n,m-1}| \\ &\leq 2d_m \cdot \|A\|_{(h_d, [c_\infty])} < \infty \text{ for all } m. \end{aligned}$$

This completes the proof of Part (a).

(b) and (c) Since  $h_d$  is a *BK* space with *AK* and  $[c_0]$  and  $[c]$  are closed subspaces of the *BK* space  $[c_\infty]$  by Proposition 1.3, Parts (b) and (c) follow by (Wilansky, 1984, Theorem 8.3.6).

(d) Finally we assume that  $L \in \mathcal{B}(h_d, Y)$ , where  $Y \in \{[c_0], [c], [c_\infty]\}$ . Then  $A_n \in h_d^\beta$  for all  $n$  and  $h_d^\beta = bs_d$  by Proposition 1.2 (b). We obtain for  $A_n x = L_n(x)$  ( $x \in h_d$ )

$$|A_n x| \leq \sum_{k=1}^\infty d_k |\Delta x_k| \frac{1}{d_k} \left| \sum_{j=1}^k a_{nj} \right| \leq \|A_n\|_{bs_d} \cdot \|x\|_{h_d} \text{ for all } n \in \mathbb{N} \text{ and all } x \in h_d. \tag{2.6}$$

To prove (2.6), let  $m \in \mathbb{N}$  be given. Then Abel's summation by parts yields

$$\begin{aligned} L_n(x^{[m]}) &= A_n x^{[m]} = \sum_{k=1}^m a_{nk} x_k = \sum_{k=1}^{m-1} \Delta x_k \sum_{j=1}^k a_{nj} + x_m \sum_{j=1}^m a_{nj} \\ &= \sum_{k=1}^{m-1} d_k \Delta x_k \frac{1}{d_k} \sum_{j=1}^k a_{nj} + d_m x_m \frac{1}{d_m} \sum_{j=1}^m a_{nj}. \end{aligned}$$

Since  $h_d$  has *AK* and  $x \in h_d$ , it follows that

$$\begin{aligned} 0 \leq |d_m x_m| &= \sum_{k=m}^\infty d_k \left| \Delta x_k^{[m]} \right| \leq \sum_{k=1}^\infty d_k \left| \Delta(x_k^{[m]} - x_k) \right| + \sum_{k=m}^\infty d_k |\Delta x_k| \\ &= \|x^{[m]} - x\|_{h_d} + \sum_{k=m}^\infty d_k |\Delta x_k| \rightarrow 0 \text{ (} m \rightarrow \infty \text{)}. \end{aligned}$$

Thus the continuity of  $L_n$  yields

$$\begin{aligned} |A_n x| = |L_n(x)| &= \lim_{m \rightarrow \infty} |L_n(x^{[m]})| \leq \sum_{k=1}^{\infty} d_k |\Delta x_k| \frac{1}{d_k} \left| \sum_{j=1}^k a_{nj} \right| \\ &\leq \sum_{k=1}^{\infty} d_k |\Delta x_k| \|A_n\|_{bs_d} = \|A_n\|_{bs_d} \cdot \|x\|_{h_d}, \end{aligned}$$

that is, (2.6).

Now we write  $B = (b_{nk})_{n,k=1}^{\infty}$  for the matrix with the rows  $B_n = nA_n - (n-1)A_{n-1}$  for  $n = 1, 2, \dots$ . Then we obtain from (2.6) for  $l = 1, 2, \dots$

$$\begin{aligned} \frac{1}{l} \sum_{n=1}^l |nA_n x - (n-1)A_{n-1} x| &= \frac{1}{l} \sum_{n=1}^l |B_n x| \leq \frac{1}{l} \sum_{n=1}^l \sum_{m=1}^{\infty} d_m |\Delta x_m| \frac{1}{d_m} \left| \sum_{j=1}^m b_{nj} \right| \\ &= \frac{1}{l} \sum_{m=1}^{\infty} d_m |\Delta x_m| \left( \frac{1}{d_m} \sum_{n=1}^l \left| \sum_{j=1}^m b_{nj} \right| \right) \\ &\leq \frac{1}{l} \left( \sup_m \frac{1}{d_m} \sum_{n=1}^l \left| \sum_{j=1}^m b_{nj} \right| \right) \cdot \|x\|_{h_d} \\ &\leq \left( \sup_{l,m} \frac{1}{ld_m} \sum_{n=1}^l \left| \sum_{j=1}^m (na_{nj} - (n-1)a_{n-1,j}) \right| \right) \|x\|_{h_d} \\ &\leq \|A\|_{(h_d, [c_{\infty}])} \|x\|_{h_d}. \end{aligned}$$

This implies

$$\|L\| = \sup_{\|x\|_{h_d}=1} \|L(x)\|_{[c_{\infty}]} = \sup_{\|x\|_{h_d}=1} \frac{1}{l} \sum_{n=1}^l |nA_n x - (n-1)A_{n-1} x| \leq \|A\|_{(h_d, [c_{\infty}])}. \tag{2.7}$$

To prove the converse inequality, let  $m \in \mathbb{N}$  be given. We put  $x^{(m)} = (1/d_m)e^{[m]}$ . Then

$$\|x^{(m)}\|_{h_d} = \frac{1}{d_m} \sum_{k=1}^m d_k |\Delta x_k^{(m)}| = \frac{d_m}{d_m} = 1$$

and

$$\begin{aligned} \|L(x^{(m)})\|_{[c_{\infty}]} &= \sup_l \frac{1}{l} \sum_{n=1}^l |nA_n x^{(m)} - (n-1)A_{n-1} x^{(m)}| \\ &= \sup_l \frac{1}{ld_m} \sum_{n=1}^l |c_{nm} - c_{n-1,m}| \leq \|L\|. \end{aligned}$$

Since  $m \in \mathbb{N}$  was arbitrary, we have  $\|A\|_{(h_d, [c_{\infty}])} \leq \|L\|$ .

Finally, this and (2.7) together imply (2.5). □

Now we establish a formula for the  $[c]$ -limits of  $L(x)$  and  $x \in h_d$ , when  $L \in \mathcal{B}(h_d, w)$ .

**Theorem 2.5** Let  $L \in \mathcal{B}(h_d, [c])$  and  $\alpha_k$  for  $k \in \mathbb{N}$  be the complex numbers in (2.3). Then the  $[c]$ -limit  $\eta(x)$  of  $L(x)$  for each sequence  $x \in h_d$  is given by

$$\eta(x) = \sum_{k=1}^{\infty} \alpha_k x_k. \tag{2.8}$$

**Proof.** Let  $L \in \mathcal{B}(h_d, [c])$ . We write  $B = (b_{nk})_{n,k=1}^{\infty}$  for the matrix with the rows  $B_n = nA_n - (n-1)A_{n-1}$  for all  $n$ . First we show

$$(\alpha_k)_{k=1}^{\infty} \in bs_d. \tag{2.9}$$

We have for all  $l, m \in \mathbb{N}$

$$\begin{aligned} \frac{1}{d_m} \left| \sum_{k=1}^m \alpha_k \right| &= \frac{1}{d_m} \cdot \frac{1}{l} \sum_{n=1}^l \left| \sum_{k=1}^m \alpha_k \right| \\ &\leq \frac{1}{d_m} \cdot \frac{1}{l} \sum_{n=1}^l \left| \sum_{k=1}^m b_{nk} - \alpha_k \right| + \frac{1}{d_m} \cdot \frac{1}{l} \sum_{n=1}^l \left| \sum_{k=1}^m b_{nk} \right| \\ &\leq \frac{1}{d_m} \sum_{k=1}^m \frac{1}{l} \sum_{n=1}^l |b_{nk} - \alpha_k| + \|A\|_{(h_d, [c_{\infty}])}. \end{aligned} \tag{2.10}$$

Since, for each fixed  $m$ , the first term in the last inequality above tends to 0 as  $l$  tends to infinity by (2.3), it follows that

$$\sup_m \frac{1}{d_m} \left| \sum_{k=1}^m \alpha_k \right| \leq \|A\|_{(h_d, [c_{\infty}])} < \infty, \tag{2.11}$$

and so (2.9) is satisfied.

By Proposition 1.2 (b) and (2.9), we have  $(\alpha_k)_{k=1}^{\infty} \in h_d^{\beta}$ . Also  $A \in (h_d, [c])$  implies  $A_n \in h_d^{\beta}$  for each  $n$ , and consequently  $B_n - (\alpha_k)_{k=1}^{\infty} \in h_d^{\beta}$  for each  $n$ . Now we obtain for all  $m$  and  $l$  by (2.11)

$$\frac{1}{ld_m} \sum_{n=1}^l \left| \sum_{k=1}^m (b_{nk} - \alpha_k) \right| \leq \frac{1}{ld_m} \sum_{n=1}^l \left| \sum_{k=1}^m b_{nk} \right| + \frac{1}{ld_m} \sum_{n=1}^l \left| \sum_{k=1}^m \alpha_k \right| \leq 2\|A\|_{(h_d, [c_{\infty}])} < \infty,$$

and so

$$\sup_{m,l} \frac{1}{ld_m} \sum_{n=1}^l \left| \sum_{k=1}^m na_{nk} - (n-1)a_{nk} - \alpha_k \right| < \infty,$$

that is,  $(a_{nk} - \alpha_k)_{n,k=1}^{\infty} \in (h_d, [c_{\infty}])$  by Theorem 2.4 (a). Finally, this and (2.3) imply  $(a_{nk} - \alpha_k)_{n,k=1}^{\infty} \in (h_d, [c_0])$ , so the  $[c]$ -limit of  $L(x)$  for  $x \in h_d$  is given by (2.8).  $\square$

### 3. The Hausdorff Measure of Noncompactness of Operators

In this section, we establish an identity for the Hausdorff measure on noncompactness of operators in  $\mathcal{B}(h_d, [c_0])$  and an estimate for the Hausdorff measure of noncompactness of operators in  $\mathcal{B}(h_d, [c])$ . We also characterise the classes  $\mathcal{K}(h_d, [c_0])$  and  $\mathcal{K}(h_d, [c])$ .

We list the necessary, known concepts and results concerning the Hausdorff measure of noncompactness. First we recall the definition of the Hausdorff measure of noncompactness of bounded

sets in complete metric spaces (Toledano et al., 1997, Definition II.2.1), and the Hausdorff measure of noncompactness of operators between Banach spaces (Malkowsky and Rakočević, 2019, Definition 7.11.1). The interested reader is also referred to the research articles Mursaleen and Noman (2010, 2011).

Let  $X$  be a complete metric space and  $\mathcal{M}_X$  be the class of bounded subsets of  $X$ . Then the function  $\chi : \mathcal{M}_X \rightarrow [0, \infty)$  with  $\chi(Q) = \inf\{\varepsilon > 0 : Q \text{ has a finite } \varepsilon\text{-net in } X\}$  is called the *Hausdorff measure of noncompactness on  $X$* .

Let  $\chi_1$  and  $\chi_2$  be Hausdorff measures of noncompactness on the Banach spaces  $X$  and  $Y$ , respectively. Then an operator  $L : X \rightarrow Y$  is said to be  $(\chi_1, \chi_2)$ -bounded, if  $L(Q) \in \mathcal{M}_Y$  for all  $Q \in \mathcal{M}_X$  and there exists a non-negative real number  $c$  such that

$$\chi_2(L(Q)) \leq c \cdot \chi_1(Q) \text{ for all } Q \in \mathcal{M}_X. \quad (3.1)$$

If an operator  $L$  is  $(\chi_1, \chi_2)$ -bounded, the the number

$$\|L\|_{(\chi_1, \chi_2)} = \inf\{c \geq 0 : (3.1) \text{ is satisfied}\}$$

is called the  $(\chi_1, \chi_2)$ -*measure of noncompactness of the operator  $L$* . If  $\chi_1 = \chi_2$ , we write  $\|L\|_\chi = \|L\|_{(\chi, \chi)}$ , for short, and refer to  $\|L\|_\chi$  as the *Hausdorff measure of noncompactness of the operator  $L$* .

We need the following known results.

**Theorem 3.1 (Goldenštein, Gohberg, Markus)** (Malkowsky and Rakočević, 2000, Theorem 2.23) *Let  $X$  be a Banach space with a Schauder basis  $(b_n)$ ,  $\mathcal{R}_n : X \rightarrow X$  for each  $n$  be defined by*

$$\mathcal{R}_n(x) = \sum_{k=n+1}^{\infty} \lambda_k b_k \text{ for all } x = \sum_{k=1}^{\infty} \lambda_k b_k \in X,$$

and  $\mu : \mathcal{M}_X \rightarrow \mathcal{M}_X$  be the function with

$$\mu(Q) = \limsup_{n \rightarrow \infty} \left( \sup_{x \in Q} \|\mathcal{R}_n(x)\| \right).$$

Then

$$\frac{1}{a} \cdot \mu(Q) \leq \chi(Q) \leq \inf_n \left( \sup_{x \in Q} \|\mathcal{R}_n(x)\| \right) \leq \mu(Q) \text{ for all } x \in \mathcal{M}_X, \quad (3.2)$$

where  $a = \limsup_{n \rightarrow \infty} \|\mathcal{R}_n\|$  is the basis constant of the Schauder basis.

**Proposition 3.2** *Let  $X$  and  $Y$  be Banach spaces and  $L \in \mathcal{B}(X, Y)$  and  $S_X$  denote the unit sphere in  $X$ . Then we have*

$$\|L\|_\chi = \chi(L(S_X)) \text{ (Malkowsky and Rakočević, 2019, Theorem 7.11.4)} \quad (3.3)$$

and  $L \in \mathcal{K}(X, Y)$  if and only if

$$\|L\|_\chi = 0 \text{ (Malkowsky and Rakočević, 2019, Theorem 7.11.5).} \quad (3.4)$$

We obtain the following results for the Hausdorff measure of noncompactness of bounded sets in  $[c_0]$  and  $[c]$ .

**Corollary 3.3** *We have*

$$\chi(Q) = \mu(Q) \text{ for all } Q \in \mathcal{M}_{[c_0]} \tag{3.5}$$

and

$$\frac{1}{2} \cdot \mu(Q) \leq \chi(Q) \leq \mu(Q) \text{ for all } Q \in \mathcal{M}_{[c]}. \tag{3.6}$$

**Proof.** We show  $a = 1$  for  $\mathcal{R}_n : [c_0] \rightarrow [c_0]$  and  $a \leq 2$  for  $\mathcal{R}_n : [c] \rightarrow [c]$ . Then (3.5) and (3.6) follow from (3.2).

We have  $x = \sum_{k=1}^{\infty} x_k e^{(k)}$  for all  $x = (x_k)_{k=1}^{\infty} \in [c_0]$  by Proposition 1.3, hence for each  $m \in \mathbb{N}$

$$\begin{aligned} \|\mathcal{R}_m(x)\|_{[c_{\infty}]} &= \sup_{n \geq m+1} \frac{1}{n} \sum_{k=m+1}^n |kx_k - (k-1)x_{k-1}| \\ &= \sup_{n \geq m+1} \frac{1}{n} \left( (m+1)|x_{m+1}| + \sum_{k=m+2}^n |kx_k - (k-1)x_{k-1}| \right) \\ &= \sup_{n \geq m+1} \frac{1}{n} \left( \left| \sum_{k=1}^{m+1} (kx_k - (k-1)x_{k-1}) \right| + \sum_{k=m+2}^n |kx_k - (k-1)x_{k-1}| \right) \\ &\leq \sup_{n \geq 1} \frac{1}{n} \sum_{k=1}^n |kx_k - (k-1)x_{k-1}| = \|x\|_{[c_{\infty}]}, \end{aligned}$$

hence

$$\|\mathcal{R}_m(x)\|_{[c_{\infty}]} \leq \|x\|_{[c_{\infty}]}. \tag{3.7}$$

This implies  $\|\mathcal{R}_m\| \leq 1$  for all  $m$ . Since  $\mathcal{R}_m$  is a projector, we also have  $\|\mathcal{R}_m\| \geq 1$  for all  $m$ . Thus we have shown  $a = 1$ .

By (1.3), every sequence  $x = (x_k)_{k=1}^{\infty} \in [c]$  has a unique representation

$$x = \xi e + \sum_{k=1}^{\infty} (x_k - \xi) e^{(k)},$$

where  $\xi$  is the  $[c]$ -limit of the sequence  $x$ . Now we have

$$\begin{aligned} \|\mathcal{R}_m(x)\|_{[c_{\infty}]} &= \sup_{n \geq m} \frac{1}{n} \left( |(m+1)(x_{m+1} - \xi)| + \sum_{k=m+2}^n |k(x_k - \xi) - (k-1)(x_k - \xi)| \right) \\ &\leq \sup_{n \geq m} \frac{1}{n} (|(m+1) - (n - (m+1))|\xi| + |(m+1)x_{m+1}| \\ &\quad + \sum_{k=m+2}^n |kx_k - (k-1)x_{k-1}|) \\ &\leq |\xi| + \sup_{n \geq 1} \frac{1}{n} \sum_{k=1}^n |kx_k - (k-1)x_{k-1}| \end{aligned}$$

and (3.7) yields

$$\|\mathcal{R}_m\|_{[c_{\infty}]} \leq |\xi| + \|x\|_{[c_{\infty}]}. \tag{3.8}$$

We also obtain for all  $n$

$$|\xi| = \frac{1}{n} \sum_{k=1}^n |\xi| \leq \frac{1}{n} \sum_{k=1}^n |kx_k - (k-1)x_{k-1} - \xi| + \frac{1}{n} \sum_{k=1}^n |kx_k - (k-1)x_{k-1}|$$

$$\leq \frac{1}{n} \sum_{k=1}^n |kx_k - (k-1)x_{k-1} - \xi| + \|x\|_{[c_\infty]}.$$

Since  $\xi$  is the  $[c]$ -limit of the sequence  $x$ , the first term in the last inequality tends to 0 as  $n$  tends to  $\infty$ , and so  $|\xi| \leq \|x\|_{[c_\infty]}$ . Now (3.8) yields  $\|\mathcal{R}_m(x)\|_{[c_\infty]} \leq 2\|x\|_{[c_\infty]}$  for all  $m$ , hence  $a \leq 2$ .  $\square$

Now we prove an estimate for  $\|L\|_\chi$ , if  $L \in \mathcal{B}(h_d, [c])$ , and an identity for  $\|L\|_\chi$ , if  $L \in \mathcal{B}(h_d, [c_0])$ .

**Theorem 3.4** (a) *Let  $L \in \mathcal{B}(h_d, [c])$ . Then we have*

$$\begin{aligned} \frac{1}{2} \cdot \lim_{r \rightarrow \infty} \left( \sup_{m; l \geq r} \frac{1}{ld_m} \sum_{n=r}^l \left| \sum_{k=1}^m (na_{nk} - (n-1)a_{n-1,k} - \alpha_k) \right| \right) &\leq \|L\|_\chi \\ &\leq \lim_{r \rightarrow \infty} \left( \sup_{m; l \geq r} \frac{1}{ld_m} \sum_{n=r}^l \left| \sum_{k=1}^m (na_{nk} - (n-1)a_{n-1,k} - \alpha_k) \right| \right), \end{aligned} \quad (3.9)$$

where the complex numbers  $\alpha_k$  are defined in (2.3).

(b) *Let  $L \in \mathcal{B}(h_d, [c_0])$ . Then we have*

$$\|L\|_\chi = \lim_{r \rightarrow \infty} \left( \sup_{m; l \geq r} \frac{1}{ld_m} \sum_{n=r}^l \left| \sum_{k=1}^m (na_{nk} - (n-1)a_{n-1,k}) \right| \right). \quad (3.10)$$

**Proof.** Let  $A = (a_{nk})_{n,k=1}^\infty$  be any infinite matrix and  $r \in \mathbb{N}$ . We write  $A^{<r>} = (a_{nk}^{<r>})_{n,k=1}^\infty$  for the matrix with the rows  $A_n^{<r>} = 0$  for  $1 \leq n \leq r$  and  $A_n^{<r>} = A_n$  for  $n \geq r+1$ .

(a) Let  $L \in (h_d, [c])$  and  $A = (a_{nk})_{n,k=1}^\infty$  be the matrix that represents  $L$ .

First we show that the limits in (3.9) exist.

Let  $x \in h_d$  be given. We write  $y_n = A_n x = L_n(x)$  for  $n = 1, 2, \dots, \eta(x)$  for the  $[c]$ -limit of the sequence  $y = (y_n)_{n=1}^\infty$  and  $\mu_r(x) = \|\mathcal{R}_r(x)\|_{[c_\infty]}$  for all  $r$ . Then we have for all  $r$

$$\begin{aligned} \mu_r(y) = \|\mathcal{R}_r(y)\|_{[c_\infty]} &= \sup_{m \geq r+1} \frac{1}{m} \sum_{n=r+1}^m |ny_n - (n+1)y_{n-1} - \eta(x)| \\ &\geq \sup_{m \geq r+2} \frac{1}{m} \sum_{n=r+2}^m |ny_n - (n+1)y_{n-1} - \eta(x)| = \|\mathcal{R}_{r+1}(y)\|_{[c_\infty]} = \mu_{r+1}(y), \end{aligned}$$

hence  $\sup_{x \in Q} \mu_r(y) \geq \sup_{x \in Q} \mu_{r+1}(y) \geq 0$  for all  $r$  and for all  $Q \in \mathcal{M}_{h_d}$ . Consequently

$$\mu(Q) = \lim_{r \rightarrow \infty} \mu_r(Q) \text{ exists for all } Q \in \mathcal{M}_{h_d}.$$

Now we define the matrix  $B = (b_{nk})_{n,k=1}^\infty$  by  $b_{nk} = a_{nk} - \alpha_k$  for all  $n$  and  $k$ , and denote the unit sphere in  $h_d$  by  $S_{h_d}$ . Since  $\eta(x) = \sum_{k=1}^\infty \alpha_k x_k$  for all  $x \in h_d$  by (2.8), it follows that  $(\mathcal{R}_r \circ L)(x) = B^{<r>}x$  for all  $x \in h_d$ , and so by (2.2) and (2.5)

$$\begin{aligned} \sup_{x \in S_{h_d}} \|\mathcal{R}_r \circ L(x)\|_{[c_\infty]} &= \|B^{<r>}\|_{(h_d, [c_\infty])} \\ &= \sup_{l, m} \frac{1}{ld_m} \sum_{n=1}^l \left| n \sum_{k=1}^m b_{nk}^{<r>} - (n-1) \sum_{k=1}^m b_{n-1,k} \right| \\ &= \sup_{m; l \geq r+1} \frac{1}{ld_m} \sum_{n=r+1}^l \left| \sum_{k=1}^m na_{nk} - (n-1)a_{n-1,k} - \alpha_k \right|. \end{aligned}$$

Finally we get (3.9) by (3.6) and by (3.3).

(b) The proof is similar to that of Part (a) with  $\alpha_k = 0$  for all  $k$  and (3.5) instead of (3.6).  $\square$

Finally the characterisations of the classes  $\mathcal{K}(h_d, [c])$  and  $\mathcal{K}(h_d, [c_0])$  are immediate consequences of (3.4) and Theorem 3.4.

**Corollary 3.5** (a) Let  $L \in \mathcal{B}(h_d, [c])$ . Then  $L \in \mathcal{K}(h_d, [c])$  if and only if

$$\lim_{r \rightarrow \infty} \left( \sup_{m; l \geq r} \frac{1}{ld_m} \sum_{n=r}^l \left| \sum_{k=1}^m (na_{nk} - (n-1)a_{n-1,k} - \alpha_k) \right| \right) = 0,$$

where the complex numbers  $\alpha_k$  are defined in (2.3).

(b) Let  $L \in \mathcal{B}(h_d, [c_0])$ . Then  $L \in \mathcal{K}(h_d, [c_0])$  if and only if

$$\lim_{r \rightarrow \infty} \left( \sup_{m; l \geq r} \frac{1}{ld_m} \sum_{n=r}^l \left| \sum_{k=1}^m na_{nk} - (n-1)a_{n-1,k} \right| \right) = 0.$$

We close with an application of our results.

*Example 3.6* We consider the Hahn space  $h = h_d$ , where  $d_k = k$  for all  $k = 1, 2, \dots$  and the Cesàro matrix  $C_1 = A = (a_{nk})_{n,k=1}^{\infty}$  of order 1, where  $a_{nk} = 1/n$  for  $1 \leq k \leq n$  and  $a_{nk} = 0$  for  $k > n$  ( $n = 1, 2, \dots$ ). Then  $L_{C_1} \in \mathcal{K}(h, [c_0])$  and  $\|L_{C_1}\| = 1$ .

**Proof.** We write

$$\begin{aligned} \sigma_{lm} &= \sum_{n=1}^m \left| \sum_{k=1}^n na_{nk} - (n-1)a_{n-1,k} \right|, \\ \tau_{lm} &= \sum_{n=m+1}^l \left| \sum_{k=1}^m na_{nk} - (n-1)a_{n-1,k} \right| \end{aligned}$$

and

$$s_{lm} = \frac{1}{lm} \sum_{n=1}^l \left| \sum_{k=1}^m na_{nk} - (n-1)a_{n-1,k} \right| \text{ for all } l \text{ and } m.$$

Then  $s_{lm} = (1/lm)(\sigma_{lm} + \tau_{lm})$  for all  $m$  and  $l$ .

We obtain

$$\sigma_{lm} = \sum_{n=1}^m \left| \sum_{k=1}^n na_{nk} - (n-1)a_{n-1,k} \right| = m,$$

and

$$\tau_{lm} = \begin{cases} 0 & (l \leq m) \\ \sum_{n=m+1}^l \left| \sum_{k=1}^m na_{nk} - (n-1)a_{n-1,k} \right| = 0 & (l \geq m+1), \end{cases}$$

hence  $s_{lm} = (1/l)$  for all  $l$  and  $m$ . So  $\sup_{lm} s_{lm} = 1$ , that is,  $L_{C_1} \in \mathcal{B}(h_d, [c_\infty])$  and  $\|L_{C_1}\| = 1$  by Theorem 2.4 (a) and (d). Also, for each fixed  $k$ ,

$$0 \leq \frac{1}{l} \sum_{n=1}^l |na_{nk} - (n-1)a_{n-1,k}| = \frac{1}{l} \sum_{n=k}^l |na_{nk} - (n-1)a_{n-1,k}| \frac{1}{l} \rightarrow 0 \quad (l \rightarrow \infty),$$

and this and  $L_{C_1} \in \mathcal{B}(h_d, [c_\infty])$  together imply  $L_{C_1} \in \mathcal{B}(h_d, [c_0])$  by Theorem 2.4 (c).

Finally, we write for all  $l \geq r$ ,  $m$  and  $r$

$$\begin{aligned} s_{lm}^{(r)} &= \frac{1}{lm} \sum_{n=r}^l \left| \sum_{k=1}^m na_{nk} - (n-1)a_{n-1,k} \right| \\ &= \frac{1}{lm} \left( \sum_{n=r}^m \left| \sum_{k=1}^n na_{nk} - (n-1)a_{n-1,k} \right| + \sum_{n=m+1}^l \left| \sum_{k=1}^m na_{nk} - (n-1)a_{n-1,k} \right| \right) \\ &= \frac{1}{lm} (m-r+1) \leq \frac{1}{l}, \end{aligned}$$

hence

$$\sup_{m;l \geq r} s_{lm}^{(r)} \leq \frac{1}{r},$$

and so

$$\lim_{r \rightarrow \infty} \sup_{m;l \geq r} s_{lm}^{(r)} = 0.$$

Consequently we have  $L_{C_1} \in \mathcal{K}(h, [c_0])$  by Corollary 3.5 (b). □

## 4. Conclusion

The paper adds new results in recent research concerning the studies of bounded linear and compact operators between  $BK$  spaces. In particular, the main results are Theorems 2.4, 2.5, 3.4 and Corollary 3.5. Theorem 2.4 establishes the characterisations of the classes  $\mathcal{B}(h_d, Y)$  for  $Y \in \{[c]_0, [c], [c]_\infty\}$  by necessary and sufficient conditions on the entries of the infinite matrices  $A$  that represent these operators; furthermore it contains a formula for the corresponding operator norms. Theorem 2.5 gives a formula for the  $[c]$ -limit of  $L(x)$ , when  $L \in \mathcal{B}(h_d, [c])$ . Theorem 3.4 establishes an identity and an estimate for the Hausdorff measures  $\|L\|_\chi$  of  $L \in \mathcal{B}(h_d, [c]_0)$  and  $L \in \mathcal{B}(h_d, [c])$ , respectively, in terms of the entries of the infinite matrices  $A$  that represent  $L$ . Corollary 3.5 yields the characterisations of the compact operators in the classes  $\mathcal{B}(h_d, [c]_0)$  and  $L \in \mathcal{B}(h_d, [c])$ . Finally, the results of the paper are applied in Example 3.5 to obtain that the operator  $C_1 : h_d \rightarrow [c]_0$  of the arithmetic means is compact.

Suggestions for further research would be the characterisations of the dual classes  $(Y, h_d)$  for  $Y \in \{[c]_0, [c], [c]_\infty\}$ , and their subclasses of compact matrix operators, and possible extensions of the results, when  $Y$  is generalised to  $Y_p \in \{[c]_0^p, [c]^p, [c]_\infty^p\}$  ( $1 \leq p < \infty$ ); here the spaces  $Y_p$  obtained by replacing the modulus  $|\cdot|$  in the definition the sets in  $Y$  by  $|\cdot|^p$ .

## Author statement

The author confirms sole responsibility for the writing, interpretation of results and editing of the manuscript.

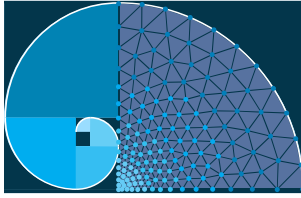
## Conflict of Interest

The author declares no conflict of interest.

## References

- Boos, J. (2000). *Classical and Modern Methods in Summability*. Oxford University Press, Oxford.
- Borwein, D. (1960). On strong and absolute summability. *Proc. Glasgow Math. Assoc.*, 4:122–139.
- Das, R. (2017). On the fine spectrum of the lower triangular matrix  $B(r; s)$  over the Hahn sequence space. *Kyungpook Math. J.*, 57:441–455.
- de Malafosse, B., Malkowsky, E., and Rakočević, V. (2021). *Operators Between Sequence Spaces and Applications*. Springer Nature Singapore, 152 Beach Road, #21 – 01/04 Gateway East, Singapore 18972, Singapore.
- Djoločić, I. and Malkowsky, E. (2012). On matrix mappings into some strong Cesàro sequence spaces. *Appl. Math. Comput.*, 218:6155–6163.
- Djoločić, I. and Malkowsky, E. (2013). Banach algebras of matrix transformations between some sequence spaces related to  $\Lambda$ -strong convergence and boundedness. *Appl. Math. Comput.*, 219:8779–8789.
- Goes, G. (1972). Sequences of bounded variation and sequences of Fourier coefficients II. *JMAA*, 39:477–494.
- Hahn, H. (1922). Über Folgen linearer Operationen. *Monatsh. Math. Phys.*, 32:3–88.
- Jarrah, A. M. and Malkowsky, E. (2002). Linear operators between some matrix domains. *Rend. Circ. di Mat. Palermo, Ser II* 68:641–655.
- Jarrah, A. M. and Malkowsky, E. (2003). Ordinary, absolute and strong summability and matrix transformations. *Filomat*, 17:59–78.
- Kamthan, P. K. and Gupta, M. (1981). *Sequence Spaces and Series*. Marcel Dekker, New York.
- Kirişci, M. (2013a). The Hahn sequence space defined by the Cesàro mean. *Abstr. Appl. Anal.*, 2013. Article ID 817659, 6 pages.
- Kirişci, M. (2013b). A survey of the Hahn sequence space. *Gen. Math. Notes*, 19(2):37–58.
- Kuttner, B. and Thorpe, B. (1979). Strong convergence. *J. Reine Angew. Math.*, 311/312:42–55.
- Malkowsky, E. (1995). The continuous duals of the spaces  $c_0(\Lambda)$  and  $c(\Lambda)$  for exponentially bounded sequences. *Acta Sci. Math. (Szeged)*, 61:241–250.
- Malkowsky, E. (2000). The dual spaces of the sets of  $\Lambda$ -strongly bounded sequences. *Novi Sad J. Math.*, 30(3):99–110.
- Malkowsky, E. (2013). Characterization of compact operators between certain  $BK$  spaces. *Filomat*, 27(3):447–457.
- Malkowsky, E. (2017). On strong summability and convergence. *Filomat*, 31(11):3095–3123.

- Malkowsky, E. and Nergiz, H. (2015). Matrix transformations and compact operators on spaces of strongly Cesàro summable and bounded sequences of order  $\alpha$ . *CAAM Contemporary Analysis and Applied Mathematics*, 3(263–279).
- Malkowsky, E. and Rakočević, V. (1998). The measure of noncompactness of linear operators between certain sequence spaces. *Acta Sci. Math. (Szeged)*, 64:151–170.
- Malkowsky, E. and Rakočević, V. (2000). *An Introduction into the Theory of Sequence Spaces and Measures of Noncompactness*, volume 9(17) of *Zbornik radova, Matematički institut SANU*, pages 143–234. Mathematical Institute of SANU, Belgrade.
- Malkowsky, E. and Rakočević, V. (2019). *Advanced Functional Analysis*. CRC Press, Taylor & Francis Group, Boca Raton, London, New York.
- Malkowsky, E., Rakočević, V., and Tuđ, O. (2021). Compact operators on the Hahn space. *Monatsh. Math.*, pages <https://doi.org/10.1007/s00605-021-01588-8>.
- Mòricz, F. (1989). On  $\Lambda$ -strong convergence of numerical sequences and Fourier series. *Acta Math. Hung.*, 54:319–327.
- Mursaleen, M. and Noman, A. K. (2010). Compactness by the Hausdorff measure of noncompactness. *Nonlinear Anal.*, 73:2541–2557.
- Mursaleen, M. and Noman, A. K. (2011). The Hausdorff measure of noncompactness of matrix operators on some *BK* spaces. *Oper. Matrices*, 5(3):473–486.
- Raj, K. and Kiliçman, A. (2014). On generalized difference Hahn sequence spaces. *Hindawi Publishing Corporation, The Scientific World Journal Volume 2014*, 2014. Article ID 398203, 7 pages.
- Rao, K. C. (1990). The Hahn sequence space. *Bull. Cal. Math. Soc.*, 82:72–78.
- Rao, K. C. and Srinivasalu, T. G. (1996). The Hahn sequence space–II. *Y. Y. U. Journal of Faculty of Education*, 1(2):43–45.
- Rao, K. C. and Subramanian, N. (2002). The Hahn sequence space–III. *Bull. Malaysian Math. Sc. Soc. (Second Series)*, 25:163–171.
- Ruckle, W. H. (1981). *Sequence Spaces*. Pitman, Boston, London, Melbourne. Research Notes in Mathematics 49.
- Toledano, J. M. A., Benavides, T. D., and Acedo, G. L. (1997). *Measures of Noncompactness in Metric Fixed Point Theory*, volume 99 of *Operator Theory Advances and Applications*. Birkhäuser Verlag, Basel, Boston, Berlin.
- Wilansky, A. (1984). *Summability through Functional Analysis*, volume 85. North-Holland, Amsterdam. Mathematical Studies.
- Zeller, K. and Beekmann, W. (1968). *Theorie der Limitierungsverfahren*. Springer Verlag, Heidelberg, Berlin, New York.



# Watt Six-Bar Compliant Mechanism Analysis Based on Kinematic and Dynamic Responses

Çağlar Uyulan<sup>1,\*</sup>, Batuhan İpek<sup>2</sup>

<sup>1</sup> Dept. of Mechatronics Eng., Bülent Ecevit University, Zonguldak, Turkey

<sup>2</sup> Dept. of Mech. Eng., Bülent Ecevit University, Zonguldak, Turkey

\*Corresponding author: caglaruyulan1@gmail.com

Received: 30.04.2021

Accepted: 09.06.2021

## Abstract

In this study, a complete guide to kinematic and kinetic analyses of a Watt type six-bar compliant mechanism is conducted incorporating the flexible buckling of the initially straight element. In the analysis procedure, the hybrid utilization of the pseudo-rigid-body model (PRBM) and the nonlinear elastic theory of beam buckling is presented. This partially compliant mechanism comprises three rigid links and two flexible links. The kinematic analyses of the mechanisms are done by using the vector loop closure equations, the PRBM of a large deflection cantilever beam, and derivation of nonlinear algebraic equations considering the quasi-static equilibrium and load-deflection curve of the flexible parts. Each of the elastic parts makes up a buckling pinned-pinned flexible Euler beam. The vector loop equations are combined with Newton-Euler dynamic formulations to provide the simultaneous constraint matrix. After these operations, the full mechanism is simulated to get both accelerations and forces for each time step. Finally, the design method is validated through experimental results. The findings derived from the combination of buckling elastica solution and PRBM approach enable the analysis of Watt's six-bar compliant mechanism.

**Keywords:** Compliant mechanism; pseudo-rigid-body model; large-deflection analysis; elastica theory; Watt type mechanism

## 1. Introduction

Compliant mechanisms consist of elastic elements that are used to accomplish the desired motion, and compliant mechanisms can have rigid links and flexible links. compliant mechanisms gain their mobility due to the constrained bending of flexible parts from simple topologies (Howell et al., 2013). In compliant mechanisms, force is transferred to other mechanism parts by making use of elastic deformation. The elastic links produce partially or completely the motion of a mechanism (Midha et al., 2000). The popularity of the compliant mechanisms has been increasing during the last decade, because of their superiority and suitability in the micro-electromechanical system (MEMS) design & micro-and nano-fabrication. It is relatively easy to manufacture a compliant mechanism using an injection molding method (Her and Midha, 1987). There are many advantages of compliant mechanisms as compared to rigid-body mechanisms. Integrated functions, high reliability,

high precision, repeatability, and backlash-free motion, reduced and simplified manufacturing processes, and necessitating fewer parts can also be counted. Therefore, they are suitable to be applied in micro-machining (Khosraviani and Leung, 2012).

They also have some significant challenges. The compliant revolute joints can exhibit small displacements, their mobility is restricted, and cannot sustain continuous rotation. Fatigue failure is observed at the elastic joints. The elastic potential energy is stored due to the deflection of flexible membranes in the compliant mechanism. The strain energy that is stored, is distributed to the entire body and released energy can be used for the desired purpose as a deflection feature. Compliant mechanism performance is affected by material properties, and factors such as thermal and structural loads, and various environment-induced effects (Howell and Midha, 1994).

The compliant mechanisms contribute to many disciplines for countless and versatile engineering solutions (i.e. artificial spinal disc, compliant centrifugal clutch, compliant suspension element, digital micromirrors, piezoresistive pressure sensors). The analysis of the compliant mechanism is quite difficult with large nonlinear elastic deflections with reasonable off-axis stiffness of its flexible elements exist. Their kinematic responses exhibit unique characteristics as compared to the quasi-static response. In synthesizing the compliant mechanisms, the simulation of the mechanism is validated experimentally investigating the complexity of the dynamic relations (Lefebvre et al., 2005; Luo, 2006; Wang and Chen, 2009). The function and structure of mechanisms have been investigated in many studies (Wang et al., 2014; Pieber and Gerstmayr, 2020; Nikham and Farhang, 2018). A method for assisting the design of flexure-based compliant mechanisms for dimensional synthesis, an optimization procedure, and experimental validation has been presented in (Berselli et al., 2015). The mobility of the compliant mechanism was analyzed under the influence of the geometry, material type, and different compliant joints (Pavlovic and Pavlovic, 2005). Realizable joint integration into elastically movable structures for motion tasks was investigated in (Ghosh and Corves, 2015).

Some papers have explained the influence of geometry and material properties on the compliant mechanisms (Gouker et al., 2006; Linß et al., 2019; Jovanova and Frecker, 2017; Venkiteswaran and Su, 2016). Topology optimization technique to design distributed compliant mechanisms was studied in (Zhang and Zhu, 2018). A comparative study for the synthesis of the design variables of the flexible slider-crank mechanism between PSO and GA was presented (Khemili et al., 2018). The theory of the curves generated in six-link motion has been described (Primrose et al., 1967a; Primrose et al., 1967b). Six-link mechanisms have been used in many applications (i.e., sewing machine (Eren and Aydemir, 2004), prosthetic limbs (Gezgin et al., 2016), legged and jumping robot (Zhang et al., 2020), wheel-track mobile robot (Luo et al., 2018), micro-aerial-vehicle design (Prosser et al., 2011). Design, kinematic synthesis, path, and motion generation with the six-bar linkage mechanism have been investigated in many papers (Chen and Tzeng, 2006; Chen and Huang, 2005; Yi and Leinonen, 2003; Plecnik and McCarthy, 2014; Zu and Wei, 2013; Mirth and Chase, 1993). A mathematical model of a six-bar linkage parametric design investigated an auto-feeding soup machine. The motion of the mechanism is simulated in ADAMS. The design parameters were also optimized to get a smooth predetermined trajectory, high movement precision, and the smallest extreme acceleration of the soup ladle in motion (Xi et al., 2010).

In another paper, the automated type synthesis of planar mechanisms and multi-body systems were developed by including topology as a design variable in a GA-based methodology. It is possible to design mechanisms that closely match the pre-described kinematic conditions by fusing the GA with a multi-body analysis program (Liu and Mecphee, 2004). A procedure for

the kinematic synthesis and analysis of a Watt I six-bar linkage was presented to apply in the vehicle suspension design. This approach degrades to the task-based synthesis of a Watt I six-bar where both ground pivots and end effector pivots are particularized (Plecnik et al., 2014). The kinematic performance of the six-bar mechanism used in the prosthetic knee was investigated through the optimization method and the advantages of the six-bar linkage over the four-bar linkage to better achieve the expected trajectory of the ankle joint in the swing phase was revealed (Jin et al., 2003; Bapat and Sujatha, 2017). A software system for the synthesis of spherical Watt I six-bar linkages based on constraining 3R open chain with randomized search in tolerance zones was designed by using SolidWorks Add-In MechGen (Sonawale et al., 2013). The design method of six-bar linkages that reach an over-specified set of task positions explained in (Tsuge and McCarthy, 2014) expands the number of candidate linkages that approximate an over-specified task. A method of optimization of structural error in a closed kinematic chain of four-bar planar mechanism with six design parameters using the Chebyshev-Freudstein method was applied to increase the global accuracy in the mechanism (Aiswal and Jawale, 2018). In another paper (Mirth, 2012), the GCP to the synthesis of six-bar planar linkages was investigated.

The primary focus of this paper is to design, synthesize and analyze a Watt six-bar compliant mechanism that exploits buckling of pinned-pinned beam elements and large deformed nonlinear beams. Although buckling is usually an unwanted phenomenon, the flexibility of linkages is very useful in applications. Investigating the buckling event can strengthen the compliant mechanism of design space by enabling the flexibility itself for versatile aims. For this purpose, the quasi-static simulation and experimentally validated simulation of the Watt six-bar compliant mechanism response is conducted. Modelling of these mechanisms contributes wide information in several areas, which comprises kinematics, compliant mechanisms, and nonlinear analysis. The sensitivity of the joint clearances and friction are omitted in this paper. The context and content of this paper are as follows. In Section 2.1., a conceptual basis of theories including the theory of elastica and the large-deflection analysis of the cantilever beam is represented by explaining the elliptic integral formulations and polynomial curve fitting application. In Section 2.2., the formulation of the Watt six-bar compliant mechanism, which comprises the vector loop closure method, kinematic analysis, and PRBM, is stated. In Section 2.3., the procedures of the dynamic simulations are investigated considering the simultaneous constraint method and quasi-static analysis, respectively. In Section 3, the simulation and experimental results are presented. The concluding remarks and discussions are given in Section 4.

## 2. Experimental Methods

### 2.1. The Theoretical Basis

Elastica theory predicts the movement of the large deflecting beams incorporated in the compliant mechanisms and is utilized in compliant mechanism design and synthesis (Howell and Midha, 1994; Konopasek, 1980). Jacob Bernoulli has pioneered the large-deflection-based analysis by proposing the proportional relation between the beam curvature at any point and bending moment, and Euler solved elastica problems in a closed-form. The main restriction is that it is only valid for simple geometries and simple loading conditions. The large deflection equations of the pinned-pinned buckling mounted to a slider can be stated in normalized form as in Eq. (1) (Sönmez and Tutum, 2008; Sönmez, 2000).

$$\begin{aligned}
 &-(p^2 + q^2)^{0.25} \pm 2F(\chi, \varphi) = 0 \\
 &-w(p^2 + q^2)^{0.75} \pm p(4E(\chi, \varphi) - 2F(\chi, \varphi)) = 0 \\
 &-h(p^2 + q^2)^{0.75} \pm q(4E(\chi, \varphi) - 2F(\chi, \varphi)) = 0,
 \end{aligned}
 \tag{1}$$

where  $p = \frac{PL^2}{EI}$  is the normalized load and  $q = \frac{QL^2}{EI}$  is the normalized deflection.  $P$  is the horizontal force,  $Q$  is the vertical reaction force applied on the beam by the slider.  $w = \frac{W}{L}$ ,  $h = \frac{H}{L}$  are normalized flexible beam horizontal displacement and vertical offset, respectively.  $L$  is the length of the compliant beam.

In Eq. (1),  $F(\chi, \varphi)$  and  $E(\chi, \varphi)$  are completely first and second kind of elliptic integrals, respectively.  $\varphi = \frac{\pi}{2}$  and  $\chi$  are the amplitude and the modulus. The formulation is represented in Eq. (2):

$$\begin{aligned}
 F(\chi, \varphi) &= \int_0^\varphi \frac{d\varphi}{\sqrt{1-\chi^2\sin^2(\varphi)}} \\
 E(\chi, \varphi) &= \int_0^\varphi \sqrt{1-\chi^2\sin^2(\varphi)}d\varphi
 \end{aligned}
 \tag{2}$$

Equation (2) is solved to evaluate the nonlinear load-deflection behaviour of a pinned-pinned beam subjected to a horizontal load. The forces exerted to a simple pinned-pinned section are collinear along the line among the two-pin joints and the deflections are also along this line. The moments are not carried by pin ends. A nonlinear spring defined with a polynomial load-deflection equation defines the pin-pin segment model.

To conduct the large deflection analysis, assume an initially straight cantilever beam subjected to an end force having a vertical force component ( $Q$ ) along the positive y-axis and a horizontal force component ( $nQ$ ) along the negative x-axis, as demonstrated in Figure 1.

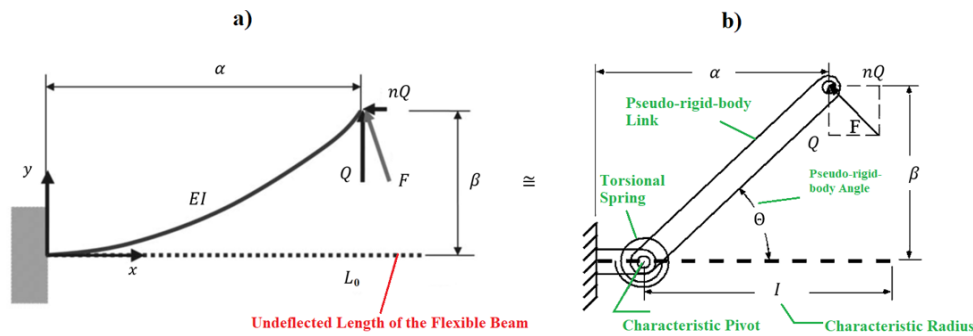


**Figure 1.** The demonstration of the large deflecting cantilever beam subjected a force at the free end; a) fixed-pinned segment, b) its equivalent pseudo-rigid-body model.

The parameter  $n$  is the force coefficient, which implies the proportion of the horizontal force to the vertical force, and positive if the beam is compressed. The parameters presented in Figure 1 are also modelled considering elliptic integrals in Eq. (3). The reader should refer to (Zhang and Chen, 2012; Bishopp and Drucker, 1945), or (Sönmez and Tutum, 2008) for their derivation.

$$\alpha = \frac{1}{\sqrt{\eta}}(F(t, \varphi) - F(\gamma, t)) \text{ for } \theta_0 < \varphi_1$$

$$\frac{\alpha}{l} = \frac{1}{\varpi\eta^{5/2}} [-n\eta((F(t, \varphi) - F(\gamma, t) + 2E(\gamma, t) - 2E(t, \varphi)) + \sqrt{2\eta(\eta + \lambda)}\cos(\gamma))]$$

$$\frac{\beta}{l} = \frac{1}{\varpi\eta^{5/2}} [\eta(F(t, \varphi) - F(\gamma, t) + 2E(\gamma, t) - 2E(t, \varphi)) + n\sqrt{2\eta(\eta + \lambda)}\cos(\gamma)]$$

$$\eta = \sqrt{1 + n^2}, \quad \gamma = \arcsin\left(\sqrt{\frac{\eta - n}{\eta + \lambda}}\right), \quad t = \sqrt{\frac{\eta + \lambda}{2\eta}}, \quad (3)$$

where  $\alpha$  is the horizontal position,  $\beta$  is the vertical deflection of the tip of the beam,  $\lambda = \sin(\theta_0) - n\cos(\theta_0)$  is an end angle related parameter,  $\theta_0$  is the deflected beam end angle, and  $\varphi_1 = \arctan\left(\frac{1}{n}\right)$  is the exerted load angle accepted positive from the  $x$ -axis.  $\varpi = \frac{QL_0^2}{EI}$  is the corresponding loading parameter. The exact elastica solution of the flexible beams and its trajectories are used for the kineostatic analysis simulation results.

### 2.2. Formulation of Watt Six-Bar Compliant Mechanism

The concept of the vector closed-loop equation (or loop closure equation) is presented in Figure 2.

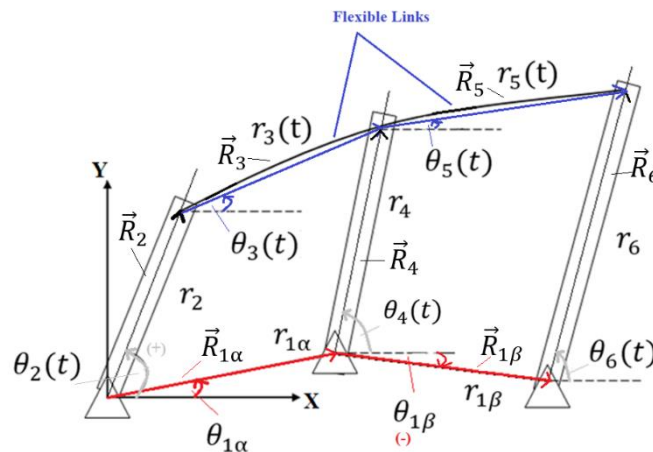


**Figure 2.** Parameterization of the dimensions and conceptualization of vector loop closure. Note that the angles of the vectors (measured from the positive  $x$ -axis to the vector at its tail) are the same as the corresponding link angle. The angles are defined as counterclockwise positive from the positive  $x$ -direction and drawn to the tail of each vector.

As seen in Figure 2, arbitrary coordinates are assigned at the ground joint, which is the leftmost in the figure. Each link (including the ground links) is represented by a displacement vector. The closed-loop vector equations are stated in Eq. (4):

$$\vec{R}_2 + \vec{R}_3 = \vec{R}_{1\alpha} + \vec{R}_4$$

$$\vec{R}_4 + \vec{R}_5 = \vec{R}_{1\beta} + \vec{R}_6 \quad (4)$$

The vector loop equation is a very compact expression of the constraints that exist between the various bodies of mechanism. The displacement achieved when vectors at the LHS of the equation are added is the same as that achieved when vectors at the RHS of the equation are added. This vector loop equation must be satisfied by the mechanism, regardless of the pose,

it takes, as long as it remains assembled as a mechanism. Eq. (5) is obtained by summing independently the horizontal (x-direction) and vertical (y-direction) vector components.

$$\begin{aligned}
 r_2 \cos(\theta_2(t)) + r_3(t) \cos(\theta_3(t)) &= r_{1\alpha} \cos(\theta_{1\alpha}) + r_4 \cos(\theta_4(t)) \\
 r_2 \sin(\theta_2(t)) + r_3(t) \sin(\theta_3(t)) &= r_{1\alpha} \sin(\theta_{1\alpha}) + r_4 \sin(\theta_4(t)) \\
 r_4 \cos(\theta_4(t)) + r_5(t) \cos(\theta_5(t)) &= r_{1\beta} \cos(\theta_{1\beta}) + r_6 \cos(\theta_6(t)) \\
 r_4 \sin(\theta_4(t)) + r_5(t) \sin(\theta_5(t)) &= r_{1\beta} \sin(\theta_{1\beta}) + r_6 \sin(\theta_6(t)) \quad (5)
 \end{aligned}$$

The derived vector loop equations are compact, elegant expressions of the simple fact the various links of the mechanism are constrained in some manner. The evaluations of the link velocities and accelerations can be obtained by taking the first and second derivatives w.r.t time of the Eq. (5), respectively. The vectors are time-varying and their orientation (vector direction) changes as the mechanism moves. Due to the flexible structure of the link-3 and link-5, their magnitude of link lengths also changes while the other link lengths (link-2, link-4, link-6) remain constant. There are seven link angles, two of which ( $\theta_{1\alpha}, \theta_{1\beta}$ ) can be taken to be constant. The other five angles are time-varying, and that must be taken into account when taking the derivatives. Eq. (6), which specifies the relationship among the rotational rates of the moving links as long as the mechanism remains assembled.

$$\begin{aligned}
 r_2 \dot{\theta}_2(t) \sin(\theta_2(t)) + r_3(t) \dot{\theta}_3(t) \sin(\theta_3(t)) - \dot{r}_3(t) \cos(\theta_3(t)) &= r_4 \dot{\theta}_4(t) \sin(\theta_4(t)) \\
 r_2 \dot{\theta}_2(t) \cos(\theta_2(t)) + \dot{r}_3(t) \sin(\theta_3(t)) + r_3(t) \dot{\theta}_3(t) \cos(\theta_3(t)) &= r_4 \dot{\theta}_4(t) \cos(\theta_4(t)) \\
 r_4 \dot{\theta}_4(t) \sin(\theta_4(t)) + r_5(t) \dot{\theta}_5(t) \sin(\theta_5(t)) - \dot{r}_5(t) \cos(\theta_5(t)) &= r_6 \dot{\theta}_6(t) \sin(\theta_6(t)) \\
 r_4 \dot{\theta}_4(t) \cos(\theta_4(t)) + \dot{r}_5(t) \sin(\theta_5(t)) + r_5(t) \dot{\theta}_5(t) \cos(\theta_5(t)) &= r_6 \dot{\theta}_6(t) \cos(\theta_6(t)) \quad (6)
 \end{aligned}$$

Link-2 is attached to a large DC motor that is capable of providing enough torque. Under this condition,  $\dot{\theta}_2(t)$  is the input to the mechanism. The second derivative of the loop equation is obtained in Eq. (7):

$$\begin{aligned}
 &\ddot{r}_3(t) \cos(\theta_3(t)) + r_4 \dot{\theta}_4(t)^2 \cos(\theta_4(t)) + r_4 \ddot{\theta}_4(t) \sin(\theta_4(t)) \\
 &= 2\dot{r}_3(t) \dot{\theta}_3(t) \sin(\theta_3(t)) + r_2 \dot{\theta}_2(t)^2 \cos(\theta_2(t)) + r_2 \ddot{\theta}_2(t) \sin(\theta_2(t)) \\
 &\quad + r_3(t) \dot{\theta}_3(t)^2 \cos(\theta_3(t)) + r_3(t) \ddot{\theta}_3(t) \sin(\theta_3(t)) \\
 &\quad \ddot{r}_3(t) \sin(\theta_3(t)) + 2\dot{r}_3(t) \dot{\theta}_3(t) \cos(\theta_3(t)) + r_4 \dot{\theta}_4(t)^2 \sin(\theta_4(t)) \\
 &\quad + r_2 \ddot{\theta}_2(t) \cos(\theta_2(t)) + r_3(t) \ddot{\theta}_3(t) \cos(\theta_3(t)) \\
 &= r_2 \dot{\theta}_2(t)^2 \sin(\theta_2(t)) + r_4 \ddot{\theta}_4(t) \cos(\theta_4(t)) + r_3(t) \dot{\theta}_3(t)^2 \sin(\theta_3(t)) \\
 &\quad \ddot{r}_5(t) \cos(\theta_5(t)) + r_6 \dot{\theta}_6(t)^2 \cos(\theta_6(t)) + r_6 \ddot{\theta}_6(t) \sin(\theta_6(t)) \\
 &= 2\dot{r}_5(t) \dot{\theta}_5(t) \sin(\theta_5(t)) + r_4 \dot{\theta}_4(t)^2 \cos(\theta_4(t)) + r_4 \ddot{\theta}_4(t) \sin(\theta_4(t)) \\
 &\quad + r_5(t) \dot{\theta}_5(t)^2 \cos(\theta_5(t)) + r_5(t) \ddot{\theta}_5(t) \sin(\theta_5(t)) \\
 &\quad \dot{\theta}_5(t) \sin(\theta_5(t)) + 2\dot{r}_5(t) \dot{\theta}_5(t) \cos(\theta_5(t)) + r_6 \dot{\theta}_6(t)^2 \sin(\theta_6(t)) \\
 &\quad + r_4 \ddot{\theta}_4(t) \cos(\theta_4(t)) + r_5(t) \ddot{\theta}_5(t) \cos(\theta_5(t)) \\
 &= r_4 \dot{\theta}_4(t)^2 \sin(\theta_4(t)) + r_6 \dot{\theta}_6(t) \cos(\theta_6(t)) + r_5(t) \dot{\theta}_5(t)^2 \sin(\theta_5(t)) \quad (7)
 \end{aligned}$$

PRBM concept analyses large beam deflections as rigid links with pin joints and torsional springs. PRBM's have been classified based on various types of compliant segments (i.e. small-

length flexural pivots, fixed-pinned segments, fixed-guided parts, binary pinned-pinned components, functionally binary pinned-pinned segments). PRBM simplifies the nonlinear analysis of the flexible beam elements by reducing the exact solution time while keeping the accuracy high. The reduced-order approach is essential for optimization and control. The PRBM consists of a rigid-body mechanism tracking trajectory with the tip of the original flexible beam and a nonlinear spring, which gives the same angular deflection (Yu et al., 2018; Ramirez and Lusk, 2011; Luo et al., 2015).

The deflections can be modelled by two rigid links pinned at the centre of the circular path. Pivot location is defined by the nondimensional “characteristic radius factor ( $\gamma$  – Figure 1). The length of the pseudo-rigid link is  $r_i = L_i + \varepsilon l_i = \gamma l_i$ , where  $l_i$  is the flexible segment length (“characteristic radius-Figure 1”) and  $L_i$  is the length of the rigid part. Flexible beam deflections are obtained as  $\alpha = l_i(1 - \gamma) \cos(\Theta)$ ,  $\beta = l_i \gamma \sin(\Theta)$ .

Deflection resistance is modelled by a torsional spring with a torsional spring constant as in Eq. (8):

$$K_i = \gamma K_{\Theta,i} \frac{EI_i}{l_i} \quad (8)$$

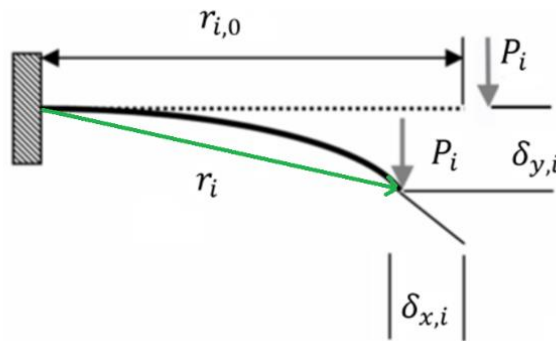


**Figure 3.** Cantilever beam subject to an end load.

Formulas used for nonlinear large deflections of pinned-pinned flexible link depicted in Figure 3 are stated as in Eq. (9):

$$\begin{aligned} \vartheta_i(t) &= \delta_{y,i}(t)r_{i,0} = (r_{i,0} - r_i(t)) \\ I_{ci} &= \frac{1}{12} h_{f,i}(b_{f,i})^3 \\ F_i(t) &= \frac{EI_i}{(r_{i,0})^2} P_i(t), \end{aligned} \quad (9)$$

where  $\delta_{y,i}$  and  $P_i$  are normalized deflection and load matrix, respectively.

The forces produced by flexible links are modelled using 4<sup>th</sup> order polynomial functions derived from nonlinear inextensible exact elastic theory.  $F_i(t)$  can be approximated with a 4<sup>th</sup> order polynomial function of deflection given in Eq. (10):

$$F_i(t) = K_{i,5}(\vartheta_i(t))^4 + K_{i,4}(\vartheta_i(t))^3 + K_{i,3}(\vartheta_i(t))^2 + K_{i,2}\vartheta_i(t) + K_{i,1} \quad (10)$$

The force-deflection curve of the flexible joints are plotted in Figure 4.

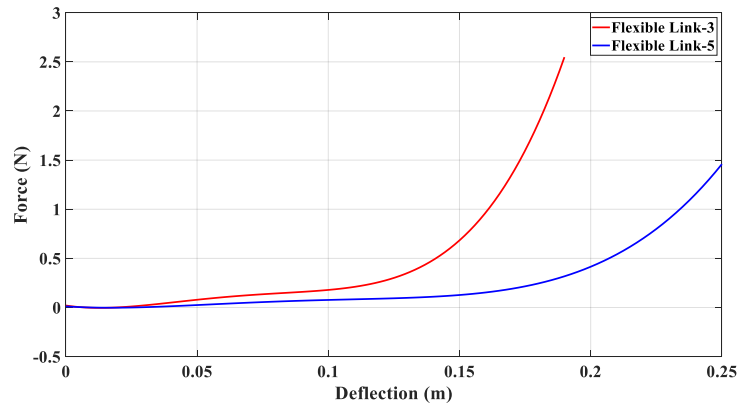


**Figure 4.** The force-deflection curves of the flexible joints. the pin-pin beam buckling; derived from the solution of the exact elastica.

The coefficients of the polynomial function are evaluated from the flexible links force-deflection curve through the curve fitting algorithm. The values of the coefficients are presented in Table 1.

**Table 1.** Curve-fitted coefficients of the flexible joints.

$K_{3,5}$	9673
$K_{3,4}$	-2418
$K_{3,3}$	201.7
$K_{3,2}$	-4.078
$K_{3,1}$	0.02046
$K_{5,5}$	1864
$K_{5,4}$	-613.1
$K_{5,3}$	67.09
$K_{5,2}$	-1.79
$K_{5,1}$	0.01182

### 2.3. Dynamic Simulation via Simultaneous Constraint Method

The simultaneous constraint method builds on the kinematic relationships described in this section. The second derivatives of the loop equation are obtained. Then, simple force balances are applied to each link to relate the forces on each link to its acceleration. Next, an approach similar to the vector loop methodology yields additional information on the link acceleration of the centre of mass. The equations are combined into a sparse matrix that can be evaluated through MATLAB/SIMULINK as a component of a full simulation. The free-body diagrams (FBD's) of the components of the Watt six-bar compliant mechanism drawn in Solidworks are represented in Figure 5.

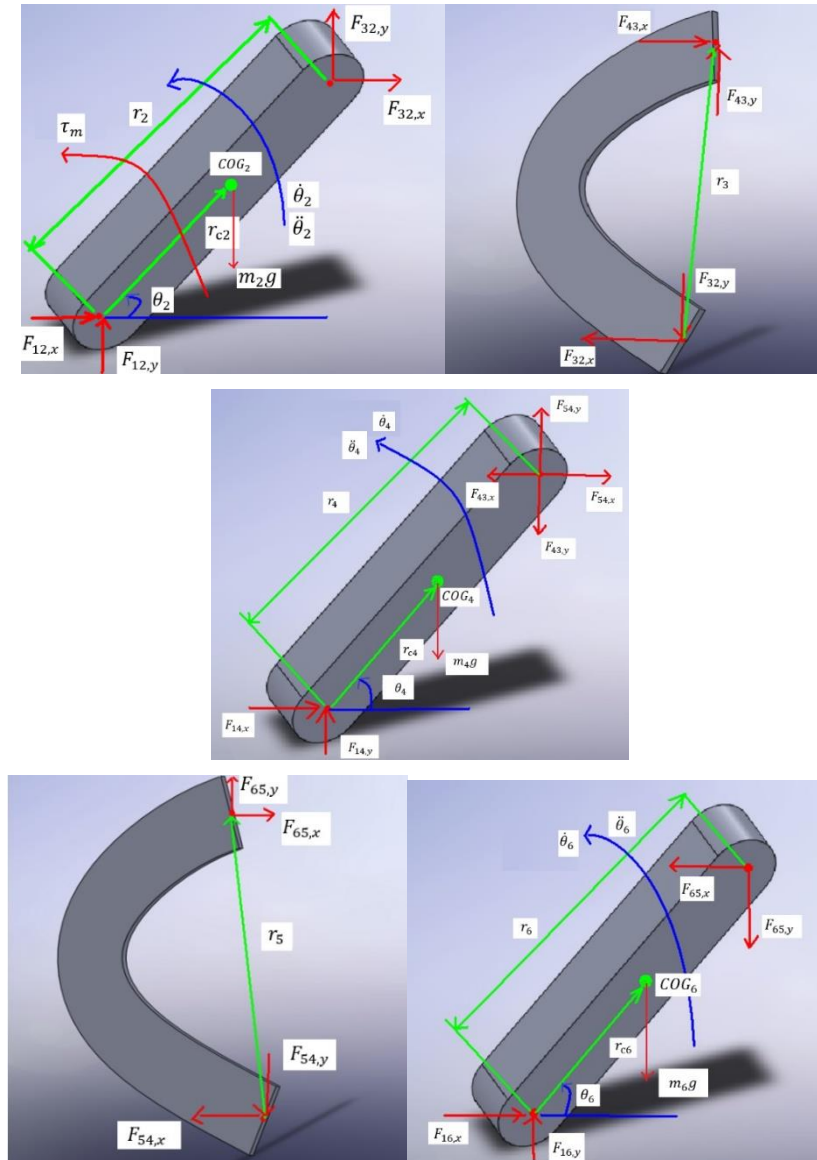


Figure 5. FBD's of link-2, link-3, link-4, link-5, link-6, respectively.

### 2.3.1. Dynamic Equations

Each joint can sustain only a force and that the forces are broken down into x-and y-components. In general,  $\vec{F}_{ij}$  will be for the force exerting on the link  $j$ , originating from the link  $i$ . An essential point here is that  $\vec{F}_{ji}$  is equal and opposite  $\vec{F}_{ij}$ . Force equations are the result of Newton's Second Law, applied to the links.

The equations of motion (EOM) for the  $i^{th}$  link can be written as in Eq. (11).

$$\begin{aligned}
 F_{ji,x} + F_{ki,x} &= m_i a_{ci,x} \\
 F_{ji,y} + F_{ki,y} - m_i g &= m_i a_{ci,y},
 \end{aligned}
 \tag{11}$$

where the acceleration terms ( $a_{ci,x}, a_{ci,y}$ ) are the x- and y-projections of the acceleration of the centre of mass of the link. Those accelerations are hidden in the vector loop equations for the entire mechanism. For each link, another position vector equation should be derived that maps the acceleration of the COG of each link to the other state variables.

The vector relationships to derive the acceleration of the centre of mass of links are given in Eq. (12):

$$\begin{aligned}
 a_{c2,x}(t) &= -r_{c2}\dot{\theta}_2(t)^2 \cos(\theta_2(t)) - r_{c2}\ddot{\theta}_2(t)\sin(\theta_2(t)) \\
 a_{c2,y}(t) &= -r_{c2}\dot{\theta}_2(t)^2 \sin(\theta_2(t)) + r_{c2}\ddot{\theta}_2(t)\cos(\theta_2(t)) \\
 a_{c4,x}(t) &= -r_{c4}\dot{\theta}_4(t)^2 \cos(\theta_4(t)) - r_{c4}\ddot{\theta}_4(t)\sin(\theta_4(t)) \\
 a_{c4,y}(t) &= -r_{c4}\dot{\theta}_4(t)^2 \sin(\theta_4(t)) + r_{c4}\ddot{\theta}_4(t)\cos(\theta_4(t)) \\
 a_{c6,x}(t) &= -r_{c6}\dot{\theta}_6(t)^2 \cos(\theta_6(t)) - r_{c6}\ddot{\theta}_6(t)\sin(\theta_6(t)) \\
 a_{c6,y}(t) &= -r_{c6}\dot{\theta}_6(t)^2 \sin(\theta_6(t)) + r_{c6}\ddot{\theta}_6(t)\cos(\theta_6(t))
 \end{aligned} \tag{12}$$

The general form of the relationships between the summation of moments and the angular acceleration can be reduced by choosing the centre of gravity ( $COG_j$ ) of the links as an axis about which the moments are taken. The summation of moments leads to Eq. (13):

$$F_{ij,x}r_{ci} \sin(\theta_i) - F_{ij,y}r_{ci} \cos(\theta_i) - F_{ki,x}(r_i - r_{ci}) \sin(\theta_i) + F_{ki,y}(r_i - r_{ci}) \cos(\theta_i) = I_{ci}\ddot{\theta}_i \tag{13}$$

After all, the force and moment equilibrium of the rigid links is built as in Eq. (14):

$$\begin{aligned}
 F_{12,x}(t) + F_3(t)\cos(\theta_3(t)) &= m_2 a_{c2,x}(t) \\
 F_{12,y}(t) + F_3(t)\sin(\theta_3(t)) - m_2 g &= m_2 a_{c2,y}(t) \\
 \tau_m(t) + F_{12,x}(t)r_{c2} \sin(\theta_2(t)) - F_{12,y}(t)r_{c2} \cos(\theta_2(t)) \\
 - F_3(t)\cos(\theta_3(t))(r_2 - r_{c2}) \sin(\theta_2(t)) + F_3(t)\sin(\theta_3(t))(r_2 - r_{c2}) \cos(\theta_2(t)) &= I_{c2}\ddot{\theta}_2(t) \\
 F_{14,x}(t) + F_5(t) \cos(\theta_5(t)) + F_3(t) \cos(\theta_3(t)) &= m_4 a_{c4,x}(t) \\
 F_{14,y}(t) + F_5(t) \sin(\theta_5(t)) + F_3(t) \sin(\theta_3(t)) - m_4 g &= m_4 a_{c4,y}(t) \\
 F_{14,x}(t)r_{c4} \sin(\theta_4(t)) - F_{14,y}(t)r_{c4} \cos(\theta_4(t)) \\
 - F_5(t)\cos(\theta_5(t))(r_4 - r_{c4}) \sin(\theta_4(t)) \\
 + F_5(t)\sin(\theta_5(t))(r_4 - r_{c4}) \cos(\theta_4(t)) \\
 - F_3(t) \cos(\theta_3(t)) (r_4 - r_{c4}) \sin(\theta_4(t)) \\
 + F_3(t) \sin(\theta_3(t)) (r_4 - r_{c4}) \cos(\theta_4(t)) &= I_{c4}\ddot{\theta}_4(t) \\
 F_{16,x}(t) + F_5(t) \cos(\theta_5(t)) &= m_6 a_{c6,x}(t) \\
 F_{16,y}(t) + F_5(t)\sin(\theta_5(t)) - m_6 g &= m_6 a_{c6,y}(t) \\
 F_{16,x}(t)r_{c6} \sin(\theta_6(t)) - F_{16,y}(t)r_{c6} \cos(\theta_6(t)) \\
 - F_5(t)\cos(\theta_5(t))(r_6 - r_{c6}) \sin(\theta_6(t)) \\
 + F_5(t)\sin(\theta_5(t))(r_6 - r_{c6}) \cos(\theta_6(t)) &= I_{c6}\ddot{\theta}_6(t)
 \end{aligned} \tag{14}$$

### 2.3.2. Solution Procedure of the Flexible Pin-Pin Large Deflection

The deflections of the elastic links are calculated by using quasi-static analysis (Lobontiu, 2014) while the mechanism moves. The simulation of the mechanism is conducted under the condition of quasi-statically slow speeds while omitting the beam and joints inertial forces&damping forces. System modelling and simulation can be made by adding the inertia and the damping forces. When the mass of the flexible beam is small compared to the rigid parts, it may not be included in the inertia of the system. The inertia of the flexible moving parts might then be modelled as a lumped mass. Newton-Raphson method is utilized to reveal this equation set starting from the initially compressed state of the mechanism. As the link-2 turns quasi-statically through the full cycle of 360° in the reverse direction, the solution for the previous step is utilized as the initial guess for the next iteration. The unknowns  $r_3(t)$ ,  $\theta_3(t)$ ,  $r_5(t)$ ,  $\theta_5(t)$ ,  $\theta_4(t)$ ,  $\theta_6(t)$ , and  $\tau_m(t)$  are evaluated after solving Eq. (15) simultaneously.

$$\begin{aligned}
 r_2 \cos(\theta_2(t)) + r_3(t) \cos(\theta_3(t)) - r_{1\alpha} \cos(\theta_{1\alpha}) - r_4 \cos(\theta_4(t)) &= 0 \\
 r_2 \sin(\theta_2(t)) + r_3(t) \sin(\theta_3(t)) - r_{1\alpha} \sin(\theta_{1\alpha}) - r_4 \sin(\theta_4(t)) &= 0 \\
 r_4 \cos(\theta_4(t)) + r_5(t) \cos(\theta_5(t)) - r_{1\beta} \cos(\theta_{1\beta}) - r_6 \cos(\theta_6(t)) &= 0 \\
 r_4 \sin(\theta_4(t)) + r_5(t) \sin(\theta_5(t)) - r_{1\beta} \sin(\theta_{1\beta}) - r_6 \sin(\theta_6(t)) &= 0 \\
 \tau_m(t) + F_3(t) \sin(\theta_3(t))(r_2) \cos(\theta_2(t)) - F_3(t) \cos(\theta_3(t))(r_2) \sin(\theta_2(t)) &= 0 \\
 -F_5(t) \cos(\theta_5(t))(r_4) \sin(\theta_4(t)) & \\
 +F_5(t) \sin(\theta_5(t))(r_4) \cos(\theta_4(t)) - F_3(t) \cos(\theta_3(t))(r_4) \sin(\theta_4(t)) & \\
 +F_3(t) \sin(\theta_3(t))(r_4) \cos(\theta_4(t)) &= 0 \\
 -F_5(t) \cos(\theta_5(t))(r_6) \sin(\theta_6(t)) + F_5(t) \sin(\theta_5(t))(r_6) \cos(\theta_6(t)) &= 0 \quad (15)
 \end{aligned}$$

To solve these nonlinear equations, one should develop a numerical method having proper initial conditions. The mechanism is simulated by using Matlab codes that contain "lsqnonlin" command with options [options = optimset('maxfunvals',3000000,'maxiter',400000,'TolFun',1e-20,'TolX',1e-20)], and trust-region-reflective-algorithm.

For kinematic analysis,  $r_3(t)$  and  $r_5(t)$  elastic link deflections must be known. At this point, the results of the quasi-static analysis help us to calculate elastic link deflections and also reduce the number of unknown equations. Nonlinear load-deflection analysis of the flexible beam is represented by a polynomial fitted by using nonlinear inextensible exact elastic theory.  $\theta_2 - r_3$  and  $\theta_2 - r_5$  curves represented in Figure 6 obtained from quasi-static results.

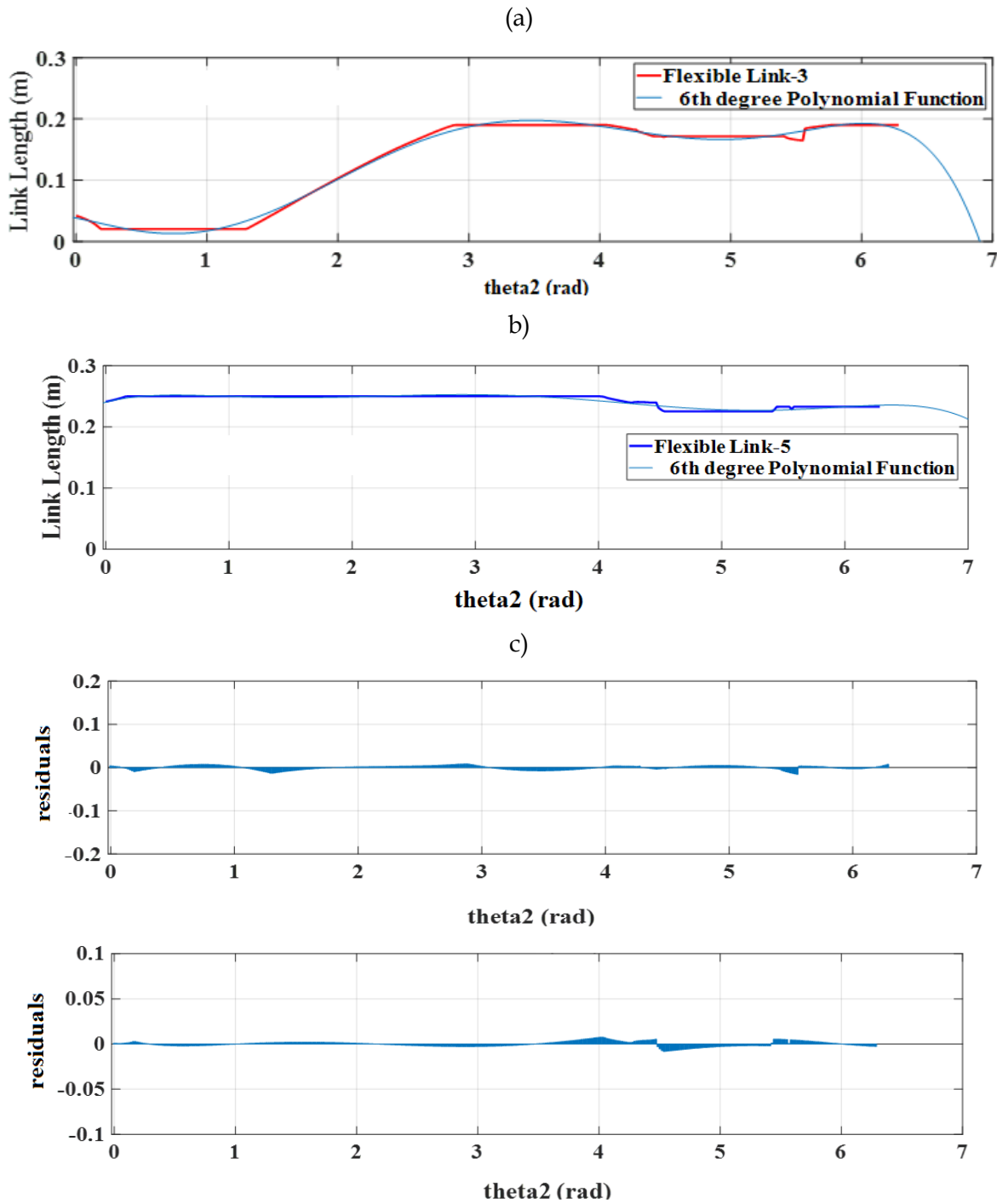


**Figure 6.** Change of the a)  $r_3$  and b)  $r_5$  flexible link lengths w.r.t.  $\theta_2$  and c) their residuals, respectively.

The related polynomial equations are given in Eq. (16):

$$\begin{aligned}
 r_3(z(\theta_2)) &= -0.014z^6 - 0.0072z^5 \\
 &+ 0.087z^4 + 0.016z^3 - 0.17z^2 + 0.057z + 0.19, \quad z(\theta_2) = (\theta_2 - 3.1)/1.8 \\
 r_5(z(\theta_2)) &= -0.037z^6 + 0.0023z^5 + 0.019z^4 \\
 &- 0.005z^3 - 0.029z^2 - 0.0074z + 0.25, \quad z(\theta_2) = (\theta_2 - 3.1)/1.8
 \end{aligned} \tag{16}$$

### 2.3.3. The Simultaneous Constraint Matrix

Combining 10 kinematic constraint equations (Eq. 7 and Eq. 12) with the 9 dynamic equations (Eq. 14), 19 unknown variables ( $[\ddot{\theta}_3, \ddot{r}_3, \ddot{\theta}_5, \ddot{r}_5, a_{c2,x}, a_{c2,y}, a_{c4,x}, a_{c4,y}, a_{c6,x}, a_{c6,y}, F_{12,x}, F_{12,y}, \tau_m, F_{14,x}, F_{14,y}, \ddot{\theta}_4, F_{16,x}, F_{16,y}, \ddot{\theta}_6]$ ) are determined by solving the simultaneous constraint matrix equation (Gardner, 2001) as demonstrated in Eq. (17):

$$\begin{bmatrix}
 -r_3 s \theta_3 & c \theta_3 & 0 & 0 & 0 & 0 & 0 & 0 & 0 & 0 & 0 & 0 & 0 & 0 & r_4 s \theta_4 & 0 & 0 & 0 & 0 \\
 r_3 c \theta_3 & s \theta_3 & 0 & 0 & 0 & 0 & 0 & 0 & 0 & 0 & 0 & 0 & 0 & 0 & -r_4 c \theta_4 & 0 & 0 & 0 & 0 \\
 0 & 0 & -r_5 s \theta_5 & c \theta_5 & 0 & 0 & 0 & 0 & 0 & 0 & 0 & 0 & 0 & 0 & -r_4 s \theta_4 & 0 & 0 & r_6 s \theta_6 & 0 \\
 0 & 0 & r_5 c \theta_5 & s \theta_5 & 0 & 0 & 0 & 0 & 0 & 0 & 0 & 0 & 0 & 0 & r_4 c \theta_4 & 0 & 0 & -r_6 c \theta_6 & 0 \\
 0 & 0 & 0 & 0 & 1 & 0 & 0 & 0 & 0 & 0 & 0 & 0 & 0 & 0 & 0 & 0 & 0 & 0 & 0 \\
 0 & 0 & 0 & 0 & 0 & 1 & 0 & 0 & 0 & 0 & 0 & 0 & 0 & 0 & 0 & 0 & 0 & 0 & 0 \\
 0 & 0 & 0 & 0 & 0 & 0 & 1 & 0 & 0 & 0 & 0 & 0 & 0 & 0 & r_{c4} s \theta_4 & 0 & 0 & 0 & 0 \\
 0 & 0 & 0 & 0 & 0 & 0 & 0 & 1 & 0 & 0 & 0 & 0 & 0 & 0 & -r_{c4} c \theta_4 & 0 & 0 & 0 & 0 \\
 0 & 0 & 0 & 0 & 0 & 0 & 0 & 0 & 1 & 0 & 0 & 0 & 0 & 0 & 0 & 0 & 0 & r_{c6} s \theta_6 & 0 \\
 0 & 0 & 0 & 0 & 0 & 0 & 0 & 0 & 0 & 1 & 0 & 0 & 0 & 0 & 0 & 0 & 0 & -r_{c6} c \theta_6 & 0 \\
 0 & 0 & 0 & 0 & -m_2 & 0 & 0 & 0 & 0 & 0 & 1 & 0 & 0 & 0 & 0 & 0 & 0 & 0 & 0 \\
 0 & 0 & 0 & 0 & 0 & -m_2 & 0 & 0 & 0 & 0 & 0 & 1 & 0 & 0 & 0 & 0 & 0 & 0 & 0 \\
 0 & 0 & 0 & 0 & 0 & 0 & 0 & 0 & 0 & 0 & r_{c2} s \theta_2 & -r_{c2} c \theta_2 & 1 & 0 & 0 & 0 & 0 & 0 & 0 \\
 0 & 0 & 0 & 0 & 0 & 0 & -m_4 & 0 & 0 & 0 & 0 & 0 & 0 & 1 & 0 & 0 & 0 & 0 & 0 \\
 0 & 0 & 0 & 0 & 0 & 0 & 0 & -m_4 & 0 & 0 & 0 & 0 & 0 & 0 & 1 & 0 & 0 & 0 & 0 \\
 0 & 0 & 0 & 0 & 0 & 0 & 0 & 0 & 0 & 0 & 0 & 0 & r_{c4} s \theta_4 & -r_{c4} c \theta_4 & -I_{c4} & 0 & 0 & 0 & 0 \\
 0 & 0 & 0 & 0 & 0 & 0 & 0 & 0 & -m_6 & 0 & 0 & 0 & 0 & 0 & 0 & 1 & 0 & 0 & 0 \\
 0 & 0 & 0 & 0 & 0 & 0 & 0 & 0 & 0 & 0 & -m_6 & 0 & 0 & 0 & 0 & 0 & 0 & 1 & 0 \\
 0 & 0 & 0 & 0 & 0 & 0 & 0 & 0 & 0 & 0 & 0 & 0 & 0 & 0 & 0 & 0 & r_{c6} s \theta_6 & -r_{c6} c \theta_6 & -I_{c6}
 \end{bmatrix}
 \begin{bmatrix}
 \ddot{\theta}_3 \\
 \ddot{r}_3 \\
 \ddot{\theta}_5 \\
 \ddot{r}_5 \\
 a_{c2,x} \\
 a_{c2,y} \\
 a_{c4,x} \\
 a_{c4,y} \\
 a_{c6,x} \\
 a_{c6,y} \\
 F_{12,x} \\
 F_{12,y} \\
 \tau_m \\
 F_{14,x} \\
 F_{14,y} \\
 \ddot{\theta}_4 \\
 F_{16,x} \\
 F_{16,y} \\
 \ddot{\theta}_6
 \end{bmatrix}
 =
 \begin{bmatrix}
 b(1) \\
 b(2) \\
 b(3) \\
 b(4) \\
 b(5) \\
 b(6) \\
 b(7) \\
 b(8) \\
 b(9) \\
 b(10) \\
 b(11) \\
 b(12) \\
 b(13) \\
 b(14) \\
 b(15) \\
 b(16) \\
 b(17) \\
 b(18) \\
 b(19)
 \end{bmatrix}
 \tag{17}$$

In this matrix, notation s is for sin(.) function and c for cos(.) function.

The notations representing the known vector in Eq. (17) are given in Eq. (18).

$$\begin{aligned}
b(1) &= r_3(t)\dot{\theta}_3(t)^2 \cos(\theta_3(t)) - r_4\dot{\theta}_4(t)^2 \cos(\theta_4(t)) + 2\dot{r}_3(t)\dot{\theta}_3(t)\sin(\theta_3(t)) \\
&+ r_2\dot{\theta}_2(t)^2 \cos(\theta_2(t)) + r_2\ddot{\theta}_2(t)\sin(\theta_2(t)) \\
b(2) &= r_2\dot{\theta}_2(t)^2 \sin(\theta_2(t)) + r_3(t)\dot{\theta}_3(t)^2 \sin(\theta_3(t)) - 2\dot{r}_3(t)\dot{\theta}_3(t)\cos(\theta_3(t)) \\
&- r_4\dot{\theta}_4(t)^2 \sin(\theta_4(t)) - r_2\ddot{\theta}_2(t)\cos(\theta_2(t)) \\
b(3) &= 2\dot{r}_5(t)\dot{\theta}_5(t)\sin(\theta_5(t)) + r_4\dot{\theta}_4(t)^2 \cos(\theta_4(t)) \\
&+ r_5(t)\dot{\theta}_5(t)^2 \cos(\theta_5(t)) - r_6\dot{\theta}_6(t)^2 \cos(\theta_6(t)) \\
b(4) &= r_4\dot{\theta}_4(t)^2 \sin(\theta_4(t)) \\
&+ r_5(t)\dot{\theta}_5(t)^2 \sin(\theta_5(t)) - 2\dot{r}_5(t)\dot{\theta}_5(t)\cos(\theta_5(t)) - r_6\dot{\theta}_6(t)^2 \sin(\theta_6(t)) \\
b(5) &= -r_{c2}\dot{\theta}_2(t)^2 \cos(\theta_2(t)) - r_{c2}\ddot{\theta}_2(t)\sin(\theta_2(t)) \\
b(6) &= -r_{c2}\dot{\theta}_2(t)^2 \sin(\theta_2(t)) + r_{c2}\ddot{\theta}_2(t)\cos(\theta_2(t)) \\
b(7) &= -r_{c4}\dot{\theta}_4(t)^2 \cos(\theta_4(t)) \\
b(8) &= -r_{c4}\dot{\theta}_4(t)^2 \sin(\theta_4(t)) \\
b(9) &= -r_{c6}\dot{\theta}_6(t)^2 \cos(\theta_6(t)) \\
b(10) &= -r_{c6}\dot{\theta}_6(t)^2 \sin(\theta_6(t)) \\
b(11) &= -F_3(t)\cos(\theta_3(t)) \\
b(12) &= -F_3(t)\sin(\theta_3(t)) + m_2g \\
b(13) &= F_3(t)\cos(\theta_3(t))(r_2 - r_{c2})\sin(\theta_2(t)) \\
&- F_3(t)\sin(\theta_3(t))(r_2 - r_{c2})\cos(\theta_2(t)) + I_{c2}\ddot{\theta}_2(t) \\
b(14) &= -F_5(t)\cos(\theta_5(t)) - F_3(t)\cos(\theta_3(t)) \\
b(15) &= -F_5(t)\sin(\theta_5(t)) - F_3(t)\sin(\theta_3(t)) + m_4g \\
b(16) &= F_5(t)\cos(\theta_5(t))(r_4 - r_{c4})\sin(\theta_4(t)) \\
&- F_5(t)\sin(\theta_5(t))(r_4 - r_{c4})\cos(\theta_4(t)) \\
&+ F_3(t)\cos(\theta_3(t))(r_4 - r_{c4})\sin(\theta_4(t)) - F_3(t)\sin(\theta_3(t))(r_4 - r_{c4})\cos(\theta_4(t)) \\
b(17) &= -F_5(t)\cos(\theta_5(t)) \\
b(18) &= -F_5(t)\sin(\theta_5(t)) + m_6g \\
b(19) &= F_5(t)\cos(\theta_5(t))(r_6 - r_{c6})\sin(\theta_6(t)) \\
&- F_5(t)\sin(\theta_5(t))(r_6 - r_{c6})\cos(\theta_6(t))
\end{aligned} \tag{18}$$

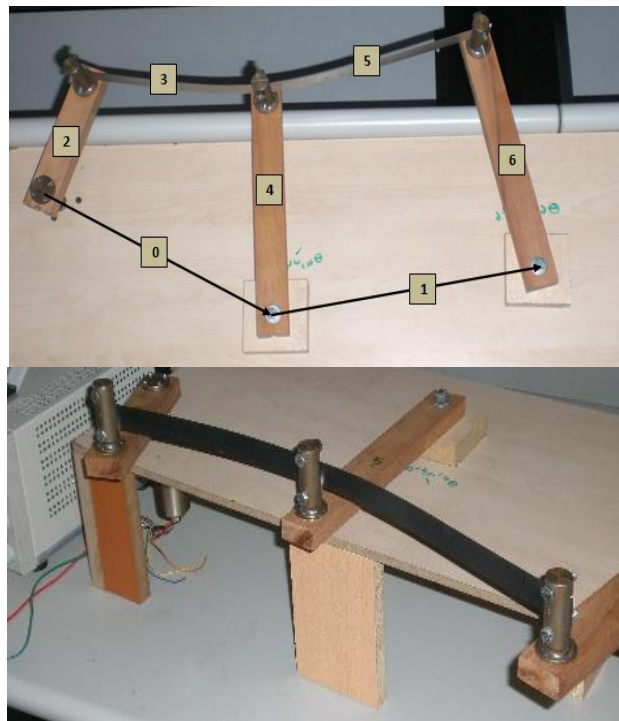
The unknown vector can be evaluated from the theory of linear algebra by multiplying the inverse of matrix A (coefficient matrix) and B (known vector), which implies as  $X = A^{-1}B$ . This matrix equation is embedded in a MATLAB function that, in turn, can be embedded into a Simulink-based simulation.

### 3. Simulation and Experimental Results

#### 3.1. Experimental Setup

The experimental setup and the prototype of the flexible Watt six-bar mechanism are demonstrated in this sub-section. The design setup of the Compliant Watt-linkage prototype is demonstrated in Figure 7. This prototype is utilized to contribute to the simulation results. The main structure of the Watt six-bar compliant mechanism is comprised of three rigid links and two flexible beams. The physical properties and their values related to the mechanism are given in Table 2.

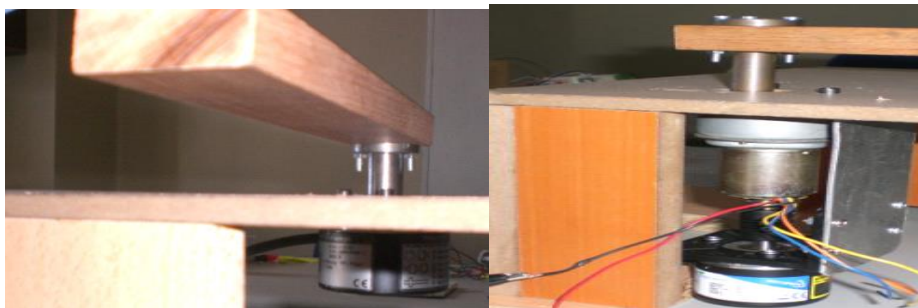
The dimensions of the cross-section of the flexible links are selected from the steel spring strips. The input of the Watt six-bar compliant mechanism is supplied by DC Motor (2.2 Volt at initial, 4 Volt at operating). To predict the movement of the whole compliant mechanism, it should be known how the flexible links buckle. The total length of the flexible links is 440 mm. The first part of the flexible link (coded as 3) is 190 mm, and the second part of the flexible link (coded as 5) is 250 mm before buckling, respectively. During the operation, the length of flexible links changes while joints that connect the flexible links and rigid links turn. An encoder is attached to each rigid link to measure the link angle and to evaluate the angular crank velocity ( $\dot{\theta}_2(t)$ ). Even though a DC motor within the house encoder is utilized in the experiments, the DC motor's encoder response was not certain. Therefore, a more accurate encoder is integrated into the motor shaft. The data from the measurements of positions are acquired with an Analogue-Digital Converter (ADC) IOTech personal data acquisition card. Encoders and ADC's are supplied with 6-7 Volt. DC Motor and encoder used in the experiments are presented in Figure 8.



**Figure 7.** The prototype of the Watt six-bar compliant mechanism.

**Table 2.** Physical properties and their values.

Physical property	Value/Dimension
Length of the flexible links (pre-buckling state) ( $r_{3,0}$ ), ( $r_{5,0}$ )	19 cm, 25 cm
Length of the rigid links ( $r_2$ ), ( $r_4$ ), ( $r_6$ )	12 cm, 22 cm, 24 cm
Length of the rigid links (from the lower end to the centre of gravity) ( $r_{c2}$ ), ( $r_{c4}$ ), ( $r_{c6}$ )	6 cm, 11 cm, 12 cm
Cross-section of the rigid links ( $b_r * h_r$ )	36 mm * 18 mm
Mass of the rigid links ( $m_2$ ) ( $m_4$ ) ( $m_6$ )	0.0389 kg, 0.0713 kg, 0.0778 kg
Moment of inertia of the rigid links ( $I_{c2}$ ), ( $I_{c4}$ ), ( $I_{c6}$ )	$1.7496 * 10^{-8} \text{ kgm}^2$
Cross-section of the flexible links ( $b_f * h_f$ )	21 mm * 0.2 mm
Young's modulus of the flexible links ( $E_3$ ), ( $E_5$ )	$2.07 * 10^{11} \text{ N/m}^2$
Ground link length ( $r_{1\alpha}$ ), ( $r_{1\beta}$ )	0.3 m
Ground link orientation ( $\theta_{1\alpha}$ ), ( $\theta_{1\beta}$ )	$25^\circ$ , $-10^\circ$ counterclockwise rotation (+)

**Figure 8.** DC motor and encoder used in the experiment.

Data processing is conducted by MATLAB/SIMULINK software. The data acquired from encoders are processed in MATLAB/SIMULINK to acquire the angular velocity and angular

position of the rigid links. The Simulink block diagram utilized for data processing is represented in Figure 9.

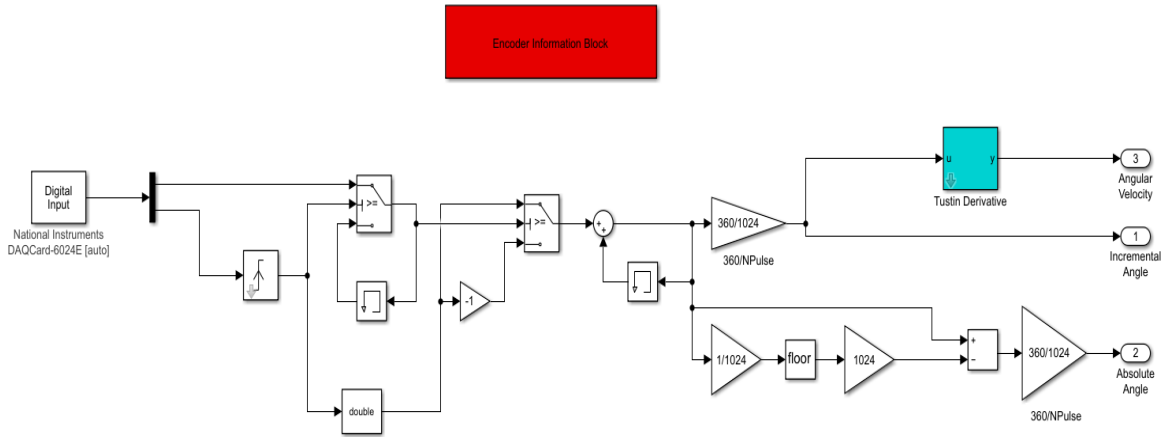


Figure 9. Simulink block diagram utilized for data processing.

The angular velocity of each rigid link is obtained from the angular displacement data of the related encoder. Unwanted noise is reduced by passing the collected raw data through differential operator and filter, respectively, given in Eq. (19):

$$D(.) = \frac{d(V(t))}{dt} \approx \frac{s}{\tau s + 1} V(s) \quad , \quad F(s) = \frac{\omega_n^2}{s^2 + 2\xi\omega_n s + \omega_n^2} \tag{19}$$

The differential operator guarantees the causality.  $\tau$  is selected as 120.51. The filter has a cut-off frequency at  $\omega_n=10$  rad/sec.  $\xi$  is selected as 0.707. The filter parameters were chosen to obtain a continuous noise-free response of the angular velocity of each rigid link.

### 3.2. Experimental and Simulation Results

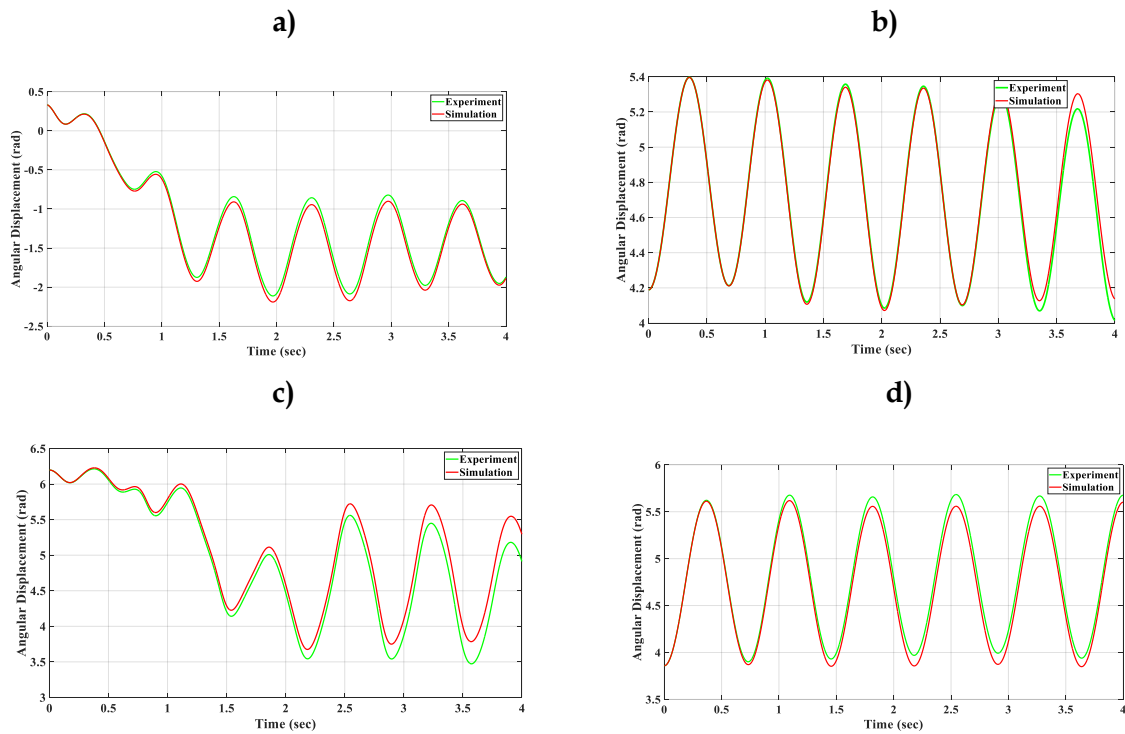
Link-2 has an initial angular velocity of 1.57 rad/s and an initial position of  $270^\circ$ . The other initial conditions (configurations) were evaluated by conducting quasi-static analysis and given in Table 3.

Table 3. Initial configuration of the mechanism.

$\theta_{3,0}$	0.3345 rad
$\theta_{4,0}$	4.1888 rad
$\theta_{5,0}$	6.1979 rad
$\theta_{6,0}$	3.8582 rad
$r_{3,0}$	0.1714 m
$r_{5,0}$	0.2253 m

The simulations were done in MATLAB/SIMULINK program. When Link-2 turns one cycle [ $270^\circ - (-90^\circ)$ ], the changes in angular positions ( $\theta_3, \theta_4, \theta_5, \theta_6$ ), angular velocities ( $\dot{\theta}_3, \dot{\theta}_4, \dot{\theta}_5, \dot{\theta}_6$ )

and angular accelerations ( $\ddot{\theta}_3, \ddot{\theta}_4, \ddot{\theta}_5, \ddot{\theta}_6$ ) w.r.t. time are presented in Figure 10a-Figure 10d, Figure 11a-Figure 11d, Figure 12a-Figure 12d, respectively.



**Figure 10.** Angular displacement trajectory. a)  $\theta_3$ -time graph, b)  $\theta_4$ -time graph, c)  $\theta_5$ -time graph d)  $\theta_6$ -time graph

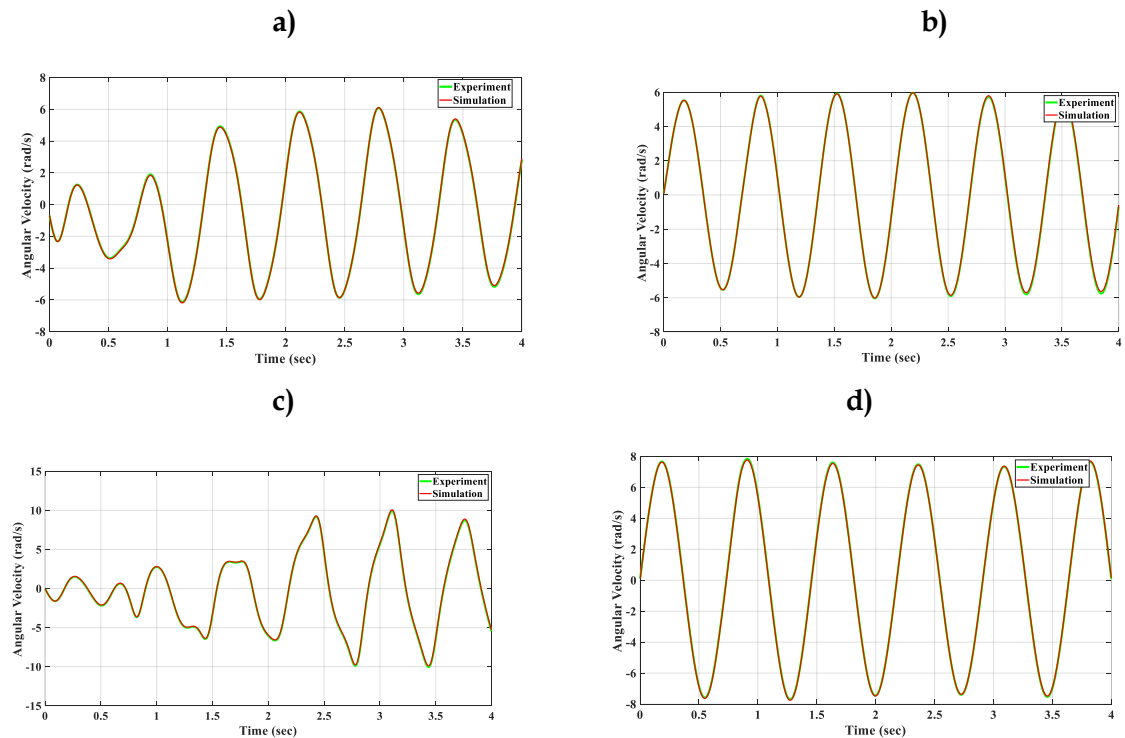


**Figure 11.** Angular velocity trajectory. a)  $w_3$ -time graph, b)  $w_4$ -time graph, c)  $w_5$ -time graph, d)  $w_6$ -time graph

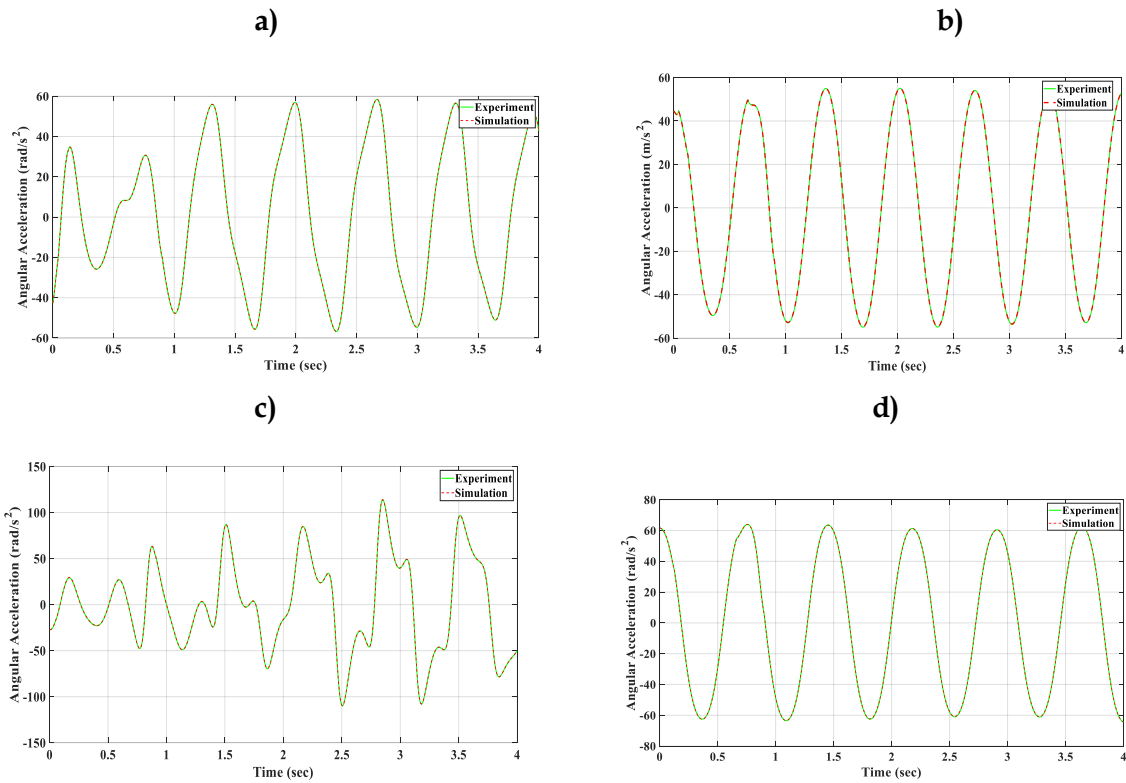


**Figure 12.** Angular acceleration trajectory. a)  $\alpha_3$ -time graph, b)  $\alpha_4$ -time graph, c)  $\alpha_5$ -time graph, d)  $\alpha_6$ -time graph

The reaction forces ( $F_{12,x}, F_{12,y}, F_{14,x}, F_{14,y}, F_{16,x}, F_{16,y}$ ), motor torque ( $\tau_m$ ) are represented in Figure 13a-Figure 13b, respectively.

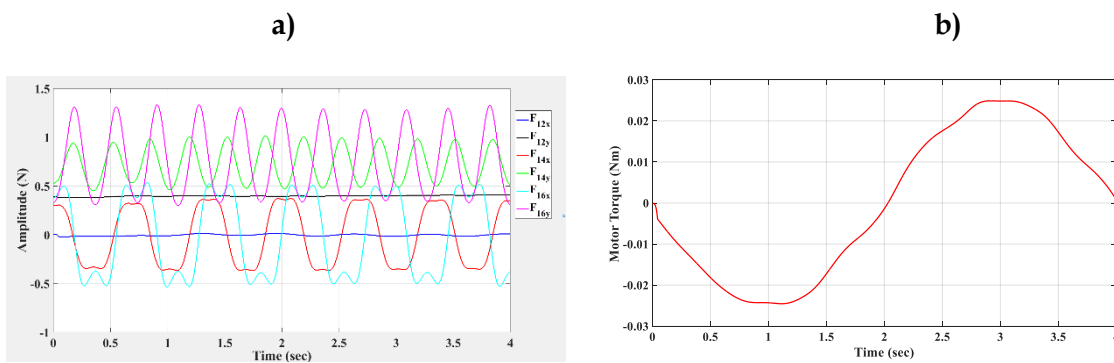


**Figure 13.** Kinetic trajectory. a) Reaction force-time, b) Motor torque-time

One can deduce from the results that the kinematic and kinetic trajectories of the mechanism were experimentally validated. The deformation of the flexible components are evident and varies in the motion cycle of the mechanism.

#### 4. Conclusions

This paper describes the design procedure and dynamic analysis of a partially compliant Watt six-bar linkage combining the PRBM and elastica buckling theory. Polynomial curve fits of the pinned-pinned flexible beam and the PRBM of the large deflecting cantilever beam are synthesized in dynamic simulation via simultaneous constraint matrix. The kinematic analysis is realized through vector loop closure, the force equilibrium of elastic elements, and numerically solving the nonlinear dynamical equations. The 4th and 6th link curves are symmetric. The path of the mechanism is almost straight in one section and completely parallel. Therefore, the compliant Watt six-bar linkage is quite suitable for legged robot design. The parallel motion of the joints leads to an extended contact surface of the leg coupled with the terrain. The balance of the legs can be sustained without damaging effects on the terrain. The number of degrees of freedom is reduced to one so that the control system synthesis and motion analysis are easily conducted. The full dynamic simulation results are verified by comparing the experimental results. The synergy of the PRBM and elastica buckling theory serves as an effective method in the analysis and synthesis of new compliant mechanism designs. The compliant synthesis approach for industrial implementations wherein accuracy is extremely important such as medical, welding and manufacturing robot cause compliant modelling wherein failures are considered.

#### Nomenclature

$r_{1\alpha}$	Ground link length ( $\alpha$ )	$F_{ij,y}$	The vertical force of link $i$ acting on the link $j$
$\theta_{1\alpha}$	Ground link orientation ( $\alpha$ )	$COG_j$	Center of gravity of the $j^{th}$ link
$r_{1\beta}$	Ground link length ( $\beta$ )	$r_{cj}$	Length from $(j - 1)^{th}$ joint to $j^{th}$ $COG_j$
$\theta_{1\beta}$	Ground link orientation ( $\beta$ )	$m_j$	$j^{th}$ rigid link mass
$r_i$	$i^{th}$ flexible link length ( $i = 3, 5$ )	$I_{cj}$	$j^{th}$ rigid link moment of inertia about the $COG_j$
$r_{i,0}$	$i^{th}$ flexible link initial length (pre-buckling state)	$g$	Acceleration due to gravity
$\dot{r}_i$	$i^{th}$ flexible link buckling velocity	$\tau_m$	Applied DC-motor torque
$\ddot{r}_i$	$i^{th}$ flexible link buckling acceleration		
$\vartheta_i$	$i^{th}$ flexible link deflection		
$\theta_i$	$i^{th}$ flexible link angle		
$\dot{\theta}_i$	$i^{th}$ flexible link angular velocity		
$\ddot{\theta}_i$	$i^{th}$ flexible link angular acceleration		
$F_i$	$i^{th}$ flexible link spring force		
$b_{f,i}$	$i^{th}$ flexible link cross-sectional width		
$h_{f,i}$	$i^{th}$ flexible link cross-sectional thickness		
$EI_i$	$i^{th}$ flexible link flexural rigidity		
$r_j$	$j^{th}$ rigid link length ( $j = 2, 4, 6$ )		
$\theta_j$	$j^{th}$ rigid link angle		
$\dot{\theta}_j$	$j^{th}$ rigid link angular velocity		
$\ddot{\theta}_j$	$j^{th}$ rigid link angular acceleration		
$b_{r,j}$	$j^{th}$ rigid link cross-sectional width		
$h_{r,j}$	$i^{th}$ rigid link cross-sectional thickness		
$F_{ij,x}$	The horizontal force of link $i$ acting on the link $j$		

## Author Statement

The authors confirm contribution to the paper as follows: Study conception, system design, analysis and data interpretation are done by Çağlar Uyulan. Experimental setup and data acquisition are done by Batuhan İpek. Draft manuscript is prepared by Çağlar Uyulan. All authors reviewed the results and approved the final version of the manuscript.

## Conflict of Interest

The authors declare no conflict of interest.

## References

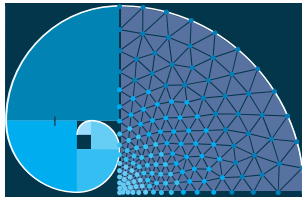
- Bapat, G. M., & Sujatha, S. (2017). A Method for Optimal Synthesis of a Biomimetic Four-Bar Linkage Knee Joint for a Knee-Ankle-Foot Orthosis. *Journal of Biomimetics, Biomaterials and Biomedical Engineering*, 32, 20-28. doi:10.4028/www.scientific.net/jbbbe.32.20
- Berselli, G., Meng, Q., Vertechy, R., & Castelli, V. P. (2015). An improved design method for the dimensional synthesis of flexure-based compliant mechanisms: Optimization procedure and experimental validation. *Meccanica*, 51(5), 1209-1225. doi:10.1007/s11012-015-0276-z
- Bishopp, K. E., & Drucker, D. C. (1945). Large deflection of cantilever beams. *Quarterly of Applied Mathematics*, 3(3), 272-275.
- Chen, F., & Huang, H. (2005). The Use Of Fuzzy Logic In The Taguchi Method For The Determination Of The Tolerance Of A Six-Bar Hinge Mechanism. *Transactions of the Canadian Society for Mechanical Engineering*, 29(3), 477-489. doi:10.1139/tcsme-2005-0029
- Chen, F., & Tzeng, Y. (2006). A Simple Approach For The Tolerance Design Of Watt-I Type Six-Bar Hinge Mechanism Using Taguchi Method. *International Journal of Reliability, Quality and Safety Engineering*, 13(02), 157-169. doi:10.1142/s0218539306002185
- Eren, R., & Aydemir, A. (2004). An Approach to Kinematic Design of Four-bar Sley Drive Mechanisms in Weaving. *The Journal of The Textile Institute*, 95(1-6), 193-205. doi:10.1533/joti.2002.0055
- Gardner, J. F. (2001). *Simulations of machines using MATLAB and Simulink*. California: Wadsworth-Thomson Learning.
- Gezgin, E., Chang, P., & Akhan, A. F. (2016). Synthesis of a Watt II six-bar linkage in the design of a hand rehabilitation robot. *Mechanism and Machine Theory*, 104, 177-189. doi:10.1016/j.mechmachtheory.2016.05.023
- Ghosh, A., & Corves, B. (2015). Microfabrication and Futuristic Issues. *Introduction to Micromechanisms and Microactuators Mechanisms and Machine Science*, 133-153. doi:10.1007/978-81-322-2144-9\_8

- Gouker, R. M., Gupta, S. K., Bruck, H. A., & Holzschuh, T. (2006). Manufacturing of multi-material compliant mechanisms using multi-material molding. *The International Journal of Advanced Manufacturing Technology*, 30(11-12), 1049-1075. doi:10.1007/s00170-005-0152-4
- Her, I., & Midha, A. (1987). A Compliance Number Concept for Compliant Mechanisms, and Type Synthesis. *Journal of Mechanisms, Transmissions, and Automation in Design*, 109(3), 348-355. doi:10.1115/1.3258802
- Howell, L. L., & Midha, A. (1994). A Generalized Loop-Closure Theory for the Analysis and Synthesis of Compliant Mechanisms. 23rd Biennial Mechanisms Conference: Machine Elements and Machine Dynamics. doi:10.1115/detc1994-0293
- Howell, L. L., & Midha, A. (1994). A Method for the Design of Compliant Mechanisms With Small-Length Flexural Pivots. *Journal of Mechanical Design*, 116(1), 280-290. doi:10.1115/1.2919359
- Howell, L. L., Magleby, S. P., & Olsen, B. M. (2013). *Handbook of compliant mechanisms*. Chichester, West Sussex, United Kingdom: John Wiley & Sons.
- Jaiswal, A., & Jawale, H. P. (2018). Synthesis and optimization of four bar mechanism with six design parameters. doi:10.1063/1.5029590
- Jin, D., Zhang, R., Dimo, H., Wang, R., & Zhang, J. (2003). Kinematic and dynamic performance of prosthetic knee joint using six-bar mechanism. *The Journal of Rehabilitation Research and Development*, 40(1), 39. doi:10.1682/jrrd.2003.01.0039
- Jovanova, J., & Frecker, M. (2017). Two Stage Design of Compliant Mechanisms With Superelastic Compliant Joints. Volume 2: Modeling, Simulation and Control of Adaptive Systems; Integrated System Design and Implementation; Structural Health Monitoring. doi:10.1115/smasis2017-3825
- Khemili, I., Abdallah, M. A., & Aifaoui, N. (2018). Multi-objective optimization of a flexible slider-crank mechanism synthesis, based on dynamic responses. *Engineering Optimization*, 51(6), 978-999. doi:10.1080/0305215x.2018.1508574
- Khosraviani, K., & Leung, A. M. (2012). Robust micromachining of compliant mechanisms using silicides. *Journal of Micromechanics and Microengineering*, 23(1), 015015. doi:10.1088/0960-1317/23/1/015015
- Konopasek, M. (1980). Classical Elastica Theory and its Generalizations. *Mechanics of Flexible Fibre Assemblies*, 255-274. doi:10.1007/978-94-011-9774-8\_14
- Lefebvre, T., Xiao, J., Bruyninckx, H., & Gerssem, G. D. (2005). Active compliant motion: A survey. *Advanced Robotics*, 19(5), 479-499. doi:10.1163/156855305323383767
- Linß, S., Henning, S., & Zentner, L. (2019). Modeling and Design of Flexure Hinge-Based Compliant Mechanisms. *Kinematics - Analysis and Applications*. doi:10.5772/intechopen.85224

- Liu, Y., & Mcphee, J. (2004). Automated Type Synthesis of Planar Mechanisms Using Numeric Optimization With Genetic Algorithms. *Journal of Mechanical Design*, 127(5), 910-916. doi:10.1115/1.1904049
- Lobontiu, N. (2014). Compliance-based matrix method for modeling the quasi-static response of planar serial flexure-hinge mechanisms. *Precision Engineering*, 38(3), 639-650. doi:10.1016/j.precisioneng.2014.02.014
- Luo, Y., Liu, W., & Wu, L. (2015). Analysis of the displacement of lumped compliant parallel-guiding mechanism considering parasitic rotation and deflection on the guiding plate and rigid beams. *Mechanism and Machine Theory*, 91, 50-68. doi:10.1016/j.mechmachtheory.2015.04.007
- Luo, Z. (2006). Theoretical And Algorithmic On Topology Optimization Design Of Distributed Compliant Mechanisms. *Chinese Journal of Mechanical Engineering*, 42(10), 27. doi:10.3901/jme.2006.10.027
- Luo, Z., Shang, J., Wei, G., & Ren, L. (2018). A reconfigurable hybrid wheel-track mobile robot based on Watt II six-bar linkage. *Mechanism and Machine Theory*, 128, 16-32. doi:10.1016/j.mechmachtheory.2018.04.020
- Midha, A., Howell, L. L., & Norton, T. W. (2000). Limit positions of compliant mechanisms using the pseudo-rigid-body model concept. *Mechanism and Machine Theory*, 35(1), 99-115. doi:10.1016/s0094-114x(98)00093-7
- Mirth, J. A. (2012). The Application of Geometric Constraint Programming to the Design of Motion Generating Six-Bar Linkages. Volume 4: 36th Mechanisms and Robotics Conference, Parts A and B. doi:10.1115/detc2012-70176
- Mirth, J. A., & Chase, T. R. (1993). Circuit Analysis of Watt Chain Six-Bar Mechanisms. *Journal of Mechanical Design*, 115(2), 214-222. doi:10.1115/1.2919180
- Niknam, A., & Farhang, K. (2018). Vibration Instability in a Large Motion Bistable Compliant Mechanism Due to Stribeck Friction. *Journal of Vibration and Acoustics*, 140(6). doi:10.1115/1.4040513
- Pavlovic, N., & Pavlovic, N. (2005). Mobility of the compliant joints and compliant mechanisms. *Theoretical and Applied Mechanics Teorijska I Primenjena Mehanika*, 32(4), 341-357. doi:10.2298/tam0504341p
- Pieber, M., & Gerstmayr, J. (2020). Six-Bar Linkages With Compliant Mechanisms for an Adaptive Robot. Volume 10: 44th Mechanisms and Robotics Conference (MR). doi:10.1115/detc2020-22546
- Plecnik, M. M., & McCarthy, J. M. (2014). Vehicle Suspension Design Based on a Six-Bar Linkage. Volume 5A: 38th Mechanisms and Robotics Conference. doi:10.1115/detc2014-35374

- Plecnik, M., McCarthy, J. M., & Wampler, C. W. (2014). Kinematic Synthesis of a Watt I Six-Bar Linkage for Body Guidance. *Advances in Robot Kinematics*, 317-325. doi:10.1007/978-3-319-06698-1\_33
- Primrose, E. J., Freudenstein, F., & Roth, B. (1967a). Six-bar motion III. Extension of the six-bar techniques to eight-bar and 2n-bar mechanisms. *Archive for Rational Mechanics and Analysis*, 24(1), 73-77. doi:10.1007/bf00251593
- Primrose, E. J., Freudenstein, F., & Roth, B. (1967b). Six-bar motion I. The Watt mechanism. *Archive for Rational Mechanics and Analysis*, 24(1), 22-41. doi:10.1007/bf00251591
- Prosser, D., Basrai, T., Dickert, J., Ratti, J., Crassidis, A., & Vachtsevanos, G. (2011). Wing kinematics and aerodynamics of a hovering flapping Micro Aerial Vehicle. 2011 Aerospace Conference. doi:10.1109/aero.2011.5747521
- Ramirez, I. A., & Lusk, C. P. (2011). Spatial-Beam Large-Deflection Equations and Pseudo-Rigid-Body Model for Axisymmetric Cantilever Beams. Volume 6: 35th Mechanisms and Robotics Conference, Parts A and B. doi:10.1115/detc2011-47389
- Sonawale, K. H., Arredondo, A., & McCarthy, J. M. (2013). Computer Aided Design of Useful Spherical Watt I Six-Bar Linkages. Volume 6A: 37th Mechanisms and Robotics Conference. doi:10.1115/detc2013-13454
- Sönmez, Ü., & Tutum, C. C. (2008). A Compliant Bistable Mechanism Design Incorporating Elastica Buckling Beam Theory and Pseudo-Rigid-Body Model. *Journal of Mechanical Design*, 130(4). doi:10.1115/1.2839009
- Sönmez, Ü. (2000). Compliant Mechanism Design and Synthesis Using Buckling and Snap-Through Buckling of Flexible Members, PhD thesis, The Pennsylvania State University, State College.
- Tsuge, B. Y., & McCarthy, J. M. (2014). Fitting Useful Planar Four-Bar and Six-Bar Linkages to Over-Specified Tasks. *Interdisciplinary Applications of Kinematics Mechanisms and Machine Science*, 171-178. doi:10.1007/978-3-319-10723-3\_18
- Venkiteswaran, V. K., & Su, H. (2016). Extension Effects in Compliant Joints and Pseudo-Rigid-Body Models. *Journal of Mechanical Design*, 138(9). doi:10.1115/1.4034111
- Wang, J., Ting, K., Zhao, D., Wang, Q., Sun, J., You, Y., & Nie, L. (2014). Full Rotatability of Watt Six-Bar Linkages. Volume 5A: 38th Mechanisms and Robotics Conference. doi:10.1115/detc2014-34207
- Wang, M. Y., & Chen, S. (2009). Compliant Mechanism Optimization: Analysis and Design with Intrinsic Characteristic Stiffness. *Mechanics Based Design of Structures and Machines*, 37(2), 183-200. doi:10.1080/15397730902761932

- Xi, Y., Xia, Y., Li, X., Sun, Y., & Wang, H. (2010). Kinematic analysis and parameter optimization of six-bar linkage based on ADAMS. 2010 International Conference on Mechanic Automation and Control Engineering. doi:10.1109/mace.2010.5536443
- Yi, L. & Leinonen, T. (2003). Computer Simulation of Path and Motion Generation With Six-Bar Linkage. Volume 2: 29th Design Automation Conference, Parts A and B. doi:10.1115/detc2003/dac-48831
- Yu, Y., Zhou, P., & Xu, Q. (2018). Kinematic and dynamic analysis of compliant mechanisms considering both lateral and axial deformations of flexural beams. Proceedings of the Institution of Mechanical Engineers, Part C: Journal of Mechanical Engineering Science, 233(3), 1007-1020. doi:10.1177/0954406218760956
- Zhang, A., & Chen, G. (2012). A Comprehensive Elliptic Integral Solution to the Large Deflection Problems of Cantilever Beams in Compliant Mechanisms. Volume 4: 36th Mechanisms and Robotics Conference, Parts A and B. doi:10.1115/detc2012-70239
- Zhang, X., & Zhu, B. (2018). Topology Optimization of Distributed Compliant Mechanisms. Topology Optimization of Compliant Mechanisms, 81-119. doi:10.1007/978-981-13-0432-3\_3
- Zhang, Z., Chang, B., Zhao, J., Yang, Q., & Liu, X. (2020). Design, Optimization, and Experiment on a Bioinspired Jumping Robot with a Six-Bar Leg Mechanism Based on Jumping Stability. Mathematical Problems in Engineering, 2020, 1-23. doi:10.1155/2020/3507203
- Zu, Y. L., & Wei, J. (2013). Simulation and Optimization Design of Inversion Six-Bar Linkage on Loader. Applied Mechanics and Materials, 416-417, 1822-1825. doi:10.4028/www.scientific.net/amm.416-417.1822



## Re-Examine Conventional Concepts in Urban Design: The Conflict Between Urban Space Utilization and the Elements of Power and Control - Case of Hawkers within Amman, Jordan

Dania Abdel-Aziz<sup>1\*</sup> 

<sup>1</sup> The University of Jordan, Dept. of Architecture, Amman, Jordan

\* archdania.aziz@gmail.com

Received: 22.02.2021

Accepted: 01.06.2021

### Abstract

Architecture and urbanism are disciplines based on knowledge of space. From this point of view, this research aims to study the challenges of dealing with hawkers (Street Vendors) in Jordan's urban centres generally by shedding light on downtown Amman. Although they succeed in acquiring and controlling space informally in Amman, hawkers have been ignored by local planners and even been harassed by local authorities for not being given space to operate their businesses. Rigid transformations should be carried in urban planning strategies in downtown Amman. Local policies need to be enforced to end this conflict and provide suitable conditions and capacities to read and respond to the hawkers' needs. They represent an integral part of the region's urban fabric. This study is based on reviewing related literature, field survey, and observations carried out for two months in the study area. In addition to several informal discussions held with the hawkers, pedestrians, merchants, and local authorities, questionnaires were used to clarify specific issues. The study suggests a few recommendations to help fulfil urban centres' effective utilization and harmonize formal activities and the hawkers in order to resolve this conflict. The study found that street hawkers are only considered troublemakers and have never been involved in decision-making when urban planning occurs. These will be an ongoing issue, not unless they are integrated into the planning processes. The study suggests different scenarios for proper allocation of hawking space can be done regarding accommodating them according to their space requirements worked out the basis of the products sold, as has been done in the present study. In short, this will help in providing suitable trading environments for the hawkers, creating a pedestrian-friendly neighbourhood, decreasing the unemployment rate, among other advantages.

**Keywords:** Street vendors; central business district; convivial urban space; national policy; hawking space

### 1. Introduction

With the continually increasing population due to the crises in its neighbouring countries (Nilsson & Borges, 2019) and pressure on jobs, Jordan is witnessing a noticeable increase in unemployment, especially among youth. The government is now unable to provide suitable job opportunities for their citizen; that's why many Jordanians were forced to work in the

informal sector to escape worsening unemployment in the country, especially as many support their families. Despite the limited income and the high cost of living, they face daily pursuit by the local authorities who seize their goods; they are forced to pay fines or give up what was confiscated from them, making their situation worse.

Jordan's unemployment rate has been alarming and has increased from 11% in 2010 to 19% by 2019 (DoS, 2020). The participation rate of Jordan's workforce has remained one of the lowest in the world at about 40% (Husseini, 2016). The youth unemployment rate in 2018 was very high, about 37.2%, and among the highest globally (The World Bank, 2019). The unemployment rates have traditionally been higher in rural areas than in urban areas due to the concentration of jobs in urban governorates and the lack of transportation or reluctance to use it (Husseini, 2016). This made many people move from rural areas running from poverty to urban areas (rural-urban migration). But those migrants do not possess the skills or education to find suitable paid and secure employment in the formal sector. This made them settle for work in the informal sector. Sharma (2016) discussed another reason why people are pushed to work in the informal sector. According to her, many businesses, factories and workshops were closed, and the previous workers could not find a proper job; hence they had to work in the informal sector to survive.

The meaning of the informal sector has been discussed by many researchers (Schneider, 1986), (Smith, 1994), (Saunders & Loots, 2015), (Dhakal, 2015) and others. The informal sector, as Smith (1994) defines it is a market-based production of goods and services, whether legal or illegal, that escapes detection in the official estimates of GDP. According to the International Labor Office (ILO) definition, the informal sector is: "The informal economy is broadly characterized as consisting of units engaged in the production of goods and services with the primary objective of generating employment and income to the persons concerned." (ILO, 1993:2). The activities in the informal sector can be categorized into two sections; (1) the self-employed and (2) the non-permanent labour (Sharma, 2016). Self-employment is one of the modern development concepts that switched perspectives in business and employment, which means the individual's quest to find a job for themselves through the reliance on their ideas, experiences, and educational and training level. A significant section of the self-employed workers are hawkers or street vendors. The rise in the number of street hawkers is due to the lack of employment in other sectors and directly linked to the informal sector's expansion.

The term "Hawkers" is an interchangeable phrase that refers to people who tends to sell goods or offer services to the public informally in any street or public place. These activities are not being protected or supervised by the government; that's why they do not have a fixed place or a permanent built-up structure. Hawkers tend to spread or display goods in open spaces or temporary static structures to attract buyers and make sales. It also refers to the person who moves from one place to another or goes to people's homes to sell goods or merchandise that he offers for sale or deals in his craft or industry by roaming (GAM, 2009). The hawker may use a trolley, kiosk, canopy, or merely using the pavement, see Figure 1.

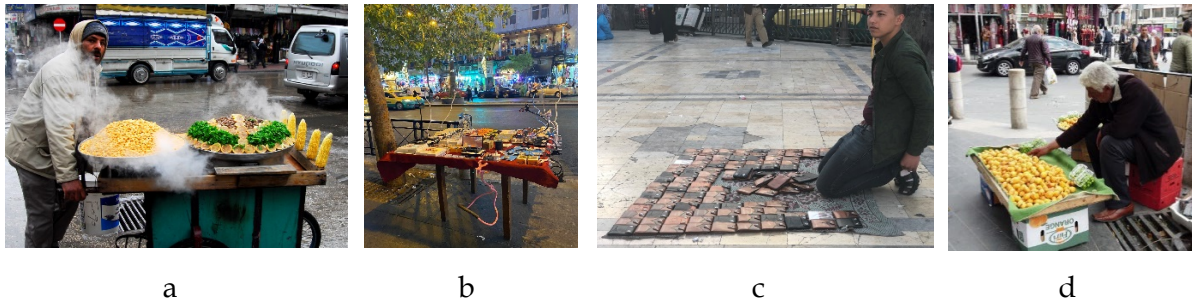


**Figure 1.** Various means used by the hawkers at the study area (Amman downtown) to present their goods and services. a) trolley, b) table, c) rug, d) boxes

Modernist planning focuses on cars' requirements rather than pedestrians' needs and expectations, making cities lose many qualities (Israt, 2019). Good accessibility is directly related to the pedestrians' thoughts and experience. It acts as a direction for the pedestrians that, as a result, affect their perception. We cannot neglect the fact that there are many problems associated with mobility and accessibility resulting from hawking in Amman downtown's streets. Simultaneously, if planners, when planning to pedestrians, took hawkers into account, many problems could be avoided. An external view of hawking in Jordan gives the impression of this sector's randomness regarding distribution and spread. In reality, it is a sector with a remarkable degree of control, and over time it had its traditions and inner life. Families are working in hawking for three generations, and there is a great deal of specialization in the sector.

The Greater Amman Municipality's (GAM) Campaigns against the phenomenon of street vending began in 1997. Some of these campaigns were very severe and targeted local markets as well (Khalil, 2019). Hawkers tended to move between many locations, while some chose to work during the night or early morning. At the same time, GAM did not provide alternative markets. GAM, as a regulatory body, is working to violate this sector because of the quality of goods that are handled since they are usually poor and not suitable for consumption. Moreover, since these workers have a specific place or are evading paying taxes and fees, it leads to a breach of security and order, the use of sidewalks, and obstructing citizens' movement. Another justification for GAM's campaigns can be in the urban landscape. But this contradicts reality, as these hawkers, especially in Amman downtown, constitute a cultural and heritage character and reflect a real image of the people. That's why these campaigns to date do not have the capabilities to withstand and continue. The GAM should see the informal sector's other sides and be aware of the critical role that the urban informal sector plays in the urban economy worldwide. An organized street vending in Amman or other urban space in Jordan could be part of city precedence for the city community's benefit.

## 2. Problem Statement

With high unemployment rates, increasing poverty, and the high cost of living in Jordan, hawkers' flow into urban centres has become a distinguishing feature of most cities. Still, they are often regarded as an 'element out of place' (Widjajanti, 2016). Their problem is the absence of reference in determining their activity's location in the city plan. Their random distribution causes many problems. For a sustainable community for its inhabitants, it must be liveable. To achieve suitable and orderly urban intervention; policy guidelines concerned with the effective use of urban centres must be formulated, customized and developed to address urban space users. In downtown Amman for example, most urban spaces are conquered by hawkers. Hawkers' rugs are spread over a wide range of different forms (see Figure 2.), on the sidewalk

inside the bazaars and local markets, in front of the Grand Hussein Mosque, see Figure 1. GAM has always fought against the hawkers. But at the same time, it did not try to understand their needs, did not provide them with job opportunities that would spare them all these conflicts. The government must provide solutions to overcome this crisis and help people. Hence the importance of recognizing them, laying down laws that regulate their work and their whereabouts in a way that achieves balance and the public interest. Sustainable planning should address spatial integration issues and resolve conflicts and hawkers' movement within the urban fabric. The purpose of this study is to examine the spatial processes and requirements in the areas where street hawkers are present. Urging the authority to propose suitable sites for hawkers, relocate them within urban spaces, plan their activities, and direct their growth and development in an organized pattern. The study assumes that the population of hawkers will continue to increase in Amman downtown. This means extra urban space is required to conduct their activities. The GAM has to restore economic growth, generate employment opportunities to absorb the unemployed's large numbers, particularly the youth, and reduce poverty levels.



**Figure 2.** Different hawkers' units spread in Amman Downtown within the study area

## 2.1. Objectives

Public spaces are open for all to use and raise the difficulties in balancing pedestrians' right to move freely in the city and the hawkers to work legally and earn money to live a better life. The research will try to solve this conflict and fill the gap and build a sustainable city community. By suggesting scenarios where hawkers can be relocated in desirable urban spaces within the urban structure, they can conduct their business, considering accessibility, comfort, and characteristics referring to their activity. From this point, the research aims to provide quantitative norms, theories and concepts for accommodating street hawkers legally in Amman downtown. See Figure 3.

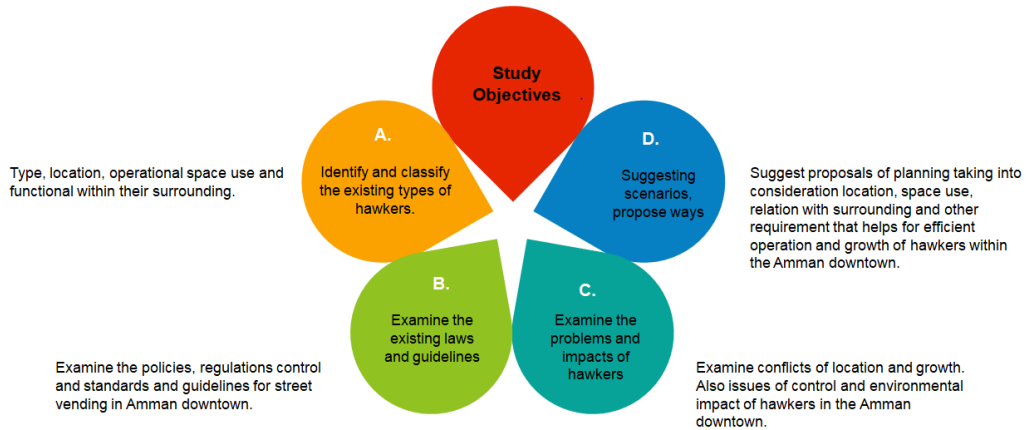


**Figure 3.** Study objectives

## 2.2. Methodology

This study is based on quantitative and qualitative methods; Figure 4 summarizes the data collection sources. This study is centred on (1) reviewing related literature; searching the concept of the informal sector, conflicts between hawkers, merchants, pedestrians and government, (2) field survey and of hawking establishments in the Amman downtown, the type of the goods, the size of the unit, etc., walking within the study area and observing pedestrian movement, the road network, how the hawkers related to the urban space and taking photographs of the activities (3) informal discussions with hawkers to collect information about the related problems and difficulties they face, the nature of their work, their needs, nature of their business, characteristics of their specific activity, their dependence on the site context, (4) questionnaires were carried out for formal business operators, pedestrians and study area visitors (5) Analysis of primary and secondary information and (6) conclusion and recommendations. The field survey was carried out after preliminary studies were made from related literature. The analysis of all collected data was presented using analytical tables. While the questionnaires were analyzed using Statistical Package for Social Science (SPSS).

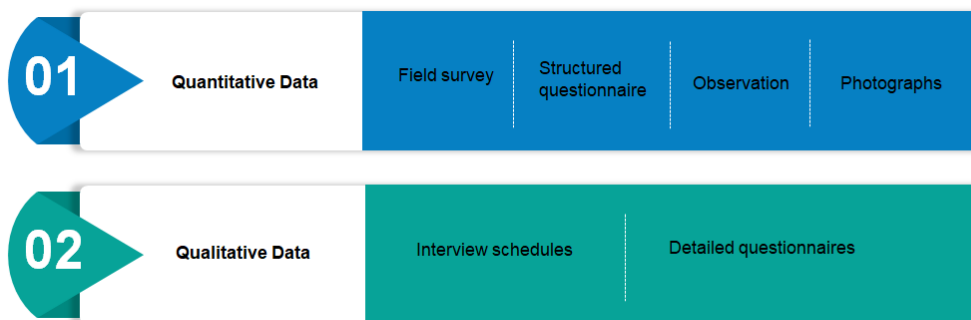


**Figure 4.** Data collection methods

## 3. Study Area

Amman is the capital of Jordan, and it covers 1680 km<sup>2</sup> of land area. 38% of Jordan's population live there; hence it is considered the most densely populated region (Potter et al., 2009). Lack of adequate housing, unemployment, poor air quality, transportation, water shortages, rapid population growth, hawking or street vending in urban centres is among the most common

problems of Amman's urbanization. These challenges are putting Amman in a massive problem in terms of its sustainability. The detailed study area in Amman downtown was defined by the area enclosed by King Faisal Square, Als-Saadeh Street, Ar-Reda Street, and the illustrated parts of King Talal Street and Shaaban Street; as shown in Figure 5 below. In the selected study area, the observation subjects were (1) spaces the hawkers were occupying and (2) the specific business venture in which the hawkers were engaged. For this study, the famous Friday market was excluded.



**Figure 5.** Study area

The target population for this research was; (1) all the hawkers who trade in the alleys of the study area, (2) pedestrians, (3) the merchants or the formal businesses owners in the surrounding area which hawkers located near their businesses and (4) the local authorities and Greater Amman Municipality departments. The activities of hawkers were extensive; this study classified them into three main “relatively” homogeneous categories; (a) food activities (such as; seasonal fruits and vegetables, local sweets, boiled corn and light snacks), see Figure 6., (b) clothing activities (such as; clothes (second hand and new ones), sunglasses, accessories, shoes, belts, watches and bags), see Figure 7. and (c) entertainment activities (such as; accessories, stationery, books, toys, lottery, perfumes, mobile accessories and magic tricks shows and home accessories), see Figure 8. Classifying them was to assess each group's different needs and specifications when relocating is being suggested.



**Figure 6.** Various hawkers who deals with food activities in the study area



**Figure 7.** Various hawkers who deals with clothing activities in the study area



**Figure 8.** Various hawkers who deals with entertainment activities in the study area

#### 4. Study Sample

The fieldwork was carried out between May 2019 and June 2019 in the selected area in Amman downtown. The observed hawkers' units were 168 units; check Tabel 1. The observation was carried out to examine the everyday use, re-use, occupation, and allocation of the urban space and the hawkers' conditions and challenges. It was noted that 152 hawking units were working in the same space uniformly. That's why, for this study, the total sample size is 152 units. The floor space occupied by hawkers is 88.5 m<sup>2</sup>. For selecting respondents, this study adopted simple random sampling to select hawkers in each category. This technique gave an equal chance to each hawker of being included in the sample.

**Table 1.** The total number and the occupied space by hawkers in the study area

Parameter	Unit
Total number of hawking units	168 unit
Total sample size	152 unit
Floor space area occupied by hawkers	88.5 m <sup>2</sup>

As a representative of the formal sector, a sample size of 12 business owners was selected in the merchants' case. The study aimed to listen to their opinions regarding relocating the hawkers next to their shops/business. While two interviews were held with the GAM staff, and data were collected from 170 respondents to the questionnaire, which was spread through this internet and targeted people who often visit Amman downtown only (respondents must be frequent visitors to the study).

A questionnaire survey was done with hawkers in the study area, most of whom cooperated by answering the questions whilst others refused to answer due to fear. That's why observation was also performed to validate the results and strengthen the findings. This

survey included structured questions to collect information about the relationship between hawking and public space to build a holistic perception of the current situation in Amman downtown. The questionnaire survey collected data on activities, hawking duration, access, the chosen location, sociability, the informal sector, safety, comfort, uses, faced problems and the user's desires. The data was analyzed using SPSS.

## 5. Analysis and Discussion

### 5.1. Site Potentials

Amman Downtown, which has served as a central commercial area, has many other different land-use activities, which have led to a high frequency of passing for local people and tourists every day. Hawkers assessed this situation as an opportunity to be a selling location and utilize the space for trading activities; Table 2 below summarizes the streets' spatial dimensions and hawkers' percentage in the study area. The accessibility to this area was easy since it is served with public transportations from different locations. Although it is considered a crowded area, the affordable prices of goods and services offered around this area attract consumers. These conditions make this place an attractive area for hawkers to construct their businesses. Moreover, easy access to public transportation relieves the load for hawkers.

**Table 2.** Spatial dimensions of the streets and hawkers' percentage in the study area

Street name	Street length*	Percentage of hawkers
King Faisal Square	205.90 m	50.66%
Ar-Reda Street	102.50 m	8.55%
As-Saadeh Street	103.30 m	9.21%
King Talal Street	380.50 m	30.26%
Shaaban Street	77 m	1.32%

\* The street's length represents the covered part that the study managed to collect data

### 5.2. Strategic Location

As concluded from the field survey, hawking activities operate in the open, pavement, lanes, and alleys, see Figure 9. The desirable location for hawkers is located within busy pedestrian routes with different activities (shops, hotels, restaurants, etc.) around public transport terminals and bazaars. In other words, the land use activities influenced them to select the space from which they operate. Each day hawkers take their respective positions with their wares ready to sell to potential buyers. They consider that the particular space is attractive for consumers and is located between various activities with a high visitor rate and a high frequency of mobility.



**Figure 9.** Various pictures show the randomness of hawkers' unit locations within the study area

Every specific space has an owner; as indicated by interviewed hawkers, no other trader would occupy the space without the original space owner's approval. This is a rule that should not be broken. Many hawkers have worked in the same space for more than 40 years, going from generation to generation. Youth hawkers indicated that their fathers were working in the same space before, and now it's their turn to keep working to live. This means that even this informal sector has its own rules. These locations, as hawkers noted, should be safe. In other words, space should be smoothly running away from and easy to be mobile to avoid arrest.

As concluded from the interviews, hawkers transport their goods by two means; 1) on foot. This is done by buying goods from a walking distance market downtown, carrying them on their backs and walking to their trading space, 2) using public transportation to move their goods. From this point, another influence can be seen in selecting its desirable location: public transportation availability. Public transportation facilitates the movement of goods as well as access to the site from their homes.

Some pedestrians complained that some pavements and alleys are just too narrow to accommodate all users and that they cannot move easily. It is recommended that hawkers be removed from streets with such issues to get rid of congestion that obstructs pedestrians' movement.

### 5.3. Right in Urban Space

The hawkers' general problem in their daily operations can be summarized as not being provided with ideal urban space to perform their activities, protecting them from climatic conditions (sun, rain), insecurity, and harassment by the GAM. From the interviews, hawkers pointed out a few critical needs to achieve a convenient place to trade; availability of ample space, ease of modification of goods' means, ease of preparation and presentation of goods, and freedom of movement to serve buyers. They are not governed by the time schedules, such as the formal sector, which gives this sector an advantage of being flexible. Pedestrians agreed that hawkers should have the right to work in the urban space and streets. They also said that they prefer in many times to buy from them because they offer good services within suitable prices compared to shops. On the other hand, many used to buy from them just to help them for living.

As indicated from the survey, the hawkers use trolleys, wooden stands, tables and mats, which they put on the ground to display their goods and services. They tend to use light materials and structures to help them smoothly run away from the GAM. The hawkers who traded in shoes and clothes displayed their goods on light mats to make it easy for customers to pick. The hawking unit's size varies depending on the goods they sell, as indicated in Table 3 below.

The most common unit size for the food activities category was 1.0\*1.0 m<sup>2</sup> while 2.0\*2.0 m<sup>2</sup> and 2.5\* 2.0 m<sup>2</sup> for clothing and entertainment activities categories.

**Table 3.** Space occupied by hawkers within the study area

Product type	Occupied Space (m <sup>2</sup> )											
	1.0*1.0	1.0*1.5	1.5*1.5	1.5*2.0	2.0*2.0	2.5*2.0	2.5*3.0	2.0*3.0	3.0*3.0	2.5*3.5	3.0*4.0	2.5*4.0
Food activities	28.5%		12.4%	16.5%		13.6%		16.5%		18.5%		
Clothing activities	15.8%	16.5%	5.5%	11.5%	17.3%	8.5%	6.5%	4.5%	6.9%	3.8%		3.2%
Entertainment activities	15.4%		20.3%	10.3%	17.4%	21.5%	3.4%		7.5%		2.2%	2.0%

#### 5.4. GAM Act with Regards to Hawking

The Greater Amman Municipality (GAM) carries out the responsibility of regulating hawking activities in Amman. The primary law is "System for monitoring and organizing hawkers, rugs, umbrellas and kiosks within the boundaries of the municipal areas No. 81 for the year 2009" (GAM, 2009). The provision of this law applies to all municipalities in Jordan except Greater Amman Municipality.

It should be mentioned that in the study area, few hawkers were legally working. When examining these cases, there is a special case or story behind every one of them. One trader has been working for 40 years, having inherited it from his past generation (Family inheritance). The trader specializes in selling Islamic rosaries and other religious products due to its location in the Grand Husseini Mosque plaza. It should be noted that it has been allowed by King Hussein bin Talal. See Figure 10. Another licensed unit is located in King Faisal Street, which a person owns with special needs. This particular trader possesses a license and identification papers that exempt him from paying any fees to the GAM due to his health condition. He noted that it was his only source of income, See Figure 11.



**Figure 10.** Grand Husseini Mosque case

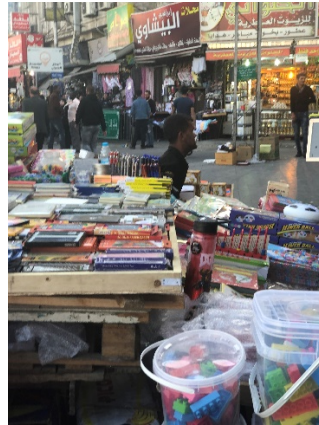


**Figure 11.** King Faisal Street case

The third one is in King Faisal Street, located at a corner in front of the Gold Market and is dedicated to selling fresh peanuts and has been trading for more than 60 years. This selling unit was distinguished by the fact that tourists were attracted to that particular sight of the owner doing his business. Taking a picture of/with him is no less important to them than taking a picture in the Roman amphitheatre in the same area. Figure 12. Below



**Figure 12.** Gold Market case (Alddemh, 2009)

From here, it should be noted that the hawkers in Amman downtown are part of the place's cultural heritage, and they are what attracts tourists to the place. The GAM should help in the economic recovery by supporting hawkers; provide them with permanent trading spaces to overcome the crisis of poverty and the high unemployment rates. This will help achieve improved services by making the urban spaces an attractive place for everyone to live and do business legally without the fear of harassment.

### 5.5. Product/Activity Type

The field study showed many different types of goods hawkers tend to deal with, such as; fruits and vegetables, clothes and bags (second hand and new ones), sunglasses, toys, stationery, lottery, mobile accessories, light snacks. The distribution and percentage of their activities are summarized in Table 4. The field survey indicates that within the different hawking activities distributed along the study area, clothes and toys (28.29%, 21%, respectively) were the most percentage of the sample size. As mentioned above, this study classified those various types of activities into three categories; check Table 5. Results showed that the maximum concentration of the different categories was located in King Faisal Square.

**Table 4.** Distribution of hawking units as per their product type

Product type	King Faisal Square	As-Saadeh Street	Ar-Reda Street	King Talal Street	Shaaban Street	In Total
Toys	15.07%	2.63%	1.98%	-	1.32%	21%
Stationary & Books	1.98%	0.66%	1.32%	1.32%	-	5.28%
Watches	0.66%	-	-	0.66%	-	1.32%
Accessories	6.58%	-	0.66%	1.32%	-	8.56%
Perfumes	-	-	0.66%	2.63%	-	3.29%
Clothes	8.55%	2.63%	1.32%	15.79%	-	28.29%
Mobile acc.	5.26%	-	0.66%	-	-	5.92%
Sunglasses	1.2%	-	-	1.97%	-	3.17%
Shoes	2.63%	1.32%	0.66%	0.66%	-	5.27%
Bags	2.63%	0.66%	-	0.66%	-	3.95%
Home stuff	3.29%	1.32%	-	3.23%	-	7.84%
Food	3.23%		1.68%	1.2%	-	6.11%

**Table 5.** Distribution of hawking units as per their main category

Main category	King Faisal Square	As-Saadeh Street	Ar-Reda Street	King Talal Street	Shaaban Street
Food activities	3.23%	-	1.68%	1.2%	-
Clothing activities	21.71%	4.61%	2.64%	21.06%	-
Entertainment activities	26.14%	4.61%	4.62%	7.18%	1.32%

## 5.6. The Formal Businesses

The study showed that most of the formal business sector's problem was that there existed an unfair competition between them and the hawkers, especially if they happen to be selling the same product. However, they have no problem with the presence of hawkers in the area, as long as it does not affect their work. The study also noted that the formal business sector is the suppliers of goods and customers to the hawkers trading in the study area. Some shop owners at the study area used to supply hawkers with products sold at competitive prices or accumulated and wanted to dispose them off and sell them at bargaining prices because there was not enough space in their warehouses.

One of the interviewed hawkers noted that many of them tended to pay a fixed price for the adjacent shop owners to guarantee a specific place for them on the street. While another one said that he has been working for eight years at the same space because the adjacent shop belongs to one of his relatives, he will not pay this amount of money. This is evidence of many points of agreement and points of disagreement between the two parties.

## 5.7. Hawking Units

The hawking unit's size is essential to be taken into consideration because planners need to ensure that the units are not infringing on the pavements and are not an obstacle to pedestrian movements. The size of a hawking unit varies depending on the specific type of product offered. Standardizing could be problematic in general, but it would be much more efficient in the same category.

The GAM would get revenue in regards to the space occupied. The study recommends that the rates charged by the GAM should reflect the space a hawking unit occupies. This will mean that hawkers pay the GAM for the size of space they need considering that every potential location has a maximum and minimum occupancy area controlling the number of hawkers that can be accommodated in an urban space. Taking into consideration that the desired unit size depends on the spatial needs of each activity, this study suggested space requirements for the hawking unit as follows:

- 1) Hawking zones should be at the entry/exit points of transport nodes and parking areas. Those zones should be at specific static structures located on pavements and footpaths to assure buses and cars smooth movement.
- 2) The GAM allowed seven markets in Amman that work during the weekdays. The Friday Market at Ras Alain area was one of them, see Figure 13. It is open every Friday and located in an empty parking area. From here rises the point of spreading this successful case by allowing specific parking areas to accommodate the hawkers during the non-working days.



**Figure 13.** The Friday Market at Ras Al-Ain area; left: designed space, right: space within working hours (Ammonnew, 2014)

- 3) To avoid clashes with the official shop owners; care must be taken into consideration; (a) maintain a precise distance between the shops and the hawking units, (b) ensure that the hawking units and the shops are not offering the same type of goods and services, (c) maintain sufficient distance for pedestrians to move between the official store and the hawking unit.
- 4) The width of the pathways should also be taken into consideration. The pathways' minimum width in which it's considered suitable for hawking should not be less than 4 meters. In comparison, units should be separated by a distance of 5 meters minimum to assure pedestrians' free movement and hawkers to work sufficiently.

## 6. Conclusions and Recommendations

Planning should consider the importance of making hawking zones in different streets/cities in Jordan a legal working space because it is believed that an organized street hawking in the urban spaces could be part of city precedence for the city community's benefit. Planners should

know the need for street hawkers to locate them in certain places may be even at certain times. Those strategic locations should be selected due to accessibility, main activity, demand and space comfort. Indeed, much care should be placed on the street design and ensure a smooth flow for pedestrian movements and the local merchants' interests.

Through participatory planning - while organizing hawkers' activity - planners should ensure all stakeholders' integration to ensure equality, sustainability, and durability of this activity. Hawkers - the urban poor - should be included in formulating and implementing a street roaming activity as part of the stakeholders. Participation will raise awareness about the problem situation, make them more understanding of proposed improvements, and feel more responsible and committed to change. By this, success has a better chance. In short, instead of treating hawkers as an outlaw that only create chaos on the streets, they should be allowed to contribute, Street hawkers can be assets to the development of the urban system. Pedestrian pathways, transport nodes and parking areas have the potential to accommodate hawkers. If adequately located despite the small space, they will find a stable job, a better income and equal dignity as other citizens. By this, hawkers will become a part of the city's socio-economic fabric rather than a problem in this fabric.

Through the development process for Amman's new master plan, the Greater Amman Municipality should provide detailed enforcement procedures for customizing its standards for hawking by specifying the implementing authority. The mechanism and criteria for allocating hawking space and assuring that hawking space allocation should be considered while planning and designing. The hawking space size needs been discussed in this research, but it cannot be generalized to include all the streets or cities in Jordan. Every street and city has a different case scenario. There are some fixed specifications, but it is advised that the space norms for hawking should be included in each zonal development plan for each city alone in Jordan.

### Author Statement

The author confirms sole responsibility for the following: study conception and design, data collection, analysis and interpretation of results, and manuscript preparation.

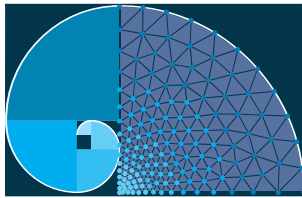
### Conflict of Interest

The author declares no conflict of interest.

### References

- Alddemh, M. (2009). *The peanut seller who became one of Amman's landmarks*. Online: <https://archive.aawsat.com/details.asp?issueno=10992&article=506263#.YiGL5Azbi c> (April, 2020).
- Ammonnew (2014). Online: <https://www.ammonnews.net/article/212250> (April, 2020).
- Bank, T. W. (2019). *World Development Indicators | The World Bank*. <http://wdi.worldbank.org/tables>
- Dhakar, R. C. (2014). *Classification of Informal sector activities in Chitwan District*. The Academia Vol. 2 No. 1, pp. 106- 120.
- DoS. (2020). *Unemployment rate during the first quarter of 2020*. [http://dos.gov.jo/dos\\_home\\_a/main/archive/unemp/2020/Emp\\_Q1\\_2020.pdf](http://dos.gov.jo/dos_home_a/main/archive/unemp/2020/Emp_Q1_2020.pdf)
- Husseini, J. Al. (2016). Challenges Facing Jordan's Labour Market. In *Atlas of Jordan* (pp. 354-368). Presses de l'Ifpo. <https://doi.org/10.4000/books.ifpo.5039>
- International Labour Organization. (1993). *Resolution concerning statistics of employment in the*

- informal sector. January, 300.* [https://www.ilo.org/wcmsp5/groups/public/---dgreports/---stat/documents/normativeinstrument/wcms\\_087484.pdf](https://www.ilo.org/wcmsp5/groups/public/---dgreports/---stat/documents/normativeinstrument/wcms_087484.pdf)
- Khalil, A. A. (2019). *Fighting rugs is definitely a losing battle.* <http://www.zamancom.com/?p=2960>
- Kjell & Borges. (2019). *Amman, one of the fastest grown cities in the world, is moving towards sustainable city planning | Nordregio.* <http://nordregio.org/amman-one-of-the-fastest-grown-cities-in-the-world-is-moving-towards-sustainable-city-planning/>
- Great Amman Municipality. (2009). *System for monitoring and organizing street vendors, rugs, umbrellas and kiosks within the boundaries of the municipal areas No. 81 for the year 2009.* <https://portal.jordan.gov.jo/>
- Saunders, S., & Loots, E. (2015). Measuring the informal economy in South Africa. *South African Journal of Economic and Management Sciences*, 8(1), 92–101. <https://doi.org/10.4102/sajems.v8i1.1286>
- Schneider, F. (1986). Estimating the Size of the Danish Shadow Economy using the Currency Demand Approach: An Attempt. *The Scandinavian Journal of Economics*, 88(4), 643. <https://doi.org/10.2307/3440435>
- Sharma, S. (2016). Hawking Space and National Policy on Urban Street Hawkers: A Study of NDMC, Delhi. *Procedia Technology*, 24, 1734–1741. <https://doi.org/10.1016/j.protcy.2016.05.207>
- Smith, P. (1994). Assessing the Size of the Underground Economy: The Statistics Canada Perspective - ARCHIVED. *Canadian Economic Observer*, 3(11-010), 16–33. <https://www150.statcan.gc.ca/n1/en/catalogue/13-604-M1994028>
- Potter, R. B., Darmame, K., Barham, N., and Nortcliff, S. (2009), “Ever-growing Amman”, Jordan: Urban expansion, social polarisation and contemporary urban planning issues. *Habitat International*, 33(1), 81- 92
- Widjajanti, R. (2016). The space utilization by street vendors based on the location characteristics in the education area of Tembalang, Semarang. *Procedia-Social and Behavioral Sciences*, 227, 186-193.



## Ensemble of Classifiers and Term Weighting Schemes for Sentiment Analysis in Turkish

Aytuğ Onan<sup>1\*</sup> 

<sup>1</sup> Department of Computer Engineering, Faculty of Engineering and Architecture, İzmir Katip Çelebi University, İzmir, Turkey

\* Corresponding author: aytug.onan@ikcu.edu.tr

Received: 21.03.2021

Accepted: 29.06.2021

### Abstract

With the advancement of information and communication technology, social networking and microblogging sites have become a vital source of information. Individuals can express their opinions, grievances, feelings, and attitudes about a variety of topics. Through microblogging platforms, they can express their opinions on current events and products. Sentiment analysis is a significant area of research in natural language processing because it aims to define the orientation of the sentiment contained in source materials. Twitter is one of the most popular microblogging sites on the internet, with millions of users daily publishing over one hundred million text messages (referred to as tweets). Choosing an appropriate term representation scheme for short text messages is critical. Term weighting schemes are critical representation schemes for text documents in the vector space model. We present a comprehensive analysis of Turkish sentiment analysis using nine supervised and unsupervised term weighting schemes in this paper. The predictive efficiency of term weighting schemes is investigated using four supervised learning algorithms (Naive Bayes, support vector machines, the k-nearest neighbor algorithm, and logistic regression) and three ensemble learning methods (AdaBoost, Bagging, and Random Subspace). The empirical evidence suggests that supervised term weighting models can outperform unsupervised term weighting models.

**Keywords:** Ensemble methods; term weighting schemes; sentiment analysis; text classification

### 1. Introduction

With the tremendous growth of social media and microblogging sites, the enormous quantity of information available will serve as an important source for decision making, regarding products, services, and policies (Onan, 2017; Onan, 2018). People may express their views, complaints, feelings, and attitudes towards subjects. They can express their ideas about current issues, and products through microblogging platforms.

Twitter is one of the most common microblogging sites in the world, in which millions of people publishing more than one hundred million text messages (referred as, tweets) every single day. On Twitter, users can send short messages with a character limit of 280. On Twitter, users can post messages about real-world events occurring around the world, aside from personal tweets. Many incidents are now being posted on Twitter for the first time, as near

real-time as it occurs (Samant et al., 2019). The content created by users on Twitter provides researchers and practitioners with a valuable source of information, which can be employed for several applications, including earthquake prediction (Sakaki et al., 2010), influenza epidemics (Woo et al., 2018), and crisis management (Hecht et al., 2011).

Sentiment analysis is a task in natural language processing, which seeks to identify the semantic orientation of text documents, with the use of tools and techniques from computer science, data science and statistics (Onan and Korukoğlu, 2017). Sentiment analysis can be employed to obtain useful information from unstructured text documents. Traditional application fields for sentiment analysis include the detection of public sentiment for policy-making purposes and the market analysis of goods and services based on feedbacks of consumers (Zhang et al., 2009; Fersini et al., 2014). In that sense, organized, insightful knowledge obtainable by recognizing subjective information from online content can be extremely useful for decision making, including decision support systems and individual decision makers (Onan et al., 2016). The approaches used in sentiment analysis can be divided into two groups, as machine learning-based and lexicon-based methods. In machine learning-based sentiment analysis, the identification of sentiment orientation has been modelled as a text classification problem, in which supervised learners, such as Naïve Bayes, support vector machines and artificial neural networks have been employed (Aggarwal and Zhai, 2012).

For short text messages, the identification of an appropriate term representation scheme is a crucial task. In the vector space model, term weighting schemes are important schemes to represent text documents.

In this paper, we present a comprehensive analysis on sentiment analysis in Turkish with two unsupervised term weighting schemes (i.e., term frequency, and TF-IDF) and seven supervised term weighting schemes (i.e., odds ratio, relevance frequency, balanced distributional concentration, inverse question frequency-question frequency-inverse category frequency, short text weighting, and inverse gravity moment and regularized entropy). Four supervised learning algorithms (i.e., Naïve Bayes, support vector machines, k-nearest neighbor algorithm and logistic regression) and three ensemble learning methods (i.e., AdaBoost, Bagging and Random Subspace) are used to explore the predictive efficiency of the term weighting schemes. To the best of our knowledge, it is the first study in Turkish text sentiment classification, where supervised and unsupervised term weighting schemes have been comprehensively evaluated in conjunction with supervised learning models and ensemble classification models. The experimental results indicate that supervised term weighting models can outperform unsupervised term weighting models.

The remainder of the paper is structured as follows: Related work on sentiment analysis is discussed in Section 2. Section 3 presents the term weighting schemes. Section 4 presents classifiers, Section 5 presents the ensemble methods. The experimental procedure, dataset and the empirical results are discussed in Section 6. The concluding remarks have been presented in Section 7.

## 2. Related Work

Sentiment analysis on the content created by users on Twitter has attracted great research attention. The early work on sentiment analysis on Twitter data is briefly reviewed in this section.

Go et al. (2009) evaluated the predictive performance of maximum entropy and support vector machine classifiers for sentiment analysis on Twitter messages. In this study, text documents are represented using different structures such as 1-gram, 2-gram, and part-of-speech tags. It

was observed that 80% correct classification performance was achieved with the developed method. In another study, Agarwal et al. (2011) examined the effectiveness of 1-gram scheme, feature engineering-based schemes and tree-based data representation for sentiment analysis on Twitter. In the 1-gram representation, the data set is represented by using around 10000 features, while the number of features in the representation based on feature engineering was reduced to 100, but the correct classification performance was kept higher. On the other hand, it has been observed that the highest accuracy classification achievements are obtained when Twitter messages are represented using the tree structure. Similarly, Kouloumpis et al. (2011) evaluated the effectiveness of n-gram features, dictionary-based features, part-of-speech tags, and Twitter-specific features for sentiment analysis on Twitter messages. In the empirical analysis, the highest predictive performance has been obtained by n-gram features. In the study performed by De Boom et al. (2016), word2vec word embedding scheme and a weighted word embedding vector extraction method based on TF-IDF weighting function were presented to capture the semantic integrity on short text documents, such as Twitter messages.

Similarly, Djaballah et al. (2019) evaluates the predictive performance of machine learning and deep learning-based schemes for sentiment analysis on Twitter messages. In experimental analysis, vectors obtained using word2vec word embedding method were considered in two different ways, namely, unweighted, and weighted vector pooling. Experimental results show that weighted vector pooling gives higher performance. The predictive performance of various n-gram models (namely unigram, bigram, and trigram) and their combinations on sentiment analysis of Turkish Twitter messages were examined by Onan (2017). In empirical research, the combination of unigram and bigram features achieves the highest predictive efficiency. In a similar way, Onan (2018) introduced an ensemble approach to sentiment analysis on Twitter based on LIWC (i.e., Linguistic Inquiry and Word Count) categories. In the study performed by Şahin (2017), vectors obtained by word2vec word embedding scheme and support vector machines have been utilized to classify Turkish text documents. In another study, Griol et al. (2020) presented an ensemble classification scheme for sentiment analysis on Twitter messages, which incorporates ensemble of feature sets based on opinion lexicons, n-grams, and word clusters in conjunction with maximum entropy classifier. Similarly, Samant et al. (2019) examined the predictive performance of supervised and unsupervised term weighting schemes for sentiment analysis on Twitter and they presented a novel improved supervised term weighting model. Recently, Carvalho and Plastino (2020) comprehensively examined the predictive performance of n-gram features, meta-level features, microblog features, part-of-speech features, surface features, emoticon features, and word embedding based features on sentiment analysis for Twitter messages.

### 3. Term Weighting Schemes

Term weighting schemes can be classified predominantly into two categories, as unsupervised and supervised term weighting schemes (Samant et al., 2019). For unsupervised term weighting schemes, category information is not utilized to allocate weight values to words, whereas supervised term weighting schemes use category information from the training data for a particular term. Let  $N$  denote the total number of documents in the corpus, let  $tf$  denote the frequency of the word indicating the number of times in the document a specific term has been encountered, and let  $df$  denote the number of documents in which at least one specific term has been encountered.

Term frequency ( $tf$ ) is an unsupervised term weighting scheme to compute weight value  $w_{d_i,t_j}$  for term  $t_j$  in document  $d_i$ , as given by Equations 1 and 2 (Samant et al., 2019):

$$w_{d_i,t_j} = tf \quad (1)$$

$$w_{d_i,t_j} = \begin{cases} 1 & , \text{ term encountered} \\ 0 & , \text{ term not encountered} \end{cases} \quad (2)$$

Term frequency-inverse document frequency (TF-IDF) is another unsupervised term weighting scheme on information retrieval and text mining. Term frequency represents the relative frequency of a word  $t$  in a text document and inverse document frequency scales with the number of documents. TF-IDF weighting scheme can be computed as given by Equation 3:

$$w_{d_i,t_j} = tf * \log\left(\frac{N}{df}\right) \quad (3)$$

Odds ratio (OR) is a supervised term weighting scheme, which is the ratio of the probability of occurrence of an event in one group to the probability of occurrence in another group. OR can be computed as given by Equation 4 (Quan et al., 2010):

$$OR = \log\left(\frac{tp * tn}{fp * fn}\right) \quad (4)$$

where  $tp$  denotes true positives,  $tn$  denotes true negatives,  $fp$  denotes false positives and  $fn$  denotes false negatives.

Relevance frequency (RF) is another supervised term weighting scheme. In this scheme, the ratio of number of positive category (positive class label) documents consisting of the word to the number of negative category (negative class label) documents containing the word has been considered to compute weight values, as given by Equation 5 (Lan et al., 2006):

$$RF = \log\left(2 + \frac{tp}{\text{Max}(1, fn)}\right) \quad (5)$$

Balanced distributional concentration ( $bdc$ ) is another supervised term weighting scheme based on entropy. Balanced distributional concentration test term  $t$ 's discriminating power based on its distribution in different categories ( $c_i$ ). Balanced distributional concentration can be computed, as given by Equation 6 (Wang et al., 2015):

$$bdc = 1 - \frac{BH_t}{\log(K)} \quad (6)$$

$$BH_t = - \sum_{i=1}^K \frac{p(t/c_i)}{\sum_{i=1}^K p(t/c_i)} \log\left(\frac{p(t/c_i)}{\sum_{i=1}^K p(t/c_i)}\right) \quad (7)$$

where  $K$  denotes total number of categories in the training data and  $p(t/c_i)$  denotes the probability of term  $t$  in category  $c_i$ .

Inverse question frequency-question frequency-inverse category frequency (IQF) is another supervised term weighting scheme for short text classification, which can be computed as given by Equation 8 (Quan et al., 2010):

$$iqf = \log\left(\frac{N}{tp + fn}\right) * \log(tp + 1) * \log\left(\frac{K}{cf} + 1\right) \quad (8)$$

where  $cf$  denotes the number of categories that have at least one document in which  $t$  has been encountered. Short text weighting (SW) is another supervised term weighting scheme for short text classification, which can be calculated as given by Equation 9:

$$W(t_{ij}) = \frac{tf_{ij} + 1}{\sum_{j=1}^{|T|} tf_{ij} + |T|} * \log \left( 1 + \frac{tp}{fp + fn + 1} \right) \quad (9)$$

where  $j$  denotes term present in document  $i$ , which contains  $|T|$  terms and  $tf_{ij}$  denotes the frequency of it.

Inverse gravity moment ( $IGM$ ) is another supervised term weighting scheme based on class-specific gravity (Chen et al., 2016). Inverse gravity moment-based weight value for a term  $t_i$  has been computed as given by Equations 10 and 11:

$$W(t_{ij}) = 1 + \lambda * IGM(t_i) \quad (10)$$

$$IGM(t_i) = \frac{f_{i1}}{\sum_{r=1}^K f_{ir} * r} \quad (11)$$

where  $\lambda$  is the parameter which has been set according to (Samant et al., 2019) and  $f_{ir}$  denotes term's frequency in category  $r$ .

Regularized entropy ( $RE$ ) is another supervised term weighting scheme, which seeks to find a balanced weighting scheme for terms by measuring term distribution. Regularized entropy can be computed as given by Equation 12 (Wu et al., 2017):

$$RE = b + (1 - b) * (1 - h), \text{ where } b \in [0,1] \quad (12)$$

$$h = -p^+ * \log(p^+) - p^- * \log(p^-) \quad (13)$$

$$p^+ = - \frac{tp/(tp + fp)}{\frac{tp}{tp + fp} + \frac{tp}{fn + tn}} \quad (14)$$

$$p^- = - \frac{fn/(fn + tn)}{\frac{tp}{tp + fp} + \frac{tp}{fn + tn}} \quad (15)$$

#### 4. Supervised Learning Models

Naïve Bayes, support vector machines, k-nearest neighbour, and logistic regression algorithm are used to evaluate the predictive efficiency of unsupervised and supervised term weighting schemes.

Naïve Bayes algorithm (NB) is a probabilistic classification algorithm based on Bayes' theorem. Owing to the assumption of conditional independence, it has a basic structure. It can be used efficiently in text and web mining applications, despite its simple structure (Onan, 2016).

Support vector (SVM) machines are supervised learning algorithms that can be used to solve problems with classification and regression based on maximum margin hyperplane. To classify both linear and non-linear data, they can be applied effectively (Onan, 2017). To solve classification or regression problems, support vector machines construct a hyperplane in a higher dimensional space. By reaching the greatest distance to the nearest training data points of classes, the hyperplane seeks to make a good separation.

An instance-based classifier is the K-nearest Neighbour Algorithm (KNN). The class label of each instance in the KNN algorithm is calculated based on the k-nearest neighbours of the instance. A majority voting mechanism is used to decide the class label, based on the predictions of neighbouring instances.

Logistic regression (LR) is a linear classification algorithm that uses a linear function of a collection of predictor variables to model the likelihood of occurrence of any event (Kantardzic, 2011). Linear regression can provide good outcomes. The membership values produced by linear regression, however, cannot always be within the [0-1] range, which is not an acceptable probability range. A linear model is based on the transformed target variable in logistic regression, while removing the stated problem.

## 5. Ensemble Learning Models

Three ensemble learning methods (i.e., AdaBoost, Bagging and Random Subspace) are used to explore the predictive efficiency of the term weighting schemes.

The AdaBoost algorithm is a common method of ensemble learning that aims to obtain a robust classification system by focusing on hard-to-classify data points (Freund and Schapire, 1996). The weight values assigned to the training set instances are modified in this method such that the weight values of misclassified instances are increased, while the weight values of properly classified instances are reduced. The learning algorithms therefore concentrate on the classification of difficult cases.

Bagging (Bootstrap aggregating) is a common method of ensemble learning that aims to achieve a single prediction with higher predictive output by combining weak algorithms of learning trained on different training sets (Breiman, 1996). Different training sets are obtained in this scheme by simple random sampling with substitution. By majority voting or weighted voting, the forecasts of poor learning algorithms are combined.

The random subspace algorithm is an ensemble learning algorithm that combines many classifiers trained on randomly selected subspaces of functions (Ho, 1998). The algorithm aims to avoid over-fitting by training the weak learning algorithms on various samples of the feature space, thus providing high predictive efficiency.

## 6. Experimental Procedure and Empirical Results

This section presents the experimental procedure, evaluation measures, and the empirical results of the study.

In the experimental analysis, a data set containing Turkish Twitter messages was created to evaluate the performance of the unsupervised and supervised term weighting schemes. The dataset was acquired over a two-month period using an application written in Python using the Twitter API. In the sentiment analysis dataset, there are a total of 21000 Twitter messages, 10500 of which are positive and 10500 are negative. On the data set, pre-processing steps such, as stemming, extraction of stop words, and root finding were applied. To annotate raw Twitter messages, we used an annotation process in which each message was assigned to one of two categories based on its sentiment orientation: positive or negative. The raw messages have been annotated by two experts. Cohen's kappa ( $\kappa$ ) metric has been calculated. We obtained a score of 0.82 for the corpus, indicating perfect agreement between the annotators.

During the stemming phase, Twitter messages reporting both a positive and a negative statement were removed from the data set. In addition, each of the letters in the messages has been converted to lowercase letters, punctuation marks, numbers, and special characters such as '@', '#' have been removed. Text messages were filtered by terms and character length, duplicate letters were removed. Lucene application development interface was used to extract the stop words, and Zemberek library was used in the root finding phase.

The performance of the data set represented by these data representation methods was evaluated with four basic classifiers, namely, k-nearest neighbour algorithm (KNN), support vector machines (SVM), logistic regression (LR) and Naive Bayes (NB). In addition, three ensemble learning methods (i.e., AdaBoost, Bagging and Random Subspace) are used to explore the predictive efficiency of the term weighting schemes. In machine learning based experimental analysis, 10-fold cross validation was used. Implementation was done with WEKA 3.9 via default parameter values.

To evaluate the performance of term weighting schemes, classification algorithms and ensemble learning methods, classification accuracy and F-measure have been utilized.

Classification accuracy (ACC) is the proportion of true positives and true negatives obtained by the classification algorithm over the total number of instances as given by Equation 16:

$$ACC = \frac{TN + TP}{TP + FP + FN + TN} \quad (16)$$

where  $TN$  denotes number of true negatives,  $TP$  denotes number of true positives,  $FP$  denotes number of false positives and  $FN$  denotes number of false negatives.

Precision (PRE) is the proportion of the true positives against the true positives and false positives as given by Equation 17:

$$PRE = \frac{TP}{TP + FP} \quad (17)$$

Recall (REC) is the proportion of the true positives against the true positives and false negatives as given by Equation 18:

$$REC = \frac{TP}{TP + FN} \quad (18)$$

F-measure takes values between 0 and 1. It is the harmonic mean of precision and recall as determined by Equation 19:

$$F - measure = \frac{2 * PRE * REC}{PRE + REC} \quad (19)$$

In Tables 1 and 2, the classification accuracy values, and F-measure values obtained by unsupervised and supervised term weighting schemes on conventional classification algorithms and ensemble learning methods have been presented, respectively. As it can be observed from the empirical results listed in Table 1, supervised term weighting schemes outperform the unsupervised term weighting schemes for short text classification in Turkish.

Regarding the empirical results presented in Tables 1 and 2, the highest predictive performance among the conventional classification algorithms has been generally obtained Naïve Bayes algorithm in conjunction with supervised and unsupervised term weighting schemes. Ensemble learning models outperform the conventional classification schemes when term weighting-based text representation models have been utilized for text representation in Turkish. The highest predictive performances among all the compared schemes have been generally obtained by random subspace ensemble of support vector machines. Among all the compared supervised and unsupervised term weighting schemes, regularized entropy (RE) outperforms the other term weighting schemes. The highest predictive performance among all the compared configurations has been achieved by regularized entropy-based term weighting in conjunction with random subspace ensemble of support vector machines.

**Table 1.** Classification accuracies by learning algorithms and term weighting methods

Weighting Scheme	TF	TF-IDF	OR	RF	BDC	IQF	SW	IGM	RE
NB	79.60	78.15	82.72	82.92	83.19	83.37	82.98	83.24	83.31
SVM	78.88	77.43	82.04	82.33	82.55	82.75	82.52	82.74	82.79
KNN	72.38	70.93	77.20	77.68	78.04	78.24	77.87	78.19	78.32
LR	76.53	75.08	79.88	80.19	80.46	80.65	80.31	80.48	80.94
AdaBoost (NB)	82.70	81.25	86.26	86.42	86.83	87.11	87.22	87.61	88.19
AdaBoost (SVM)	80.37	78.92	83.67	83.91	84.17	84.35	84.02	84.28	84.39
AdaBoost (KNN)	79.39	77.94	82.63	82.82	83.09	83.41	83.05	83.22	83.40
AdaBoost (LR)	73.82	72.37	78.58	79.05	79.37	79.48	79.17	79.49	79.61
Bagging (NB)	76.64	75.19	79.96	80.23	80.58	80.67	80.37	80.89	80.97
Bagging (SVM)	78.72	77.27	81.87	82.08	82.34	82.54	82.14	82.38	82.45
Bagging (KNN)	79.39	77.94	82.63	82.85	83.11	83.42	83.09	83.33	83.45
Bagging (LR)	80.37	78.92	83.81	83.93	84.27	84.44	84.13	84.33	84.39
Random Subspace (NB)	81.51	80.06	84.65	84.78	85.06	85.28	84.94	85.40	85.58
Random Subspace (SVM)	85.58	84.13	88.88	88.99	89.27	89.34	89.17	89.42	89.76
Random Subspace (KNN)	85.13	83.68	88.28	88.57	88.94	88.99	88.83	88.97	89.04
Random Subspace (LR)	82.48	81.03	86.21	86.41	86.80	86.93	86.67	87.48	87.77

**Table 2.** F-measure values obtained by learning algorithms and term weighting methods

Weighting Scheme	TF	TF-IDF	OR	RF	BDC	IQF	SW	IGM	RE
NB	0.80	0.79	0.83	0.84	0.84	0.84	0.84	0.84	0.84
SVM	0.80	0.78	0.83	0.83	0.83	0.83	0.83	0.83	0.83
KNN	0.73	0.72	0.78	0.78	0.79	0.79	0.78	0.79	0.79
LR	0.77	0.76	0.81	0.81	0.81	0.81	0.81	0.81	0.82
AdaBoost (NB)	0.83	0.82	0.87	0.87	0.88	0.88	0.88	0.88	0.89
AdaBoost (SVM)	0.81	0.80	0.84	0.85	0.85	0.85	0.85	0.85	0.85
AdaBoost (KNN)	0.80	0.79	0.83	0.83	0.84	0.84	0.84	0.84	0.84
AdaBoost (LR)	0.74	0.73	0.79	0.80	0.80	0.80	0.80	0.80	0.80
Bagging (NB)	0.77	0.76	0.81	0.81	0.81	0.81	0.81	0.82	0.82
Bagging (SVM)	0.79	0.78	0.83	0.83	0.83	0.83	0.83	0.83	0.83
Bagging (KNN)	0.80	0.79	0.83	0.84	0.84	0.84	0.84	0.84	0.84
Bagging (LR)	0.81	0.80	0.84	0.85	0.85	0.85	0.85	0.85	0.85
Random Subspace (NB)	0.82	0.81	0.85	0.85	0.86	0.86	0.86	0.86	0.86
Random Subspace (SVM)	0.86	0.85	0.90	0.90	0.90	0.90	0.90	0.90	0.90
Random Subspace (KNN)	0.86	0.84	0.89	0.89	0.90	0.90	0.90	0.90	0.90
Random Subspace (LR)	0.83	0.82	0.87	0.87	0.88	0.88	0.87	0.88	0.88

We observed that the relative performance of term weighting schemes varies significantly across datasets and classifiers in our experiments. Unsupervised schemes outperformed supervised schemes, while regularized entropy-based schemes outperformed supervised schemes. The empirical results indicate that the weight values for terms can be improved by employing supervised term weighting models which utilize class-specific information.

To summarize the main findings of the empirical results, Figure 1 denotes the bar chart for classification accuracies based on supervised learning models and ensemble learning methods and Figure 2 illustrate the bar chart for classification accuracies based on term weighting schemes.

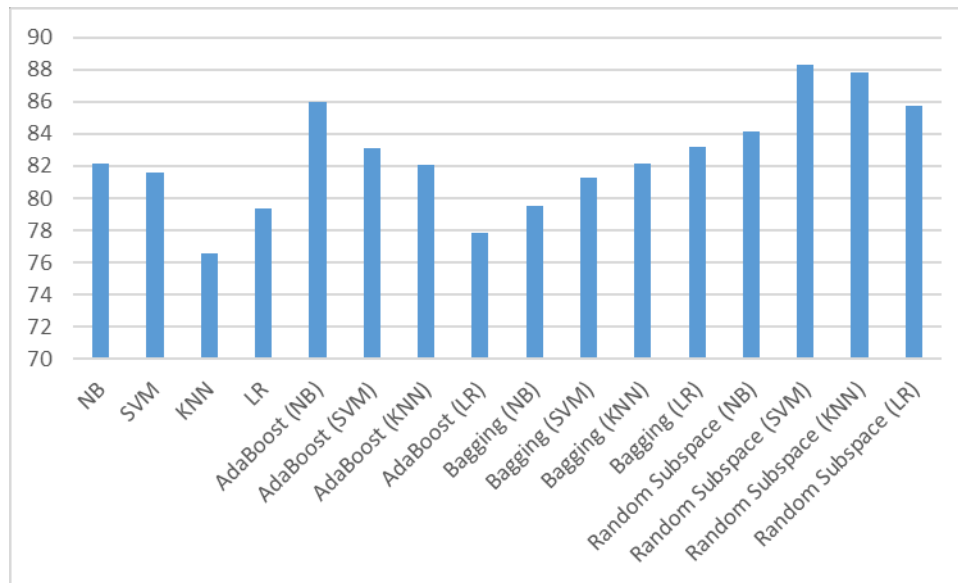


Figure 1. The bar chart for accuracy for classifiers

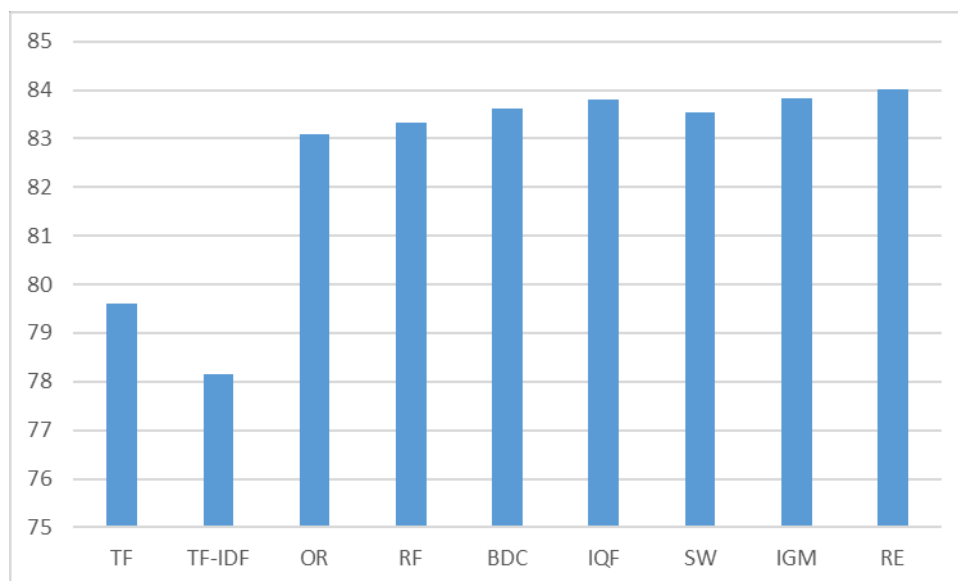


Figure 2. The bar chart for accuracy for weighting schemes

## 7. Conclusions

Social networking and microblogging sites have developed into important sources of information as information technology advances. Individuals can express their opinions, concerns, thoughts, and attitudes on a wide variety of subjects. They should make use of microblogging platforms to voice their opinions about current events and products. Sentiment analysis is a critical subfield of natural language processing research that aims to characterize the sentiment orientation of source materials. Twitter is one of the world's most popular microblogging platforms, with millions of users posting over a hundred million text messages daily (known as tweets). The task of choosing an appropriate scheme for representing terms in short text messages is critical. Term weighting schemes are advantageous when it comes to representing text documents in a vector space model. We present a comprehensive analysis of Turkish sentiment analysis in this paper, utilizing nine supervised and unsupervised term weighting schemes. To investigate the predictive efficiency of term weighting schemes, four supervised learning algorithms (Naive Bayes, support vector machines, k-nearest neighbor algorithm, and logistic regression) and three ensemble learning methods (AdaBoost, Bagging, and Random Subspace) are used. The results of the experiments indicate that supervised term weighting models can outperform unsupervised term weighting models. Regularized entropy (RE) outperforms all other term weighting schemes when supervised and unsupervised schemes are compared. Regularized entropy-based term weighting in combination with a random subspace ensemble of support vector machines produced the best predictive performance of all the configurations compared.

## Author Statement

The author confirms sole responsibility for the following: study conception and design, data collection, analysis and interpretation of results, and manuscript preparation.

## Conflict of Interest

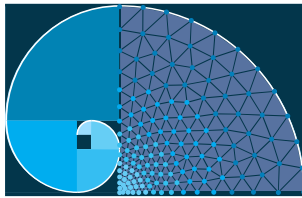
The author declares no conflict of interest.

## References

- Agarwal, A., Xie, B., Vovsha, I., Rambow, O., & Passonneau, R. J. (2011, June). Sentiment analysis of twitter data. In *Proceedings of the workshop on language in social media (LSM 2011)* (pp. 30-38).
- Aggarwal, C. C., & Zhai, C. (2012). A survey of text classification algorithms. In *Mining text data* (pp. 163-222). Springer, Boston, MA.
- Breiman, L. (1996). Bagging predictors. *Machine learning*, 24(2), 123-140.
- Carvalho, J., & Plastino, A. (2020). On the evaluation and combination of state-of-the-art features in Twitter sentiment analysis. *Artificial Intelligence Review*, 1-50.
- De Boom, C., Van Canneyt, S., Demeester, T., & Dhoedt, B. (2016). Representation learning for very short texts using weighted word embedding aggregation. *Pattern Recognition Letters*, 80, 150-156.
- Djaballah, K. A., Boukhalifa, K., & Boussaid, O. (2019, October). Sentiment Analysis of Twitter Messages using Word2vec by Weighted Average. In *2019 Sixth International Conference on Social Networks Analysis, Management and Security (SNAMS)* (pp. 223-228). IEEE.

- Fersini, E., Messina, E., & Pozzi, F. A. (2014). Sentiment analysis: Bayesian ensemble learning. *Decision support systems*, 68, 26-38.
- Freund, Y., & Schapire, R. E. (1996, July). Experiments with a new boosting algorithm. In *icml* (Vol. 96, pp. 148-156).
- Go, A., Bhayani, R., & Huang, L. (2009). Twitter sentiment classification using distant supervision. *CS224N project report, Stanford*, 1(12), 2009.
- Griol, D., Kanagal-Balakrishna, C., & Callejas, Z. (2020). Feature Set Ensembles for Sentiment Analysis of Tweets. In *Advances in Data Science: Methodologies and Applications* (pp. 189-208). Springer, Cham.
- Hecht, B., Hong, L., Suh, B., & Chi, E. H. (2011, May). Tweets from Justin Bieber's heart: the dynamics of the location field in user profiles. In *Proceedings of the SIGCHI conference on human factors in computing systems* (pp. 237-246).
- Ho, T. K. (1998). The random subspace method for constructing decision forests. *IEEE transactions on pattern analysis and machine intelligence*, 20(8), 832-844.
- Kantardzic, M. (2011). *Data mining: concepts, models, methods, and algorithms*. John Wiley & Sons.
- Kouloumpis, E., Wilson, T., & Moore, J. (2011, July). Twitter sentiment analysis: The good the bad and the omg!. In *Fifth International AAAI conference on weblogs and social media*.
- Lan, M., Tan, C. L., & Low, H. B. (2006, July). Proposing a new term weighting scheme for text categorization. In *AAAI* (Vol. 6, pp. 763-768).
- Onan, A. (2016). Classifier and feature set ensembles for web page classification. *Journal of Information Science*, 42(2), 150-165.
- Onan, A. (2017). Twitter mesajları üzerinde makine öğrenmesi yöntemlerine dayalı duygu analizi. *Yönetim Bilişim Sistemleri Dergisi*, 3(2), 1-14.
- Onan, A. (2017, April). Sarcasm identification on twitter: a machine learning approach. In *Computer Science On-line Conference* (pp. 374-383). Springer, Cham.
- Onan, A. (2018). Sentiment analysis on Twitter based on ensemble of psychological and linguistic feature sets. *Balkan Journal of Electrical and Computer Engineering*, 6(2), 69-77.
- Onan, A., & Korukoğlu, S. (2017). A feature selection model based on genetic rank aggregation for text sentiment classification. *Journal of Information Science*, 43(1), 25-38.
- Onan, A., Korukoğlu, S., & Bulut, H. (2016). A multiobjective weighted voting ensemble classifier based on differential evolution algorithm for text sentiment classification. *Expert Systems with Applications*, 62, 1-16.
- Quan, X., Wenyin, L., & Qiu, B. (2010). Term weighting schemes for question categorization. *IEEE transactions on pattern analysis and machine intelligence*, 33(5), 1009-1021.
- Şahin, G. (2017, May). Turkish document classification based on Word2Vec and SVM classifier. In *2017 25th signal processing and communications applications conference (SIU)* (pp. 1-4). IEEE.
- Sakaki, T., Okazaki, M., & Matsuo, Y. (2010, April). Earthquake shakes Twitter users: real-time event detection by social sensors. In *Proceedings of the 19th international conference on World wide web* (pp. 851-860).

- Samant, S. S., Murthy, N. B., & Malapati, A. (2019). Improving Term Weighting Schemes for Short Text Classification in Vector Space Model. *IEEE Access*, 7, 166578-166592.
- Wang, T., Cai, Y., Leung, H. F., Cai, Z., & Min, H. (2015, November). Entropy-based term weighting schemes for text categorization in VSM. In *2015 IEEE 27th International Conference on Tools with Artificial Intelligence (ICTAI)* (pp. 325-332). IEEE.
- Woo, H., Cho, H. S., Shim, E., Lee, J. K., Lee, K., Song, G., & Cho, Y. (2018). Identification of keywords from twitter and web blog posts to detect influenza epidemics in Korea. *Disaster medicine and public health preparedness*, 12(3), 352-359.
- Wu, H., Gu, X., & Gu, Y. (2017). Balancing between over-weighting and under-weighting in supervised term weighting. *Information Processing & Management*, 53(2), 547-557.
- Zhang, C., Zeng, D., Li, J., Wang, F. Y., & Zuo, W. (2009). Sentiment analysis of Chinese documents: From sentence to document level. *Journal of the American Society for Information Science and Technology*, 60(12), 2474-2487.



## The Impact of COVID-19 on Users' Visit to the Shopping Centers in Libya

Hafith Mohammed Sulayman Almansouri<sup>1,\*</sup> , Mehmet Cetin<sup>1</sup> 

<sup>1</sup> Department of Landscape Architecture, Kastamonu University, Kastamonu, Turkey

\*Corresponding author: hafithm.s.almansouri@gmail.com

Received: 30.04.2021

Accepted: 01.06.2021

### Abstract

The impacts of COVID-19 pandemic are expected to be challenging on all countries worldwide, especially from an economic concept. Reformations in the world's economic system and changes in human precautions and behaviors are expected to influence several other aspects directly and indirectly. This paper aims to evaluate the impact of the pandemic on the behaviors and perceptions of shopping malls' users. Through the performed questionnaire on the residents of Dernah, Libya, it was found that they depend on cars as a main mean of transportation. Thus, no major impacts were found on the user's choices in that aspect. However, evaluations of the scale reflect changes of people's attitudes towards their preferences for shopping malls. These results are significant indicators in directing the attention of designers and managers of shopping malls to adopt new strategies and approaches.

**Keywords:** COVID-19; shopping mall; reformation

### 1. Introduction

Tourism provides livelihoods for millions of people and allows billions more to appreciate their own and different cultures, as well as the natural world. For some countries, it can represent over 20 per cent of their GDP and, overall, it is the third largest export sector of the global economy. Tourism is one of the sectors most affected by the COVID-19 pandemic, impacting economies, livelihoods, public services, and opportunities on all continents. While sustaining the livelihoods dependent on the sector must be a priority, rebuilding tourism is also an opportunity for transformation with a focus on leveraging its impact on destinations visited and building more resilient communities and businesses through innovation, digitalization, sustainability, and partnerships (UNSDG, 2020).

Tokazhanov et al. (2020) reviewed literature material to study the impact of the pandemic on elements of sustainability in design of residential units. The authors recommended the reconsideration of architectural and engineering requirements to adjust to health and safety needed measures. Fezi (2020) suggested a "health engaged" architecture that looks into the needs of users in the new era. Effects on design elements are expected to extend to all possible elements including scales and dimensions, ventilation control, and layouts. The author

suggested that sustainability certification bodies to lead the movement towards the new requirements. Ahsan (2020) proposed several solutions for architecture in post-pandemic, which included reverting to successful techniques from historic civilizations and focusing on sustainability. Based on these studies and the persistent professional viewpoints of the eventual changes in architecture and design during and after the COVID-19 pandemic, it is important to understand the change in user behaviors and preferences.

## **2. Literature Review**

### **2.1. Pandemic Challenges to Shopping Malls**

For daily essentials – grocery, bakery, pharmacy – consumers increasingly prefer one-stop shop destinations. Our focus-group participants said they find local neighborhood centers or strip malls most convenient for meeting these daily, functional needs, and they expect to shop less in enclosed malls than they did before.

That, along with the growing strength and convenience of e-commerce, means mall owners will have to work even harder to give consumers a reason to travel beyond their neighborhood to get what they need. Single-purpose malls, where consumers go only to shop from a collection of retailers, will struggle to stay relevant.

As the restrictions imposed to protect public health during the pandemic are eased, people will likely be craving more social interaction. If their functional needs are being met close to home, malls themselves will need to build broader, more dynamic experiences that people cannot find elsewhere. Landlords and retailers need to collaborate creatively to drive foot traffic and boost dwell times to increase their revenue productivity.

Consumers told us that to capture their attention and get them to come back, the new destination mall will need to offer not only a great assortment of food options, as mentioned earlier, but also local or made-in-Canada merchants, a variety of parking and curbside pickup options, a centralized place for product returns (including those bought online), and even green spaces with trees and parkland. Progressive malls are building strategies to create mixed-use spaces that bring together residential, office, entertainment, leisure, health and wellness, and other novel experiences. Our interviewees talked about creating community living-room spaces in malls for people to meet and socialize, or building concept destinations like the mall, or health and wellness center, which would include clinics, pharmacies, and spa services.

“If the mall or store can’t provide a great experience, there is no reason to go there because you can just buy what you want online,” said one mall owner. Lower-performing enclosed community malls in urban or mature markets are (or will soon become) obsolete. Consumers will be drawn to new mixed-use projects with strong leisure and entertainment offerings that help them find the social interaction they crave, especially now (Powell, 2020).

### **2.2. Negative Effects of COVID-19 on Global Tourist Activities**

Potential tourists tend to postpone or cancel their plans for a destination that is plagued by a pandemic, especially when its main features are scarce of effective antivirus drugs and vaccines, the rapid spread of the virus and the damage that can cause to health. In cases of pandemics, tourists cancel their travels avoiding suspect places and people. Such kinds of pandemics directly affect industries such as tourism and retail service sector. The economic consequences of this outbreak will be serious, and they will cause damages not only to the tourist destinations with an important concentration of cases but also at a global level. A

similar case is the outbreak of SARS in 2002. Tourism is currently –March 2020- one of the most affected sectors and the World Tourism Organization has revised its 2020 forecast for international arrivals and receipts, though it emphasizes that such predictions are likely to be further revised. The United Nations specialized agency for tourism expects that international tourist arrivals will be down by 20% to 30% in 2020 when compared with 2019 figures. An expected fall of between 20-30% could translate into a decline in international tourism receipts (exports) of between US\$300-450 billion, almost one-third of the US\$ 1.5 trillion generated in 2019. Considering past market trends, this would mean that between five- and seven-years' worth of growth will be lost to COVID-19 (Folinas & Metaxas, 2020).

This immense shock could translate into a drop of 850 million to 1.1 billion international tourists and a loss of \$910 billion to \$1.2 trillion in export revenues from tourism, putting 100 to 120 million direct tourism jobs at risk. This is particularly critical as around 80 per cent of all tourism businesses are MSMEs. Considerable challenges lie ahead, including the unknown evolution of the pandemic and how consumer confidence will recover. The global economy is projected to contract sharply by 4.9 per cent in 2020, though the outlook is expected to pick up in 2021, according to the International Monetary Fund. Although countries and international organizations have implemented a range of measures to mitigate the socio-economic impacts of COVID-19 and to stimulate the recovery of tourism, the magnitude of the crisis requires extra efforts and continued support (UNSDG, 2020).

### 3. Methodology

The main aim of the study is to study the effect of COVID-19 pandemic on shopping mall users-based changes that occurred to their behaviors, preferences, and considerations. The scope of the study is focused on measurement in Derna, Libya. Moreover, the questionnaire tool used in the study is designed to collect data under three main sections:

1. Demographics
2. General changes
3. Specific changes in shopping malls that affect user satisfaction. This part measures using 5-point Likert scale four main aspects:
  - Habits,
  - Accessibility,
  - Design, and
  - Health and safety.

Using an electronic collection method, twenty-seven questionnaires were collected from the population. Results are analyzed through a comparison and descriptive statistics. Many limitations surround the current research, as the cause of change is an ongoing event (i.e. COVID-19). Therefore, it would be challenging to provide final and definite conclusions. The current studies available in the literature provide an initial vision to user behavior and design in the new era. Nonetheless, it is beneficial to focus on exploratory studies in order to assess the changes, which can empower future decision-making.

### 4. Results

The first section of the questionnaire collected the demographic data of the sample, which are illustrated in Figure 1. The majority of the participants were males (85%) and the sample was closely distributed between three age groups. Majority of the participants work at the public sector (54%), followed by students (31%), and employees of the private sector (15%). The vast

majority of the participants are holding a university degree as a minimum, which reflects a well-educated sample.

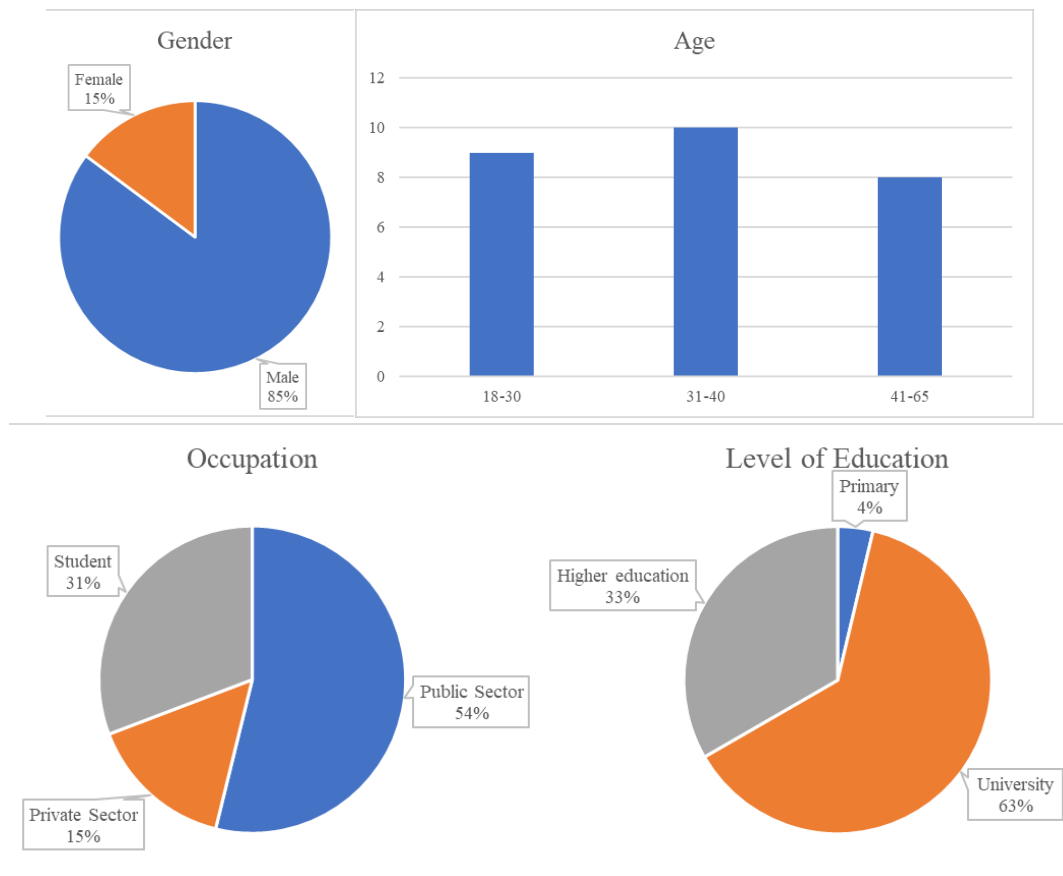
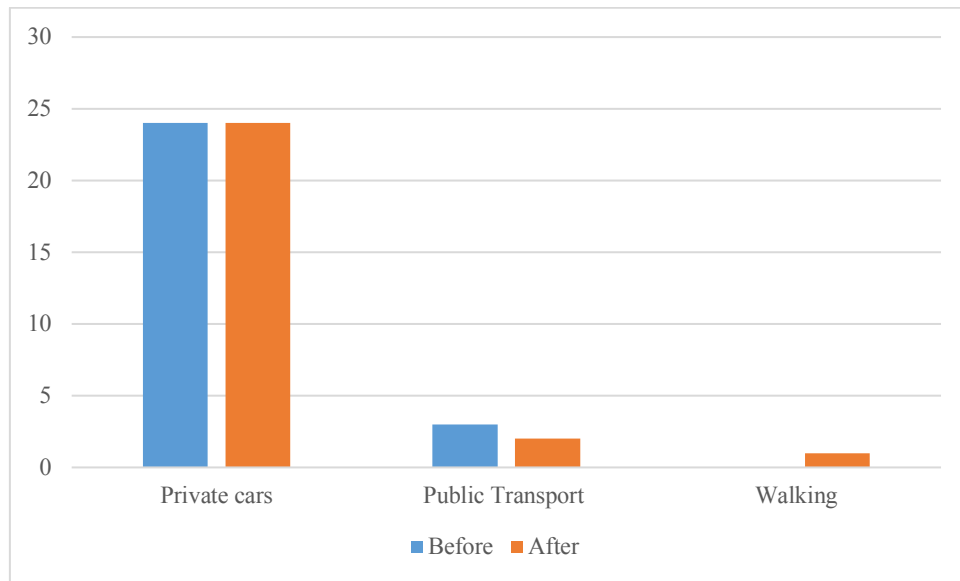


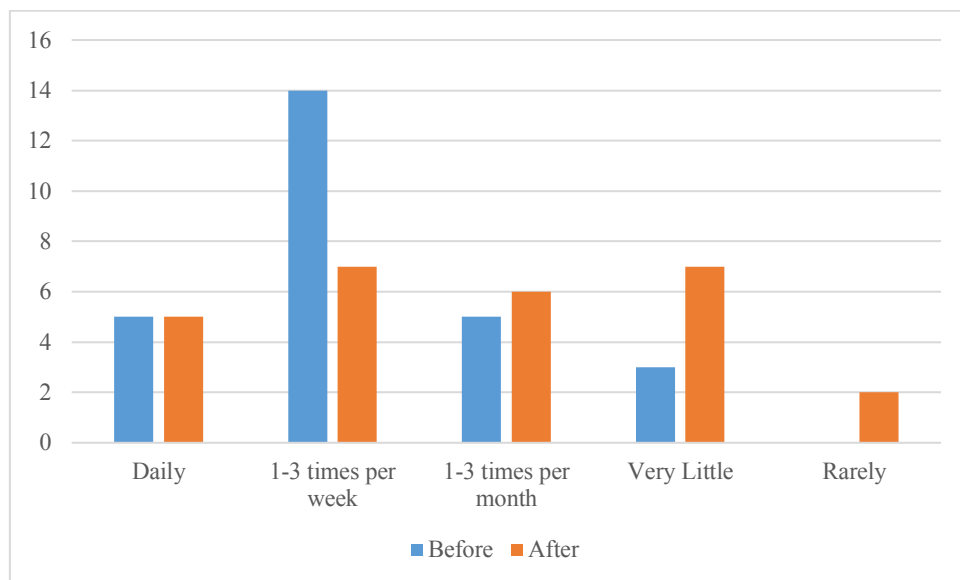
Figure 1. Demographics of participants

In the second section of the study, general differences between before and after the pandemic are measured and compared. Figure 2 compares differences in using means of transportation used to reach shopping malls between the two eras, where no major changes were noticed as users depend on private cares as the main mean of transportation.



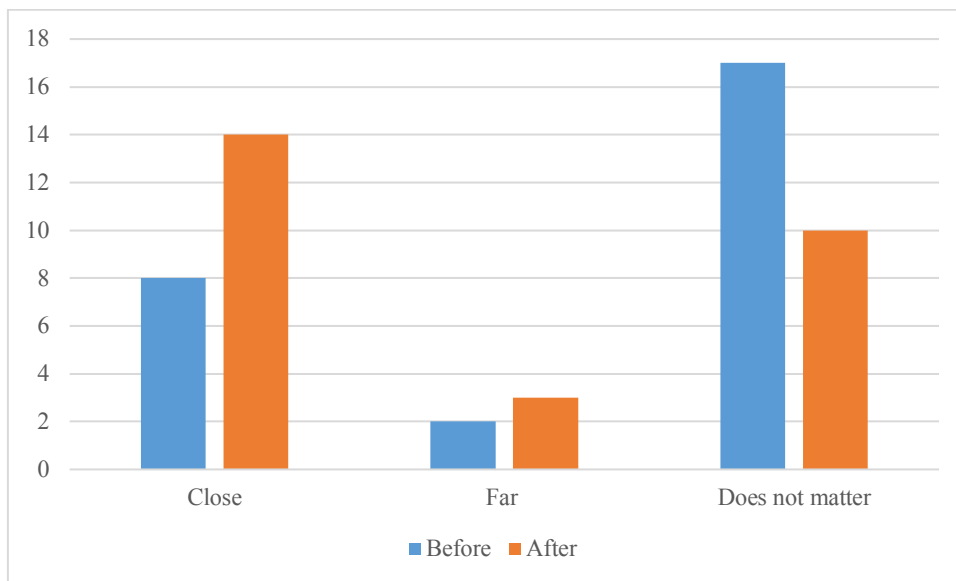
**Figure 2.** Changes in types of used transport to shopping malls

Figure 3 shows the difference in frequency of visits to shopping malls before and after the pandemic. The results show that the majority of participants were going 1 to 3 times per week, while the number was reduced after the pandemic. A research (Çokyığıt et al. 2019) carried out in three shopping centers of Antalya-Turkey before the pandemic showed that most of the participants (86%) preferred shopping malls for the aim of shopping.



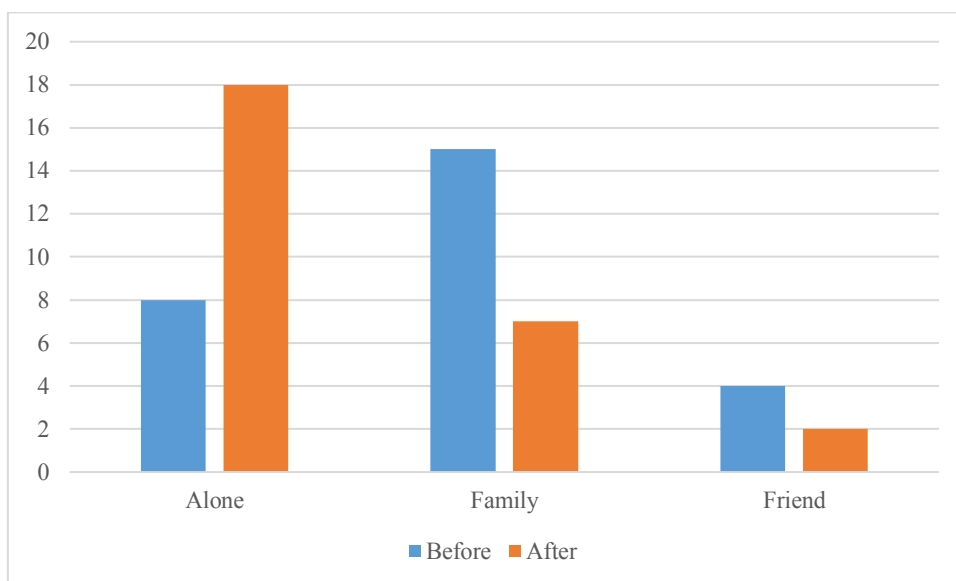
**Figure 3.** Frequency of visits to shopping malls

Figure 4 shows the preference of the participants to the distance to destination shopping malls. It is evident that more users started preferring close malls after the pandemic, where the majority did not consider distance as a factor before it.



**Figure 4.** Shopping malls preference according to distance

Figure 5 shows the behaviors of the users in visiting shopping malls, where the majority of the participants started preferring to visit it alone, instead with family or a friend, after the pandemic.



**Figure 5.** Companion preference in shopping mall visit

In the third section of the study, a scale measuring habits, accessibility, design, and health and safety was measured. Table 1 shows the mean and standard deviation values for each of the twenty-seven items. The indicator that aggregated the highest mean score was for the impact of hygiene and cleanness on reinforcing trust (3.41), followed by the preference of outdoor dining areas (3.37), the preference for shopping malls that are easier to reach (3.33), the preference of spending time in outdoor spaces (3.26), and the priority of caring about cleanness (3.22). Similar to a result in this study, Yücedağ and Çetin (2020) stated that EFL teachers mostly preferred online shopping during pandemic.

**Table 1.** Evaluation of shopping malls based on user's preferences after COVID-19 pandemic

	Items	Mean	SD
Habits	1 Shopping habits had changed	2.19	1.36
	2 My preferred working hours had changed	2.41	1.37
	3 I prefer online shopping	2.37	1.47
	4 I fear from spending long periods in closed spaces	2.70	1.49
	5 While it was an entertaining activity before, shopping had become for necessities only	2.63	1.50
Accessibility	1 After the Pandemic, the choice for means of transport had changed	2.56	1.4
	2 I go to shopping malls that are easier to reach	3.33	1.69
	3 The location being in the city center affects my decision to go there	2.37	1.50
	4 I do not prefer to reach using public transport	2.89	1.65
	5 I use public transports that do not have high density of users	2.67	1.57
	6 It is important for me to have sufficient availability of car parking	3.00	1.57
	7 I use stairs in shopping malls	2.81	1.62
	8 Warning and awareness signs affect my preference for a shopping mall	2.52	1.50
Design	1 Architectural design and construction do not affect my preference	1.78	1.09
	2 I prefer indoor open spaces	3.00	1.64
	3 I try to spend less time in closed indoor spaces	2.70	1.46
	4 I prefer spending time in outdoor spaces	3.26	1.68
	5 I prefer areas with natural sightseeing	3.04	1.74
	6 I prefer outdoor dining facilities	3.37	1.67
	7 socio-cultural facilities, e.g. cinema, playgrounds, etc., are not the reason behind my choices	2.33	1.27
	8 The use of touchless equipment affects my choices	2.33	1.27
Health & Safety	1 The first thing I care about is the feel that it is clean	3.22	1.85
	2 The keep of cleanness and hygiene reinforces trust	3.41	1.72
	3 The presence of control points increases my trust	2.96	1.72
	4 I do not find children's playgrounds safe anymore	3.11	1.72
	5 I do not find dining spaces healthy anymore	2.70	1.44
	6 I think that shopping centers will remain unsafe for a long time	2.52	1.37

## 5. Conclusions

The magnitude of event makes it imperative that COVID-19 pandemic affects and continue affecting human attitudes, habits, preferences, and lifestyles. Therefore, it is highly expected that preferences for shopping malls are also changed after the pandemic. The findings of the current study provide a general comparison between user habit for shopping malls before and after the pandemic, as well as an evaluation of the most important aspects that are considered by users while visiting a shopping mall. Comparisons show that while no effect on preferred means of transportation was found in the Libyan sample, differences were found in users' frequency of visits, preference of distance to shopping malls, and companion preferences. It is indicated that users after COVID-19 pandemic prefer less frequently visiting malls, with preferences for close malls and individual visits. Evaluation of different aspects of shopping mall experiences after the pandemic, it is indicated that hygiene and availability of outdoor spaces are the most important factors influencing user decisions.

## Acknowledgments

As the corresponding author I am studying my Ph.D. at Kastamonu University. This study conducted in Derna, Libya. Thank you for supporting to the residence of Derna, Libya. In addition, thank you for this study was conducted by Ph.D. courses of "Tourism Planning and Ecotourism". Thank you for supporting for the course of teachers.

## Author Statement

The authors confirm contribution to the paper as follows: study conception and design: Hafith; data collection: Hafith; analysis and interpretation of results: Hafith and Mehmet; draft manuscript preparation: Hafith. All authors reviewed the results and approved the final version of the manuscript.

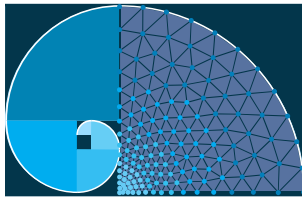
## Conflict of Interest

The authors declare no conflict of interest.

## References

- Ahsan, M. (2020). Strategic decisions on urban built environment to pandemics in Turkey: Lessons from COVID-19. *Journal of Urban Management*, 9(3), 281-285.
- Fezi, B. A. (2020). Health engaged architecture in the context of COVID-19. *Journal of Green Building*, 15(2), 185-212.
- Folinas, S., & Metaxas, T. (2020). Tourism: The Great Patient of Coronavirus COVID-2019. *Munich Personal RePEc Archive*.
- Powell, C. (2020). *Malls must focus less on shopping and more on experience: Deloitte*. Retrieved from The Message: <https://the-message.ca/2020/07/13/malls-must-focus-less-on-shopping-and-more-on-experience-deloitte/>
- Tokazhanov, G., Tleuken, A., Guney, M., Turkyilmaz, A., & Karaca, F. (2020). How is COVID-19 Experience Transforming Sustainability Requirements of Residential Buildings? A Review. *Sustainability*, 12(8732).

- UNSDG. (2020). *Policy Brief: COVID-19 and Transforming Tourism*. Retrieved from United Nations Sustainable Development Group: <https://unsdg.un.org/resources/policy-brief- COVID -19-and-transforming-tourism>
- Çokyiğit, H., Kaya, L.G., Yücedağ, C., Aşikkutlu, H.S. (2019). AVM'lerde Sergileme Elemanlarının Tüketici Davranışına Etkisi: Antalya Örneği, (Editor: Kaya, L.G. Mimarlık Planlama ve Tasarım Alanında Araştırma ve Değerlendirmeler). Gece Publishing, Basım sayısı:1, ISBN:978-605-7852-93-9.
- Yücedağ, C., Çetin, M. (2020). Identifying Leisure Perceptions and Activities of EFL Teachers in Home Isolation during the Covid-19 Pandemic. *Kastamonu Üniversitesi Mühendislik ve Fen Bilimleri Dergisi*, 6(2): 62-72.



## On Local Scouring at Single Piers

António Heleno Cardoso<sup>1,\*</sup> , Cristina Maria Sena Fael<sup>2</sup> , Rui Miguel Madeira Lança<sup>3</sup> 

<sup>1</sup> Instituto Superior Técnico, Universidade de Lisboa, Lisboa, Portugal

<sup>2</sup> Universidade da Beira Interior, C-MADE, Covilhã, Portugal

<sup>3</sup> Instituto Superior de Engenharia, Universidade do Algarve, Faro, Portugal

\*Corresponding author: antonio.cardoso@tecnico.ulisboa.pt

Received: 29.06.2021

Accepted: 16.07.2021

### Abstract

The paper mostly summarizes disperse contributions of the authors published during the last fifteen years on the scour depth at single piers. These contributions rely on unique experiments in the sense that they are systematically longer than most of those found in the literature. The characterization of the effects of flow intensity, relative sand size, flow shallowness, time and pier shape and alignment is significantly improved as compared with existing literature. Our contributions consist on refinements of the model suggested by the school of Auckland, initiated by Raudkivi and boosted by Melville and his students. A considerable number of empirical equations and charts expresses those contributions.

**Keywords:** Single piers; flow intensity; flow depth factor; sediment size factor; time factor; pier shape and alignment.

### 1. Introduction

Local scour around bridge piers and abutments is a frequent cause of partial failure or collapse of bridges. The reconstruction or rehabilitation of destroyed or damaged bridges frequently amounts to significant monetary costs. Above all, the casualties that occur in many of these disasters raise the societal claim for security. Enhanced security involves failure prevention, which in turn requires the accurate prediction of the scour depth or the adoption of proper mitigation scour countermeasures. In spite of the remarkable progresses registered since the mid-last century, scouring remains only a partly solved problem, due to the large number of variables involved in the processes and the inherent complexity of their phenomenological interactions.

The scope of this paper is scouring at single piers. Single piers are characterized by a unique cross-section along their main axes, assumed vertical. Local scouring at such single piers has been extensively studied. Research has been made mostly through experimentation. Early contributions of Chabert and Engeldinger (1956), Laursen and Toch (1956), Laursen (1963) or Shen et al. (1966) deserve to be mentioned, whereas one of the most comprehensive reviews on bridge scouring was offered by Melville and Coleman (2000).

For uniform flows in straight open channels, the maximum scour depth at a given moment,  $d_s$ , was shown to be described through the following parametric equation (see Fael (2007)):

$$\Pi_{d_s} = \phi \left( \Pi_d; \Pi_U; \Pi_{D_{50}}; \sigma_D; s; \Pi_\nu; \Pi_f; \Pi_\theta; \Pi_W; \Pi_G; \Pi_t \right) \quad (1)$$

where  $\Pi$  stands for non-dimensional parameter,  $\phi$  means “function of” and subscripts refer to the variables influencing scouring. These are, namely,  $d$  = flow depth;  $U$  = average approach flow velocity;  $D_{50}$  = median grain size of the bed sediment;  $\nu$  = kinematic water viscosity;  $f$  = pier shape;  $\theta$  = pier alignment;  $W$  = channel width;  $G$  = geometry of the channel cross-section. Non-dimensional parameters  $\sigma_D$  and  $s$  stand for, respectively, gradation coefficient and specific gravity of the bed sediment. The basic variables used to derive Eq. (1) were the characteristic length of the pier cross-section,  $D_p$ , the gravitational acceleration,  $g$ , and the water density,  $\rho$ .

$$\Pi_{d_s} = \phi \left( \Pi_d; \Pi_U; \Pi_{D_{50}}; \sigma_D; \Pi_\nu; \Pi_f; \Pi_\theta; \Pi_t \right) \quad (2)$$

In this equation, it is assumed that the effect of flow contraction on scouring at single piers vanishes in wide channels and that the specific sediment gravity is practically invariant, notably for sand. It is also assumed that the rectangular cross-section is the reference shape of open channels.

According to Melville and Coleman (2000), the previous equation can be materialized for piers as follows:

$$\Pi_{d_s} = K_d K_U K_{D_{50}} K_{\sigma_D} K_\nu K_f K_\theta K_t \quad \text{with} \quad \Pi_{d_s} = \frac{d_s}{D_p} \quad \text{or} \quad \Pi_{d_s} = \frac{d_s}{d} \quad (3)$$

It should be noted here that  $K_d$  refers to the effect of the relative flow depth or flow shallowness,  $\Pi_d = d/D_p$ ;  $K_U$  accounts for the effect of flow intensity,  $\Pi_U = U/U_c$  ( $U_c$  = critical velocity of beginning of sediment motion);  $K_{D_{50}}$  reflects the effect of relative sediment size or sediment coarseness,  $\Pi_{D_{50}} = D_p/D_{50}$ ;  $K_{\sigma_D}$  refers to the armoring effect (which mostly depends on  $\sigma_D$ );  $K_\nu$  accounts for the effect of fluid viscosity as captured through any form of the Reynolds number, e.g.,  $\Pi_\nu = u^* D_{50} / \nu$  ( $u^*$  = friction velocity);  $K_f$  and  $K_\theta$  attend, respectively, to the effects of shape and alignment of the pier; and  $K_t$  varies with the non-dimensional time,  $\Pi_t = Ut/D_p$ .

In the last fifteen years, we have revisited local scouring at single piers inserted in channel beds composed of practically uniform ( $\sigma_D < 1.5$ ;  $K_{\sigma_D} = 1.0$ ) non-ripple forming sand ( $D_{50} > 0.6$  mm). Under these conditions, we have indeed contributed to the enhanced characterization of Eq. (3). This paper reviews those contributions, synthesizing mostly the works of Lança et al. (2010), Simarro et al. (2011), Lança et al. (2013) and Fael et al. (2016). It does not cover the effects of water viscosity, bed armoring (due to the wide granular distribution of the bed material) or ripple forming bed material ( $D_{50} \leq 0.6$  mm) since we performed only a very limited number of experiments on these effects. The effect of viscosity can indeed be anticipated to be negligible since the flow field around obstacles tends to be rough turbulent, irrespective of the approach flow regime (smooth, transitional or rough).

Prior to addressing those contributions, we include a short description of the experimental facilities and granular materials used in the studies, as reported by Fael et al. (2014), and assess the calculation of the equilibrium scour depth from scour depth time records.

## 2. Experimental Facilities and Granular Materials

Three horizontal-bed flumes were used in the studies. Each flume included a central reach consisting of a rectangular recess box in the bed (Figure 1), where the piers were installed. The main features of the flumes are shown in Table 1, where  $W$  = flume width,  $L$  = flume length,  $\ell$  = distance from flume entrance to the recess box,  $\ell_1$  = length of bed recess box and  $d_r$  = its depth (Figure 1).

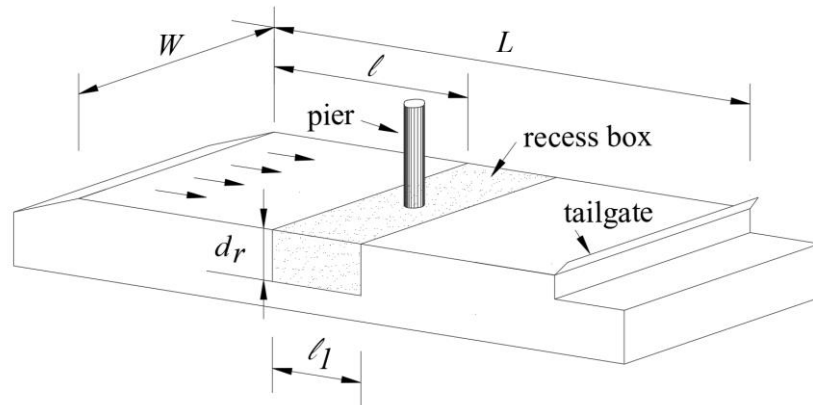


Figure 1. Sketch of the flumes

Table 1. Main features of the flumes

Flume	$W$ (m)	$L$ (m)	$\ell$ (m)	$\ell_1$ (m)	$d_r$ (m)
F <sub>1</sub>	4.00	28.00	13.90	3.00	0.60
F <sub>2</sub>	0.83	12.70	5.00	3.10	0.35
F <sub>3</sub>	1.00	33.20	16.00	3.20	0.35

Two natural quartz sands were used: sand  $S_1$ , defined by  $D_{50} = 1.28$  mm and  $\sigma_D = 1.46$ ; sand  $S_2$ , defined by  $D_{50} = 0.86$  mm and  $\sigma_D = 1.36$ ). Herein  $\sigma_D = (D_{84.1}/D_{50} + D_{50}/D_{15.9})/2$  and  $D_{50}$  = sand particle sieving diameter for which 50% are finer by weight. Both sands can be considered as uniform, since  $\sigma_D < 1.5$ . The specific gravity was verified to be  $s \approx 2.65$  in all cases.

Distinctive characteristics of the experiments were 1) the absence of contraction scour and wall effects and 2) their long duration. They typically lasted longer than 7 days, this way allowing the proper assessment of equilibrium scour depth. Another remarkable feature is the large number of experiments covering uncommon ranges of the relative sediment size or coarseness,  $\Pi_{D50} = D_p/D_{50}$ .

## 3. Experimental Equilibrium Scour Depth

Local scouring occurs for two distinct sediment transport conditions: i) under *clear-water*, i.e., in the absence of sediment movement in the bed of the approach flow, which implies the bed shear stress to be smaller or, at most, equal to the critical bed shear stress of beginning of sediment motion; ii) under *live-bed*, i.e., when noticeable bed sediment movement occurs in the approach flow, meaning that the bed shear stress is larger than the critical bed shear stress.

Conceptually, under *clear-water*, a scour hole is in equilibrium when the scour depth practically does not increase anymore, while under *live-bed*, a scour hole is in equilibrium when the time-averaged amount of sediment leaving the scour hole equals the time-averaged amount of sediment that it captures from upstream. Starting from a flatbed, the time required to reach equilibrium scour depends on the state of sediment movement. For *live-bed* conditions, there is the simultaneous removal of grains originated from the scour hole and of those trapped by the same scour hole as they move downstream. The quantity of material that initially leaves the scour hole exceeds the quantity of material coming in and the scour depth increases. After a comparatively short time, both quantities tend to be equal. This state of equilibrium is known as dynamic equilibrium since the scour depth normally oscillates. The oscillations reflect the movement of bedforms – ripples, dunes, antidunes – that, in turn, induce periodical variations of the amount of sediments falling into the scour hole. In this context, it is pertinent to define the maximum scour depth,  $d_{sm}$ , as the sum of the average equilibrium scour depth,  $d_{se}$ , with a value that depends on the semi-amplitude of bedforms.

For *clear-water* flow conditions, the increase of scour depth induces the continuous reduction of bed shear stress inside the scour hole until it becomes conceptually insufficient to transport sediment particles downstream. As scouring progresses, the scour rate decreases. The equilibrium depth is reached asymptotically and equilibrium is usually said to be static, in contrast with the *live-bed* case. It should be noticed here that, though the most frequent scour disasters occur under *live-bed* conditions associated with floods, scour due to long-lasting *clear-water* flows can originate slightly deeper scour holes.

The scour depth has classically been assumed to evolve in three phases, particularly in the *clear-water* flow case. These phases are i) the *initial phase*, where scour depth increases very quickly; ii) the *principal phase*, where the scour hole increases in depth and plan extent at a progressively decreasing rate; iii) the *equilibrium phase*, where the scour depth is assumed to stop increasing.

Until to the beginning of the present millennium, most studies assumed the existence of a finite time to reach equilibrium, both for *clear-water* and *live-bed* conditions. Many research works, including those of Cardoso and Bettess (1999), Fael et al. (2006) or Cardoso and Fael (2010), adopted this concept. At the dawn of the XXI century, Oliveto and Hager (2002; 2005) stated that “end scour as the equilibrium state between the vortical agents and the resistance of sediments to be scoured does not normally exist”, in disagreement with previous research works. Although there is no evidence supporting the inexistence of end scour, we recognize that the probability of occurrence of a sufficiently strong turbulent event capable of entraining bed grains is never null. Thus, it can be assumed that the mentioned probability decreases as scouring progresses, the scour depth evolving to a finite equilibrium value.

In other words, time to equilibrium can be conceived as infinity (notably, under *clear-water* flow conditions) although the equilibrium scour depth is indeed finite. Under these assumptions, the equilibrium scour depth of each experiment was derived by adjusting the polynomial equation,

$$d_s = p_1 \left( 1 - \frac{1}{1 + p_1 p_2 t} \right) + p_3 \left( 1 - \frac{1}{1 + p_3 p_4 t} \right) + p_5 \left( 1 - \frac{1}{1 + p_5 p_6 t} \right) \quad (4)$$

to the recorded time evolution of the scour depth. Parameters  $p_1$  to  $p_6$  were obtained through regression analysis and the equilibrium scour depth was calculated as  $d_{se} = p_1 + p_3 + p_5$  for  $t = \infty$ . The above polynomial was suggested by Lança et al. (2010) as an improvement of a similar proposal by Bertoldi and Jones (1998). Lança et al. (2010) have shown that the method leads to

practically invariant results for  $d_{se}$  as soon as experiments last for at least 7 days, which applies to the present experimental data.

#### 4. Flow Intensity Factor

Referring to Eq. (3), let us consider that scouring occurs in a uniform flow on a straight, wide and rectangular open channel. Assuming also that i) the bed material is uniform ( $K_{\sigma D} = 1.0$ ); ii) the pier is a cylinder ( $K_{\theta} = K_f = 1.0$ ); iii) viscosity does not play a significant role on scouring ( $K_v = 1.0$ ); iv) the scouring process has sufficiently approached the equilibrium stage ( $K_t = 1.0$ ); v)  $K_{D50} = \text{const.}$ , Eq. (3) comes

$$\Pi_{d_{se}} = \varphi(\Pi_d; \Pi_U) \quad \text{with} \quad \Pi_{d_{se}} = \frac{d_{se}}{D_p} \quad \text{or} \quad \Pi_{d_{se}} = \frac{d_{se}}{d} \quad (5)$$

where  $d_{se}$  stands for equilibrium scour depth. For slender cylindrical piers, when the average approach velocity,  $U$ , reaches a value of the order of  $0.5U_c$  (Chabert and Engeldinger, 1956; Hanco, 1971), the flow structure around the pier induces local bed shear stresses that promote the beginning of grains motion, i.e., the initiation of the scour process (see Figure 2) although there is no sediment transport in the approach channel. To a given value of the approach flow velocity in the range  $\approx 0.5U_c < U < U_c$  corresponds one single value of the equilibrium scour depth,  $d_{se}$ , as soon as  $\Pi_d = d/D_p$  remains constant. The scour depth,  $d_{se}$ , increases linearly with  $U/U_c$  until it reaches its maximum for  $U = U_c$  ( $\Pi_U = 1.0$ ). Increasing further the velocity, the bed grains of the approach flow will move and dunes will develop in the bed. For  $U > U_c$ , the movement of dunes downstream feeds the scour hole with successive waves of bed material that the vortical system (horseshow vortex plus wake vortices) keeps removing from the scour hole, this way reducing its capacity to erode the original bed. Through this mechanism, dunes tend to induce a small decrease of  $d_{se}$  as  $U$  increases in the range  $U_c < U < \approx 2U_c$  ( $1 < \Pi_U < \approx 2$ ). A minimum of the equilibrium scour depth occurs for  $U \approx 2U_c$ . For approach flow velocities in the range  $\approx 2U_c < U < \approx 4U_c$ , dunes become longer and their upstream slope become milder as flow velocity increases. The scouring process will be influenced by the arrival of other dunes with lower height and volume; the vortical system tends to be increasingly able to move the incoming sediments downstream. Consequently, the equilibrium scour depth increases again gradually with the approach flow velocity. A new maximum of  $d_{se}$  is reached for  $U \approx 4U_c$  ( $\Pi_U \approx 4$ ). This maximum is of the order of the one observed for  $U = U_c$  but it occurs for the upper-regime flat bed. For velocities higher than  $\approx 4U_c$ , antidunes normally develop, and the scour depth tends to decrease again for the same reasons as those why the occurrence of dunes also decreases the equilibrium scour depth.

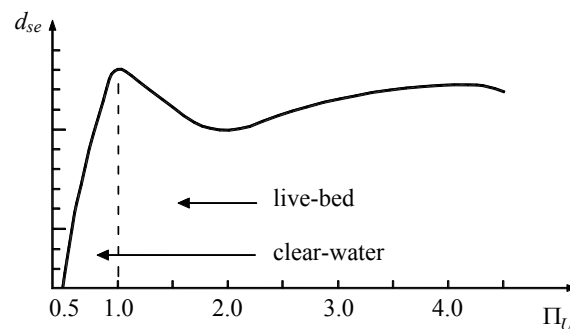


**Figure 2.** Typical variation of  $d_{se}$  with  $U$  for comparatively coarse uniform bed sediment (adapted from Breusers and Raudkivi (1991))

It should be emphasized here that the condition of scour inception – given as  $U/U_c = 0.5$  and meaning that the critical value of the flow intensity for scour inception would be  $\Pi_{Ui} = 0.5$  – has not been consensual. For instance, Chiew (1995) indicated  $\Pi_{Ui} = 0.3$ , Melville (1992, 1997) suggested charts according to which  $\Pi_{Ui} = 0$  and Hager and Oliveto (2002) proposed an equation to calculate  $\Pi_{Ui}$  as a function of the flow blockage.

In view of the lack of consensus, Fael et al. (2006) investigated the scour inception at vertical wall abutments by performing 31 long lasting (more than 7 days) experiments with sand S1 in the flume F1. Abutments' length,  $\ell_a$ , varied in the range  $0.64 \text{ m} < \ell_a < 1.86 \text{ m}$ , the flow depth was kept practically constant ( $\approx 0.06 \leq d \leq \approx 0.07 \text{ m}$ ), the relative abutment length,  $1/\Pi_d = \ell_a/d$ , spanned from 8.9 to 30.1, the flow intensity covered the range  $\approx 0.4 < \Pi_U < \approx 1.0$  and wall effects and contraction scour were absent. Fael et al. (2006) also selected 25 experiments from the literature, covering lower values of  $\ell_a/d$ , between 2.0 and 17.4, and  $\approx 0.6 < \Pi_U < \approx 1.0$ . From the data collected, Fael et al. (2006) concluded that the scour inception at vertical wall abutments is defined by

$$\Pi_{Ui} = \frac{1}{1 + 0.402(\ell_a/d)^{0.648}} \quad (6)$$

Since abutments can be conceptually regarded as half-width piers, meaning that they mimic piers with  $D_p = 2\ell_a$ , the previous equation can be written as

$$\Pi_{Ui} = \frac{1}{1 + 0.257(D_p/d)^{0.648}} \quad (7)$$

Eq(s). (6) and (7) are plotted in Figure 3 together with the equation suggested by Hager and Oliveto (2002). In this figure,  $\ell_o$  stands for pier width,  $D_p$ , or abutment length,  $\ell_a$ , depending on the equation.

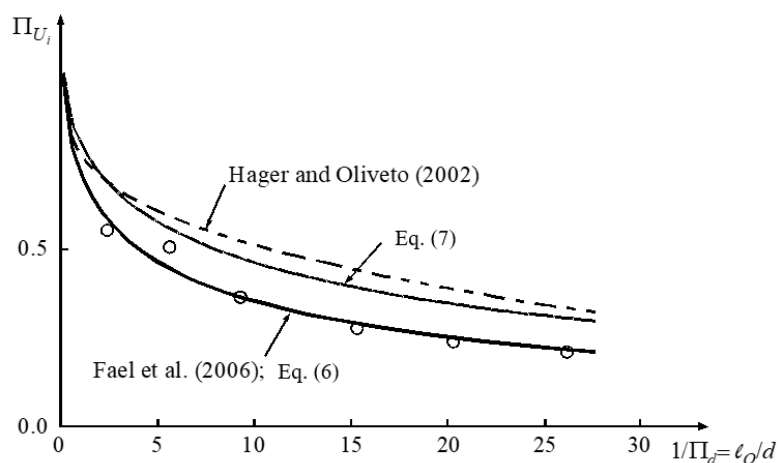


**Figure 3.** Variation of  $\Pi_{Ui}$  with  $1/\Pi_d$

Further assuming that the scour reduction occurring for  $\Pi_U \approx 2.0$  is negligible, it can be concluded that  $K_{U_i}$ , defined as

$$K_U = \frac{d_{se}}{d_{se}} \text{ (for a given } \Pi_U) \quad (8)$$

can be obtained as follows:

$$K_U = \begin{cases} 0 & \Pi_U < \Pi_{Ui} \\ \frac{1}{1 - \Pi_{Ui}} (\Pi_U - \Pi_{Ui}) & \Pi_{Ui} \leq \Pi_U < 1 \\ 1 & \Pi_U \geq 1 \end{cases} \quad (9)$$

This equation reflects the influence of  $\Pi_U$  and  $\Pi_d$  - trough  $\Pi_{Ui}$  - on  $K_U$ . It compares with other contributions according to Figure 4.

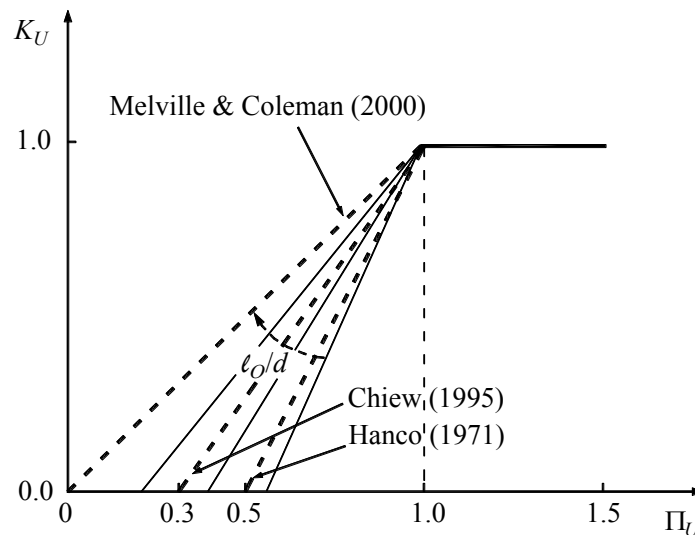


Figure 4. Variation of  $K_U$  with  $\Pi_U$

### 5. Effects of Flow Depth and Sediment Size on the Equilibrium Scour Depth

Resuming the scenario of rough turbulent uniform flows on uniform non-ripple forming sandbeds in straight, very wide, rectangular open channels and also considering constant values of flow intensity,  $\Pi_U$ , Eq. (3) reads

$$\Pi_{ds} = K_d K_{D_{50}} K_f K_\theta K_t \quad (10)$$

The equilibrium scour depth - where  $\Pi_{ds} = \Pi_{dse}$  - at cylindrical piers ( $K_f = K_\theta = 1.0$ ) can be described as

$$\Pi_{dse} = K_d K_{D_{50}} \quad (11)$$

It is unanimously recognized that the relative approach flow depth,  $\Pi_d = d/D_p$ , is a key parameter of the scour process. On the contrary, many authors (e.g. Ettema (1980), Melville

and Chiew (1999)) have successively assumed that the normalized equilibrium scour depth,  $\Pi_{d_{se}} = d_{se}/D_p$  or  $\Pi_{d_{se}} = d_{se}/d$  does not depend on the relative sediment size,  $\Pi_{D50} = D_p/D_{50}$ , as soon as  $\Pi_{D50} > \approx 25 - 50$ . Under this assumption, the equilibrium scour depth would be given as

$$\frac{d_{se}}{D_p} = \varphi\left(\frac{D_p}{d}\right) \quad \text{or} \quad \frac{d_{se}}{d} = \varphi\left(\frac{D_p}{d}\right) \quad \text{or} \quad d_{se} = \varphi(d; D_p) \quad (12)$$

Kandasamy (1989) collected scour data for piers and abutments corresponding to comparatively low values of  $\Pi_{D50}$ . In the attempt to unify the analysis of both obstacle types, he used a common characteristic length,  $\ell_o$ , to represent the abutment length (assuming  $D_p = 2.3 \ell_o$ ) and the pier diameter. He obtained the 3D representation of the surface

$$d_{se} = \varphi(d; \ell_o) \quad (13)$$

included in Figure 5 for  $\Pi_U \approx 1.0$ , i.e., corresponding to the maxima scour depths. According to Kandasamy (1989), this surface can be divided into four zones. Zone 1 consists of the planar area defined by  $d > b_1 \ell_o$  (surface OAB). In this zone, covering the domain of slender piers, the scour depth does not depend on the flow depth, meaning that

$$d_{se} = C_1 \ell_o \quad (14)$$

Zone 4 (surface ODE) would be a planar surface too, obeying the condition  $\ell_o > b_2 d$ . According to Kandasamy (1989), it would apply to long abutments, for which the equilibrium scour depth is independent of the obstacle length and only depends on the flow depth ( $d_{se} = C_2 d$ ).

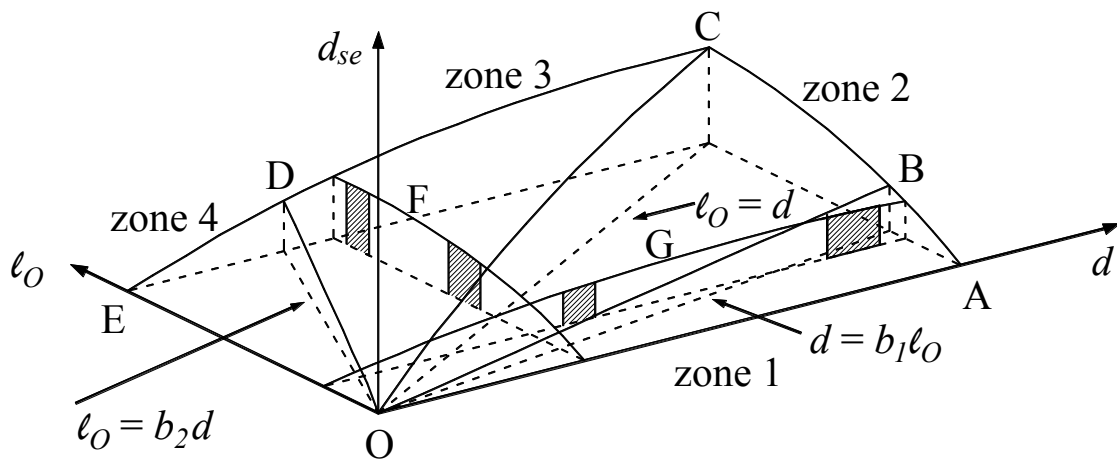


Figure 5. Shape of the function  $d_{se} = d_{se}(d; L)$  as defined by Kandasamy (1989)

Figure 5 includes curves F and G, parallel to the axis of obstacle length and to the axis of flow depth, respectively. The curve F establishes the variation of  $d_{se}$  with  $\ell_o$  for  $d = \text{const.}$ ; curve G

establishes the variation of  $d_{se}$  with  $d$  for  $\ell_o = \text{const}$ . Along curve F, which intersects zones 1, 2 and 3, the scour depth increases strong and linearly with  $\ell_o$  in zone 1; in zone 2 (where piers prevail), the increase slows down; this effect is even more pronounced in zone 3, corresponding to  $\ell_o > d$ . Had the curve crossed zone 4,  $d_{se}$  would become constant and proportional to  $d$ . Qualitatively, curve G presents the same type of variation as curve F; it is obvious that the rate of increase of scour depth diminishes from zone 4 to zone 1. To the right of the line OB,  $d_{se}$  is independent of  $d$  and becomes  $C_1\ell_o$  (see Eq. (14)).

Several contributions can be found in the literature corresponding to specific forms of Eq. (13). One of the most widely spread was obtained by Melville (1992; 1997) who suggested the following envelop curves for the calculation of equilibrium scour depth at cylindrical piers:

$$\frac{d_{se}}{D_p} = 2.4 \quad \text{for} \quad D_p / d \leq 0.7 \quad (\Pi_d \geq 1.43) \quad (15)$$

$$\frac{d_{se}}{D_p} = 2 \left( \frac{D_p}{d} \right)^{0.5} \quad \text{for} \quad 0.7 < D_p / d \leq 5 \quad (0.2 \leq \Pi_d < 1.43) \quad (16)$$

$$\frac{d_{se}}{d} = 4.5 \quad \text{for} \quad D_p / d > 5 \quad (\Pi_d < 0.2) \quad (17)$$

It should be noticed here that the contribution of Melville (1992; 1997) implicitly fixes  $b_1 = 0.7$ ,  $b_2 = 5$ ,  $C_1 = 2.4$  and  $C_2 = 4.5$ .

The cancelation of the relative sediment coarseness effect – associated with  $\Pi_{D50}$  – assumed by Ettema (1980), Kandasamy (1989) and Melville (1992; 1997), among many others, was disputed by Sheppard et al. (2004) and Lee and Sturm (2009), according to whom  $\Pi_{dse}$  decreases with increasing relative sediment size, particularly, for  $\Pi_{D50} > \approx 50$ . In spite of the importance of this contribution, it did not sufficiently pervade the hydraulics community until to the present. Consequently, Lança et al. (2013) reassessed the influence of  $\Pi_{D50}$  on scouring. They performed thirty eight tests with sand  $S_2$ , lasting between 7 and 14 days on this effect, covering values of the relative sediment size in the range  $58 \leq \Pi_{D50} \leq 465$  and relative flow depth,  $\Pi_d$ , in the range  $0.5 \leq \Pi_d \leq 5.0$ , for flow intensity close to the condition of initiation of motion ( $0.93 \leq \Pi_U \leq 1.04$ ). In their tests, there were no significant wall as well as contraction scour effects.

The collected data allowed the characterization of Eq. (11). The values of  $\Pi_{dse} = d_{se}/D_p$  are plotted against  $\Pi_{D50}$  in Figure 6. Data of six long duration clear-water experiments ( $T_d \geq 6$  days) by Sheppard et al. (2004) for  $\Pi_{D50} > 500$  and  $\Pi_U$  sufficiently close to 1.0 (0.85 to 1.21) are also included. Figure 6 renders it clear that  $\Pi_{D50}$  influences  $\Pi_{dse}$  by decreasing the normalized scour depths as  $\Pi_{D50}$  increases in the range of the study.

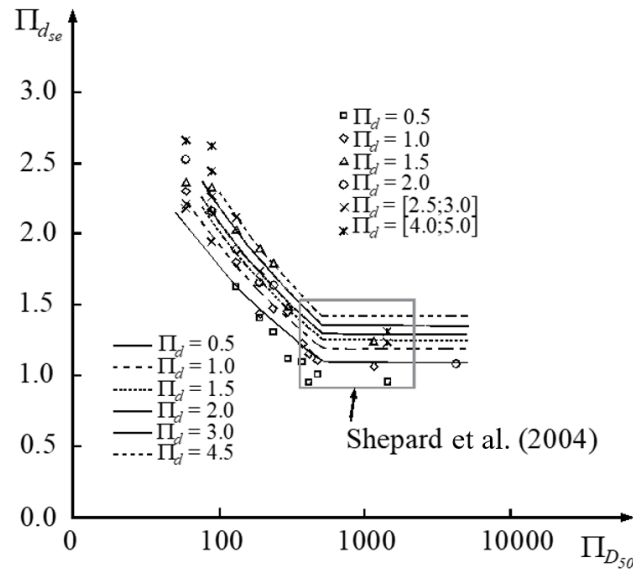


Figure 6. Effect of  $\Pi_{D50}$  and  $\Pi_d$  on  $\Pi_{d_{se}}$ , Lança et al. (2013)

Lança et al. (2013) suggested the upper-bound predictor of the equilibrium scour depth given by Eq. (11), assuming that  $K_d$  is the predictor of Melville (1997) slightly modified to read:

$$K_d = \begin{cases} 2.3(\Pi_d)^{1/3} & 0.50 \leq \Pi_d \leq 1.45 \\ 2.6 & \Pi_d > 1.45 \end{cases} \quad (18)$$

and that  $K_{D50}$  is given by:

$$K_{D50} = \begin{cases} 1.0 & 60 < \Pi_{D50} \leq 100 \\ 5.8(\Pi_{D50})^{-0.38} & 100 < \Pi_{D50} \leq 500 \\ 0.55 & \Pi_{D50} > 500 \end{cases} \quad (19)$$

In engineering practice, the use of Eq(s).(18) and (19) requires the application of appropriate multiplying factors - see Eq. (3) - to take into account the effects of flow intensity, viscosity, pier shape, pier alignment, gradation coefficient, flow contraction, channel cross-section shape and time. The effect of flow intensity was presented in section 4. Sections 6 and 7 assess the time factor and the pier shape and alignment factors, respectively.

### 6. Time Factor

The data of Lança et al. (2010), covering time durations between 24.9 and 45.6 days, complemented with data of one 58.2 days-long experiment found in the literature, were reassessed by Simarro et al. (2011) who have shown that the exponential function suggested by Franzetti et al. (1982),

$$K_t = \frac{d_s}{d_{se}} = 1 - \exp[-a_1 \Pi_t^{a_2}] \quad \text{with} \quad \Pi_t = \frac{Ut}{D_p} \quad (20)$$

is a good predictor of the scour depth time evolution for *clear-water* flow conditions. The use of this equation requires the proper knowledge of  $a_1$  and  $a_2$ , assuming that  $d_{se}$  is known.

In the sequence of the assessment performed by Simarro et al. (2011), Lança et al. (2013) also revisited the proposal of Franzetti et al. (1982). Contrary to these authors, they have concluded that  $a_1$  and  $a_2$  are not constant. The multiplying coefficient  $a_1$  varies in the range  $0.005 \leq a_1 \leq 0.080$ , with an average value of 0.031, whereas  $a_2$  varies within the range  $0.212 \leq a_2 \leq 0.458$ , with an average value of 0.311. Lança et al. (2013) have shown that  $a_1$  and  $a_2$  depend on  $\Pi_{D50}$  as follows:

$$a_1 = 1.22(\Pi_{D50})^{-0.764} \quad a_2 = 0.09(\Pi_{D50})^{0.244} \quad (21)$$

From the above, the model of Franzetti et al. (1982) for the prediction of scour depth time evolution can be applied to cylindrical piers in wide channels whose bed is composed of non-ripple forming uniform sand whenever the approach flow velocity is close to the critical velocity of beginning of motion, i.e., for  $\Pi_U \approx 1.0$ . In this case, the time factor,  $K_t$ , reads as follows:

$$K_t = 1 - \exp\left\{-1.22(\Pi_{D50})^{-0.764} [\Pi_t]^{0.09(\Pi_{D50})^{0.244}}\right\} \quad (22)$$

Further research is needed to include the effect of  $\Pi_U$  on  $K_t$ .

## 7. Pier Shape and Alignment

The pier shape multiplying factor  $K_f$  of Eq. (3) is defined as the ratio between the scour depth at a pier with a given cross-section shape and the scour depth at the standard section-shape pier (usually the circular pier), all the other parameters kept constant. Likewise, the pier alignment or orientation factor,  $K_\theta$ , is defined as the ratio between the scour depth at a pier aligned with a given angle (angle of attack) towards the flow direction and the scour depth at an equal pier aligned with the flow direction (zero angle of attack), all the other parameters kept unchanged.

The effects of pier shape and alignment have received little attention since Laursen and Toch (1956). Yet, a number of pier shape factors,  $K_f$ , were suggested by different researchers. Richardson and Davis (2001) recommended the following expression that describes the values of  $K_\theta$  obtained by Laursen and Toch (1956) for the particular case of rectangular piers:

$$K_\theta = \left(\cos \theta + \frac{\ell_p}{D_p} \sin \theta\right)^{0.65} \quad (23)$$

where  $\ell_p$  stands for pier length and  $D_p$  reads as pier width.

According to Richardson and Davis (2001),  $K_\theta$  replaces the product  $K_f K_\theta$  if the angle of attack,  $\theta$ , is larger than  $5^\circ$  and  $2 < \ell_p/D_p < 16$ . This suggestion corroborates Laursen and Toch (1956) who found that the shape effect becomes negligible ( $K_f = 1.0$ ) in the above domain.

Fael et al. (2016) extended the existing experimental evidence on  $K_f$  and  $K_\theta$  by performing fifty five tests with sand  $S_2$  in Flume  $F_1$  bisected longitudinally to render  $W = 2.0$  m. They tested rectangular square-nosed, rectangular round-nosed and oblong piers as well as zero-spacing (packed) pile-groups (see Figure 7) for skew angles  $\theta = \{0^\circ; 30^\circ; 45^\circ; 60^\circ \text{ and } 90^\circ\}$  and aspect ratios  $\ell_p/D_p = \{1.33; 2.0; 4.0\}$ , i.e., extending down the lower limit of the experiments by Laursen and Toch (1956).

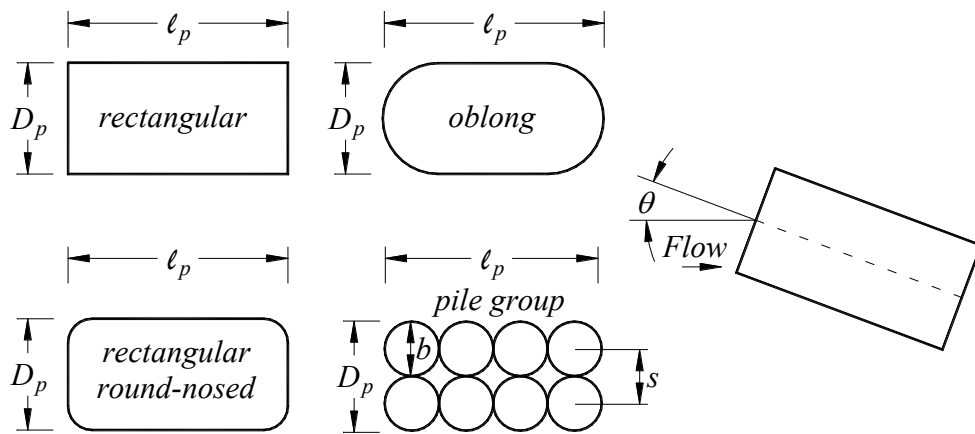


**Figure 7.** Tested pier shapes

Within their experimental domain, Fael et al. (2016) concluded that *i*) the shape factor is  $K_f = 1.0$ , for rectangular round-nosed and oblong cross-section piers, and  $K_f = 1.2$ , for rectangular square-nosed and pile-group cross-section piers; *ii*) the shape effect is non-negligible at skewed piers, contrary to what is usually accepted, although the associated shape coefficients remain in the narrow range of 1.0 to 1.2; *iii*) Eq. (23) constitutes a good predictor of  $K_\theta$  for  $l_p/D_p = 4.0$ , whereas it is better described by

$$K_\theta = \begin{cases} 1 + \frac{4\theta}{1000} & \text{for } \frac{l_p}{D_p} = 1.33 \\ 1 + \frac{8\theta}{1000} & \text{for } \frac{l_p}{D_p} = 2.00 \end{cases} \quad (24)$$

In short, the scour depth at skewed piers depends on both shape and alignment as soon as  $l_p/D_p < 4.0$ . This is relevant whenever equilibrium scour is to be calculated at piers whose cross-section is defined by small aspect ratios,  $l_p/D_p$ .

## 8. Concluding Remarks

This paper aims at reviewing contributions of the authors towards a more precise prediction of the equilibrium scour depth at single vertical piers. It covers the effects of *i*) flow intensity under *clear-water* flow conditions, *ii*) flow depth and sediment size, *iii*) time evolution, and *iv*) alignment and cross-section pier shape. The paper also deals with the controversial concept and assessment of the equilibrium scour depth. Our contributions do not accrue from a new framework; they are rather a refinement of the model suggested by the school of Auckland, initiated by Raudkivi and boosted by Melville and his students. The enhanced predictive capacity associated to our works arises from precise equilibrium scour values properly estimated from unusually long experiments covering uncommonly high laboratory relative pier sizes.

Our most important contributions express  $K$ -factors of Eq. (3) and can be summarized as follows:

- i) The critical value of flow intensity above which scouring is triggered is not a constant value but rather a function of the relative flow depth as given by Eq(s). (6) or (7).
- ii) Flow intensity factor can be predicted by Eq. (9).

- iii) The relative sediment size factor is not constant for values of  $\Pi_{D50}$  above 25 – 50, as it is frequently assumed, but it rather decreases in the range  $100 < \Pi_{D50} < 500$ . It is described by Eq. (19).
- iv) The effect of the relative flow depth or flow shallowness can be described by Eq. (18) instead of Eq(s). (15), (16) and (17).
- v) The time factor is given by Eq. (22) for flow intensities close to 1.0, reflecting the effect of the relative grain size in the range  $60 < \Pi_{D50} < 500$ .
- vi) The shape effect is non-negligible at comparatively short skewed piers.
- vii) Eq. (24) accounts for the alignment effect for small values of the pier cross-section aspect ratio.

It should be noted here that predictions of the improved Auckland's model (Eq. (3)) can be significantly smaller mostly due to the correction associated with the relative sediment size factor.

Another important contribution of the authors to the topic of local scouring is of instrumental nature and refers to the evaluation of the equilibrium scour depth in *clear-water* scour experiments. These should last for at least about one week and the issuing scour values be adjusted by the six parameters polynomial given by Eq. (4) (or a similar equation) to render the value of the scour depth at infinite time.

## Nomenclature

$a_1$	coefficient of the model of Franzetti et al. (1982)[-]	$K_{D50}$	relative sediment size factor or sediment coarseness factor [-]
$a_2$	coefficient of the model of Franzetti et al. (1982)[-]	$K_f$	pier shape factor [-]
$b_1$	experimental cst. [-]	$K_U$	flow intensity factor [-]
$b_2$	experimental cst. [-]	$K_t$	time factor [-]
$b$	pier diameter in a pile group [m]	$K_v$	fluid viscosity factor [-]
$C_1$	experimental cst. [-]	$K_\theta$	pier alignment factor [-]
$C_2$	experimental cst. [-]	$K_{\sigma_D}$	armorings factor [-]
$d$	flow depth [m]	$\ell$	distance from flume entrance to the recess box [m]
$D_{15.9}$	sand particle sieving diameter for which 15.9% are finer by weight [m]	$L$	flume length [m]
$D_{50}$	sand particle sieving diameter for which 50% are finer by weight; median grain size of the bed sediment [m]	$\ell_1$	length of bed recess box [m]
$D_{84.1}$	sand particle sieving diameter for which 84.1% are finer by weight [m]	$\ell_a$	abutment length [m]
$D_{pr}$	characteristic length of the pier cross-section [m]	$\ell_o$	obstacle length [m]
$d_r$	depth of bed recess box [m]	$\ell_p$	pier length [m]
$d_s$	scour depth [m]	$p_1 - p_6$	experimental constants [-]
$d_{se}$	equilibrium scour depth [m]	$s$	specific gravity of the bed sediment [-]
$d_{sm}$	maximum scour depth [m]	$t$	time [s]
$f$	pier shape [-]	$U$	average approach flow velocity [ $ms^{-1}$ ]
$G$	channel cross-section geometry [-]	$u^*$	friction velocity [ $ms^{-1}$ ]
$g$	gravitational acceleration [ $ms^{-2}$ ]	$U_c$	critical velocity of beginning of sediment motion [ $ms^{-1}$ ]
$K_d$	flow shallowness or relative flow depth factor [-]	$W$	channel width [-]
		$\Pi$	any non-dimensional parameter [-]

$\Pi_d = d/\ell_a$ and $\Pi_d = d/D_p$	relative flow depth or flow shallowness [-]	$\Pi_{Ui}$	scour inception parameter [-]
$\Pi_{ds}$	non-dimensional scour depth [-]	$\Pi_W$	cross-section aspect ratio [-]
$\Pi_{dse} = d_{se}/d$ and $\Pi_{dse} = d_{se}/D_p$	non-dimensional equilibrium scour depth [-]	$\Pi_v = u_*D_{50}/\nu$	particle Reynolds number [-]
$\Pi_{D50} = D_p/D_{50}$	relative sediment size or coarseness [-]	$\Pi_\theta$	alignment parameter [-]
$\Pi_f$	pier shape parameter [-]	$\phi$	function of [-]
$\Pi_G$	channel cross-section parameter [-]	$\nu$	kinematic water viscosity [ $\text{m}^2\text{s}^{-1}$ ]
$\Pi_t = Ut/D_p$	non-dimensional time [-]	$\theta$	pier alignment [°]
$\Pi_U = U/U_c$	flow intensity [-]	$\rho$	water density [ $\text{kgm}^{-3}$ ]
		$\sigma_D$	gradation coefficient of the bed sediment [-]

### Author Statement

The authors confirm contribution to the paper as follows: all authors have contributed equally to the study conception and design, analysis and interpretation of results, draft manuscript preparation. All authors reviewed the results and approved the final version of the manuscript.

### Conflict of Interest

The authors declare no conflict of interest.

### References

- Bertoldi, D.A. & Jones, J.S. (1998). Time to scour experiments as an indirect measure of stream power around bridge piers. *Proceedings of the International Water Resources Engineering '98*, Memphis, Tennessee, 264-269.
- Breusers, H.N.C. & Raudkivi, A.J. (1991). Scouring, *Hydraulics Structures Design Manual*. IAHR A.A. Balkema ed., Rotterdam.
- Cardoso, A.H. & Bettess, E. (1999). Time evolution and effect of channel geometry on local scour at bridge abutments. *Journal of Hydraulics Engineering*, 125(4), 388-399.
- Cardoso, A.H. & Fael, C.M.S. (2010). Time to equilibrium scour at vertical wall bridge abutments. *ICE Journal on Water Management*. 163(VM10), 509-513.
- Chabert, J. & Engeldinger, P. (1956). Etude des affouillements autour des piles de ponts. *Lab. Natl. d'Hydraul.*, Chatou, France.
- Chiew, Y.M. (1995). Mechanics of riprap failure at bridge piers. *Journal of Hydraulic Engineering*, 121(9), 635-643.
- Ettema, R. (1980). Scour at bridge piers. Report No. 216, University of Auckland, Auckland, New Zealand.
- Fael, C.M.S. (2007). Erosões localizadas junto de encontros de pontes e respectivas medidas de protecção. *PhD thesis*, University of Beira Interior, Covilhã, Portugal.
- Fael, C.M.S., Simarro-Grande, G., Martín-Vide, J.P. & Cardoso, A.H. (2006). Local scour at vertical-wall abutments under-clear water flow conditions. *Water Resources Research*. 42, W10408.

- Fael, C.M.S., Lança, R.M.M. & Cardoso, A.H. (2016). Effect of pier shape and pier alignment on the equilibrium scour depth at single piers. *International Journal of Sediment Research*, 31(3), 244-250.
- Fael, C.M.S, Lança, R.M.M., Couto, L. & Cardoso, A.H. (2014). Local scour at single piers revisited, *3rd IAHR European Congress*, Porto, April, paper 12.
- Franzetti, S., Larcan, E. & Mignosa, P. (1982). Influence of tests duration on the evaluation of ultimate scour around circular piers. *Proc., Int. Conf. on the Hydraulic Modeling of Civil Engineering Structures, BHRA Fluid Engineering*, England, 381-396.
- Hager W.H. & Oliveto, G. (2002). Shields' entrainment criterion in bridge piers. *Journal of Hydraulic Engineering*, 128(5), 538-542.
- Hanco, S. (1971). Sur le calcul des affouillements locaux dans la zone de piles de pont, *XIV Congrès de IAHR*, Communication C36 aux, Paris.
- Kandasamy, J.K. (1989). Abutment scour. Report n° 458, School of Engineering, University of Auckland, Auckland, New Zealand.
- Lança, R., Fael, C. & Cardoso, A.H. (2010). Assessing equilibrium clear-water scour around single cylindrical piers. *River Flow 2010*, Dittrich, A. et al., eds., Bundesanstalt für Wasserbau, Germany, 1207-1213.
- Lança, R., Fael, C., Maia, R., Pêgo, J. & Cardoso, A.H. (2013). Clear-water scour at comparatively large cylindrical piers. *Journal of Hydraulic Engineering*, 139(11), 1117-1125.
- Laursen, E.M. (1963). An analysis of relief bridge scour. *J. Hydraulic Division Am Soc. Civ. Eng.*, 89(HY3), 93-118.
- Laursen, E. & Toch, A. (1956). Scour around bridge piers and abutments. *Bulletin No. 4*, Iowa Highway Research Board.
- Lee, S., & Sturm, T. (2009). Effect of sediment size scaling on physical modeling of bridge pier scour. *Journal of Hydraulic Engineering*, 135(10), 793-802.
- Melville, B.W. (1992). Local scour at bridge abutments. *Journal of Hydraulic Engineering*, 118(4), 615-631.
- Melville, B.W. (1997). Pier and abutment scour: integrated approach. *Journal of Hydraulic Engineering*, 123(2), 125-136.
- Melville, B.W. & Coleman, S.E. (2000). Bridge scour. *Water Resources publications*, LLC, CO.
- Melville, B.W. & Chiew, Y.M. (1999). Time scale for local scour at bridge piers. *Journal of Hydraulic Engineering*, 125(1), 59-65.
- Oliveto, G. & Hager, W.H. (2002). Temporal evolution of clear-water pier and abutment scour. *Journal of Hydraulic Engineering*, 128(9), 811-820.
- Oliveto, G. & Hager, W.H. (2005). Further results to time-dependent local scour at bridge elements. *Journal of Hydraulic Engineering*, 131(2), 97-105.
- Richardson, E.V. & Davis, S.R. (2001). Evaluating scour at bridges. *Hydraulic Engineering Circular No. 18 (HEC-18)*. Rep. No. FHWA NHI 01-001, Federal Highway Administration, Washington, D.C.
- Shen, H.W., Schneider, V.R. & Karaki, S.S. (1966). *Mechanics of local scour.*, U.S. Department of Commerce, National Bureau of Standards, Institute for Applied Technology, 1966.

- Sheppard, D.M., Odeh, M. & Glasser, T. (2004). Large scale clear-water local pier scour experiments. *Journal of Hydraulic Engineering*, 130(10), 957-963.
- Simarro, G., Fael, C. & Cardoso, A.H. (2011). Estimating equilibrium scour depth at cylindrical piers in experimental studies. *Journal of Hydraulic Engineering*, 137(9), 1089-1093.